Report of Investigation 18

THE TENSLEEP PLAY OF SOUTH-CENTRAL MONTANA: A PART OF THE PERMO-PENNSYLVANIAN PETROLEUM SYSTEM OF MONTANA AND WYOMING

David A. Lopez
Montana Bureau of Mines and Geology
Montana Tech of The University of Montana

Steven W. VanDelinder
Ballard Petroleum Holdings, LLC

Michael L. Hendricks
Hendricks and Associates, Inc.

Geoffrey S. Bayliss
Geochem Laboratories, Inc.

Wayne L. Ewert
Ballard Petroleum Holdings, LLC

2007

Work performed under Contract DE-PS26-04NT15450-2B
Submitted by:
Montana Bureau of Mines and Geology
1300 North 27th Street
Billings, MT 59101

DISCLAIMER

Cover photo: Upper Soap Creek on the east side of the Big Horn Mountains. Photo shows red Chugwater Formation overlying light brown sandstones of the Tensleep Sandstone near the valley bottom. Photo by David Lopez, MBMG.

CONTENTS

FIGURES

TABLE

PLATES

ABSTRACT

Eolian sands are the main Pennsylvanian Tensleep Sandstone reservoir rocks, and were deposited in a near-shore environment interbedded with near-shore marine and sabkha calcareous and dolomitic rocks. Within the Tensleep, numerous cycles are characterized by basal marine or sabkha calcareous sandstone or dolomitic sandstone overlain by porous and permeable eolian sandstone, which in turn is capped by marine sandstone. The cycles represent the interplay of near-shore marine, sabkha, and eolian environments.

On the west side of the project area, both the lower and upper Tensleep are present and the total thickness reaches a maximum of about 240 ft. The lower Tensleep is 100 to 120 ft thick and consists of a sequence of repeating cycles of limey shallow marine sandstone, sandy limestone, and sandy dolomite. The upper Tensleep is generally characterized by cycles of sandy limestone or dolomite, overlain by light-colored, eolian dune sandstone capped by marine limey sandstone.

In the central and eastern parts of the project area, only the lower Tensleep is present, but here eolian sandstones are in cycles much like those in the west in the upper Tensleep. The lower Tensleep is quite variable in thickness, ranging from about 25 ft to over 200 ft.

Oil accumulations in the Tensleep are best described as structurally modified paleostratigraphic accumulations. At Frannie Field, the irregular oil column can be explained by a post-Tensleep channel scour on the west flank of the anticline. On the Powder River Basin side of the project area, the Soap Creek and Lodge Grass Fields produce from the Permo-Pennsylvanian system. In these two fields, erosional remnants of eolian sandstone control the production, similar to the situation at Frannie Field. At Soap Creek the trap is enhanced by structural closure. In the Lodge Grass area, Tensleep oil is trapped in preserved dunes in the footwall of a Laramide reverse fault. Oil generation and migration was early. Two hypotheses have been presented: migration occurred (1) before mid-Jurassic erosion produced a major regional unconformity or (2) about 82 million years ago. Migration pre-Laramide occurred because oil in both the Bighorn Basin and the Powder River Basin are part of the same petroleum system. Geochemical analysis of oils from producing fields across the region show the oils are all similar and have the same source and generation history. No Phosphoria source rocks exist in the project area of south-central Montana, requiring that oil migrated from distant source areas, probably in central and southwestern Wyoming.

Oil shows and production in the Tensleep are absent in the northern part of the project area. This appears to be controlled by the merging of the top of the Tensleep Sandstone and the Jurassic unconformity (top of the Triassic Chugwater Formation). There should be potential for the discovery of oil in Tensleep stratigraphic traps or combination traps everywhere south of the Jurassic–Pennsylvanian Isopach zero contour except where the Tensleep has been exposed by uplift and erosion.

Known Tensleep fields in south-central Montana are generally small in area, which agrees with outcrop studies that show eolian dune sequences are generally quite small in lateral extent, on the order of 10 to 40 acres. Although existing fields are small in area, they are very productive; individual wells will probably make 300,000 to 500,000 barrels of oil.

In the project area, hydrodynamic considerations are important. All the existing Tensleep fields have active water drives. In many cases, the reservoir pressure today is as it was when initially discovered. In areas of high structural complexity, such as the Lodge Grass–Crow Agency fault and the Lake Basin fault zone, significant structural closure may be necessary to trap oil because of the strong hydrodynamic influence exerted by the underlying Madison Formation aquifer.

EXECUTIVE SUMMARY

The Permo-Pennsylvanian stratigraphic section in the Bighorn and Powder River Basins is one of the most prolific oil-producing systems in the central Rocky Mountain Region. These reservoirs have produced in excess of 2 billion barrels of oil in the Bighorn Basin and in excess of 525 million barrels of oil in the Powder River Basin. The Tensleep–Minnelusa play is part of the much more extensive regional petroleum system sourced from the Permian Phosphoria Formation. Reservoir facies were controlled by eastward change from marine to coastal depositional environments in combination with erosional wedging in the Permian and Jurassic. Eolian sands are the main reservoir rocks where they occur, in cycles that are characterized by basal marine or sabkha calcareous sandstone or dolomitic sandstone overlain by porous and permeable eolian sandstone, which in turn is capped by marine sandstone. The cycles represent the interplay of near-shore marine, sabkha, and eolian environments.

In the western project area, both the lower and upper Tensleep Sandstone are present. The lower Tensleep is a sequence of repeating cycles of limey shallow marine sandstone, sandy limestone, and sandy dolomite. The upper Tensleep is characterized by cycles of sandy limestone or dolomite, overlain by light-colored eolian dune sandstone, which in turn is capped by marine limey sandstone.

In the central and eastern areas, only the lower Tensleep is present. But here eolian sandstones are present in cycles much like upper Tensleep cycles in the west. The lower Tensleep is quite variable in thickness, ranging from about 25 ft to over 200 ft.

The oil accumulations in the Tensleep are best described as structurally modified paleo-stratigraphic traps. Migration occurred pre-Laramide because oil in both the Bighorn Basin and the Powder River Basin have been shown to be parts of the same petroleum system. Geochemical analysis of oils from producing fields across the region show the oils are all chemically similar and have the same source and generation history.

Oil shows and production in the Tensleep are absent in the northern part of the project area, which is probably controlled by the merging of the top of the Tensleep Sandstone and the Jurassic unconformity (top of the Triassic Chugwater Formation). There should be potential for the discovery of oil in Tensleep stratigraphic traps or combination traps everywhere south of the J-Penn isopach zero contour.

Known Tensleep fields in south-central Montana are generally small in area, but are very productive; individual wells are probably capable of producing 300,000 to 500,000 barrels of oil.

Hydrodynamic considerations are also important since existing Tensleep fields in the study area have water drives. In many cases, the reservoir pressure today is as it was when initially discovered.

INTRODUCTION

The Pennsylvanian Tensleep–Minnelusa stratigraphic section in the Bighorn and Powder River Basins contains the most prolific oil-producing reservoirs in all of the central Rocky Mountain Region. These reservoirs have produced in excess of 2 billion barrels of oil in the Bighorn Basin and in excess of 525 million barrels of oil in the Powder River Basin. The Tensleep–Minnelusa play is part of the much more extensive regional petroleum system sourced from the Permian Phosphoria Formation (Johnson, 2005), which will be described in more detail in a later section of this report. Dramatic stratigraphic changes and thinning occur within the Pennsylvanian section between the Central Montana Trough and the Bighorn and Powder River Basins to the south. The erosional pinch-out of this system has been the focus of petroleum exploration in the past. However, recent work in the northern part of the Bighorn Basin has shown that petroleum accumulations are in fact controlled by more complicated stratigraphic changes that occur south of the erosional pinch-out of this stratigraphic interval.

The area considered in this project includes the northernmost portions of the Bighorn and Powder River Basins (fig. 1). In this region the Pennsylvanian Tensleep Sandstone and Minnelusa Formation provide some of the most important petroleum reservoirs. Reservoir facies were controlled by east–west transitions from marine, to marginal marine, to coastal depositional environments in combination with erosional wedging of the top of the sequence

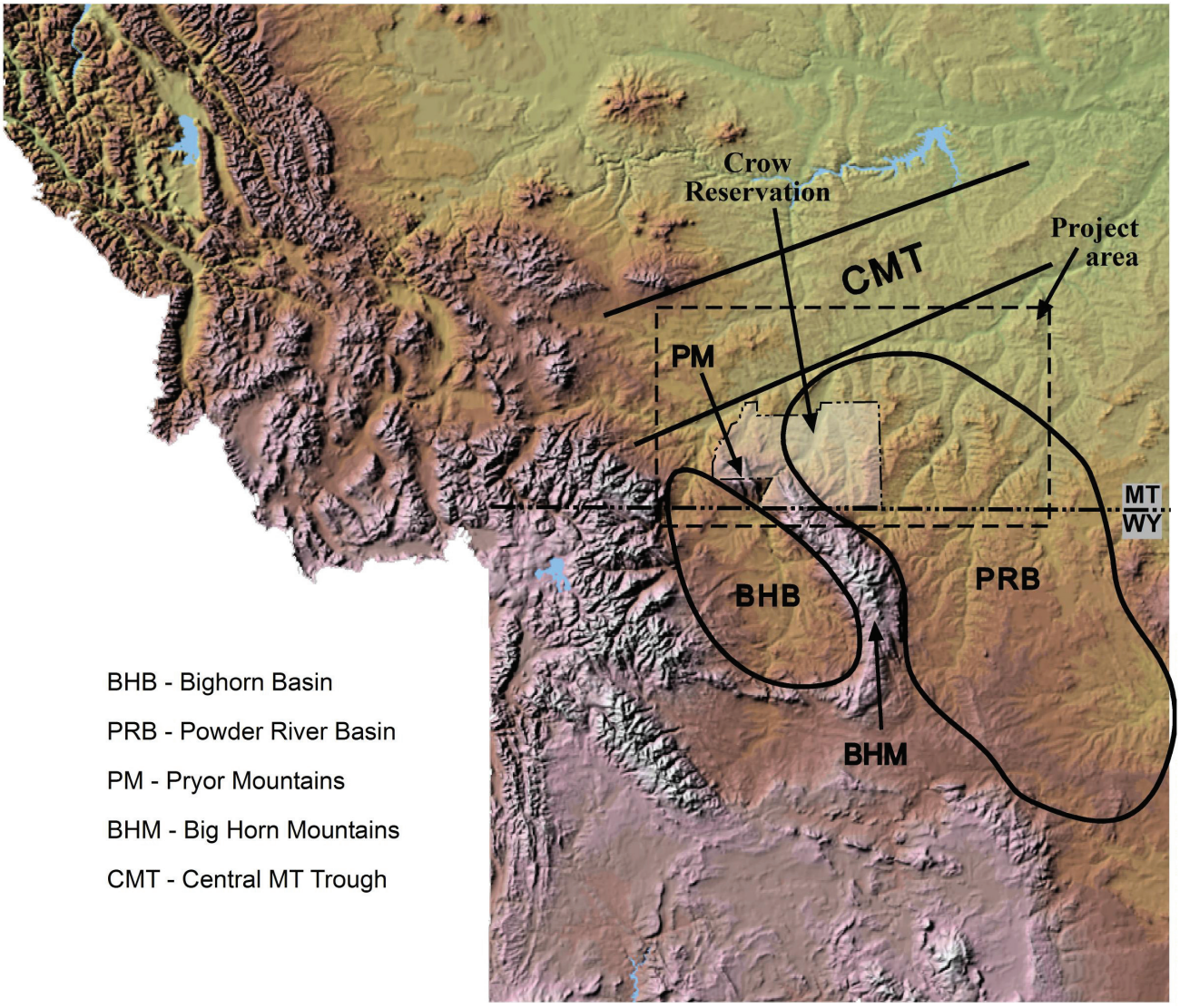

Figure 1. Index map of project area, showing structural features, basins, and the Crow Indian Reservation.

that occurred in the Permian and Jurassic. The Tensleep–Minnelusa section pinches out completely in the area of the Central Montana Trough.

The overall goals of this project were: (1) to develop a new exploration model for the Permo-Pennsylvanian petroleum system, (2) to generate maps showing an exploration fairway for oil accumulations in this system, (3) to reduce exploration costs by allowing focused exploration in the fairway and by understanding geologic controls on petroleum accumulations, and (4) to ultimately add petroleum reserves from new discoveries.

REGIONAL STRUCTURAL GEOLOGY

The project area is within the Rocky Mountain structural province, which is characterized by Laramide basins and uplifts. More specifically, it straddles the Pryor and Big Horn Mountains and includes the northern parts of the Bighorn and Powder River Basins (fig. 1). This structural region was chosen intentionally to test the idea that the two basins, now separated, are part of one petroleum system.

The Pryor and Big Horn Mountains are parts of a larger regional Laramide uplift that includes both mountain ranges and extends to the northwest to the Fromberg fault zone (plate 1). This regional structural uplift is divided into several differentially uplifted blocks by a complex system of basement involved reverse faults and tear faults (plate 1) (Lopez, 1995, 1996, 2000a,b). Many northwest-striking folds and monoclines (plate 1) are controlled by reverse faults or blind reverse faults, including the eastern flank of the Big Horn Mountains (Lopez, 2000a; Vuke and others, 2000). Two blind reverse faults were identified on seismic data in T. 3 and 4 S., R. 37 E. (fig. 2). Many of these folds are traps for oil and gas. The fold–fault relationship is probably best described for this region by the fault-propagation model of McConnell (1994).

In general, as shown by structural contours on plate 1 (in back cover), regional dips are away from the uplift in all directions. This general structural pattern is interrupted by folds and monoclines as described above and is also modified by two west–northwest-striking fault zones, the Nye-Bowler (Wilson, 1936) and Lake Basin fault zones (plate 1; Hancock, 1919, 1920). These are both left-lateral strike-slip zones at depth and are expressed at the surface by a system of northeast-striking en echelon normal faults as well as associated anticlinal and synclinal folds (Lopez, 2000a,b). These fault zones are basement-controlled fault systems that have experienced repeated recurrent episodes of movement through geologic time (Thom, 1923; Wilson, 1936; Chamberlin, 1945; Alpha and Fanshawe, 1954; Foose and others, 1961; Smith, 1965; Hoppin, 1974; Wise, 2000). In the Pryor and Big Horn Mountains the Nye-Bowler zone extends across the ranges and controlled the structural development of the Laramide uplifts. A northward fault splay off of this zone also shows clear structural control of channel development in Lower Cretaceous Greybull Sandstone (Lopez, 2000c). The Lake Basin fault zone extends at least as far east as T. 2 S., R. 40 E. (plate 1; Vuke and others, 2001). Seismic data purchased for this project to help with subsurface interpretation in areas of sparse well control show the nature of these faults and confirm the eastward extent of the Lake Basin fault zone as mapped by Vuke and others (2001; fig. 3).

STRATIGRAPHY

Regional Stratigraphy

Understanding the Permo-Pennsylvanian stratigraphy in the region is the key to understanding hydrocarbon trapping mechanisms within these rocks. The stratigraphic sequence from Mississippian through Middle Jurassic rocks in the project region was controlled by continuous depositional systems, but Laramide deformation separated the region into two basins, the Bighorn and the Powder River. The stratigraphic terminology applied to the stratigraphic sequence is different in the two basins (fig. 4).

In the Bighorn Basin the Darwin Sandstone, at the base of the section discussed here, locally fills in the karsted surfaces that were developed on the Mississippian Madison Group. In the Powder River Basin the equivalent rocks are the Bell Sandstone. The Amsden Formation, which can be divided

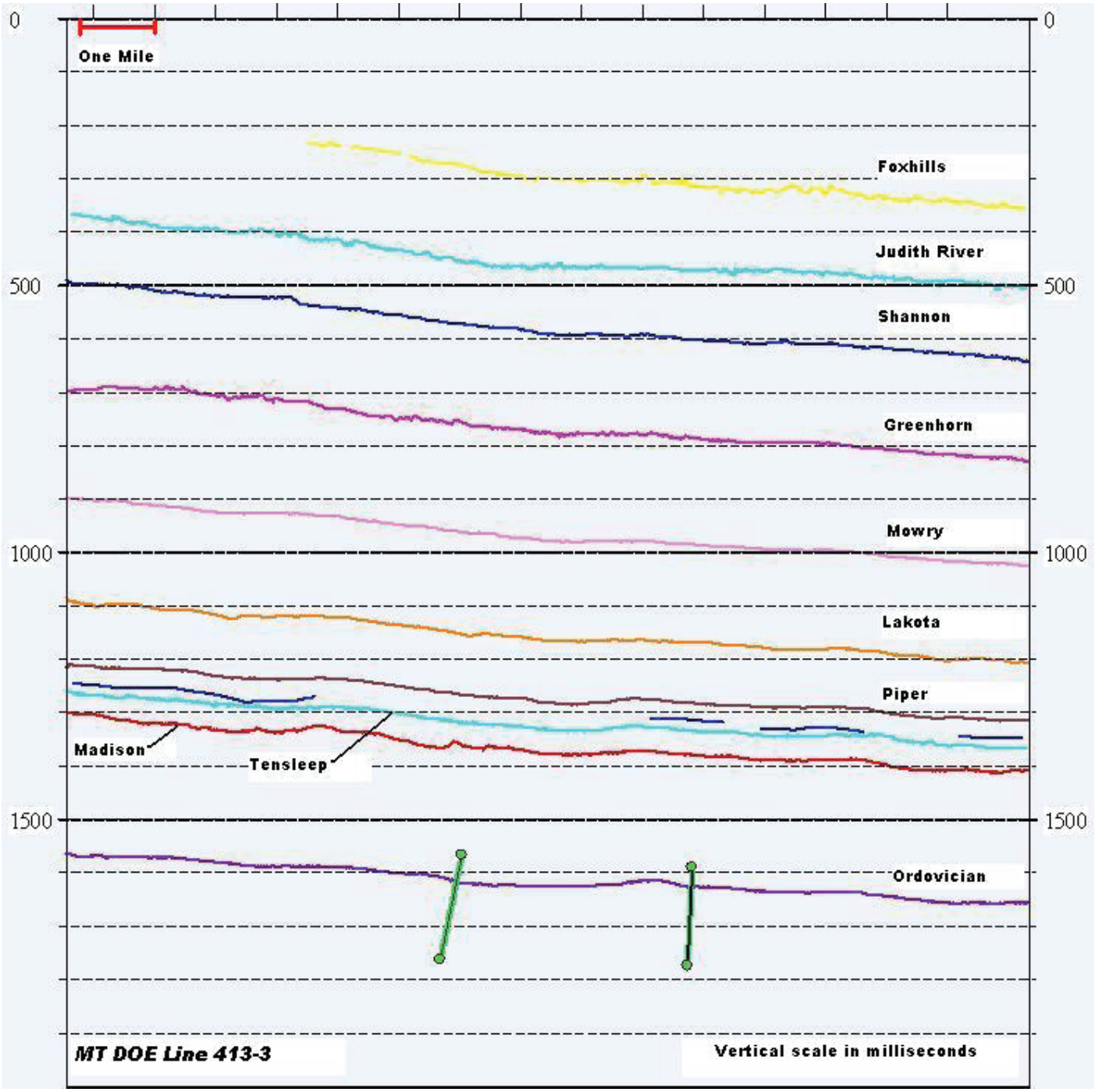

Figure 2. Interpretation of east–west seismic line in T. 3 S., R. 36, 37, and 38 E., showing blind Laramide reverse faults.

into the lower Horseshoe Shale Member and the upper Ranchester Limestone Member, overlies the Madison, or locally the Darwin, and is 70 to 150 ft thick. The Amsden grades upward from the cherty dolomite into a sandy carbonate-rich section of the Tensleep. The top of the Amsden is best picked in the subsurface using the density log to identify the uppermost dense dolomite bed.

The Tensleep Formation can be divided into two distinct lithologic cycles as described in detail by Mankiewicz and Steidtmann (1979). Overall, the lower to upper Tensleep represents a westward regression of the depositional system and is composed of a mixed marine/subaerial lower unit overlain by a dominantly eolian upper unit that periodically gave way to marine pulses. These units are so distinct in outcrop and subsurface that Moore (1984) proposed they be classified as separate members of the

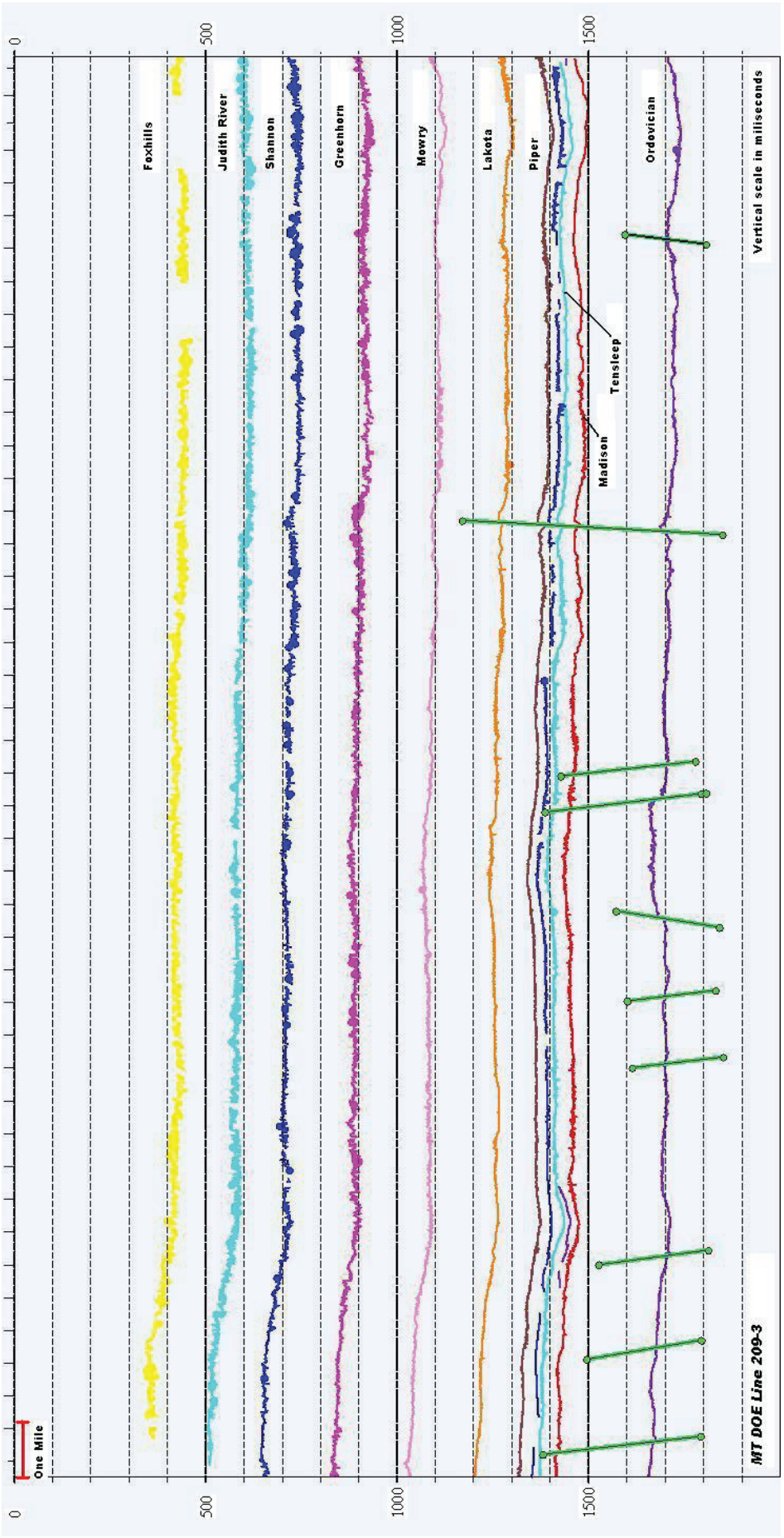

Figure 3. Interpretation of southwest–northeast seismic line in T. 2 and 3 S., R. 38–41 E., showing faulting along the Lake Basin fault zone.

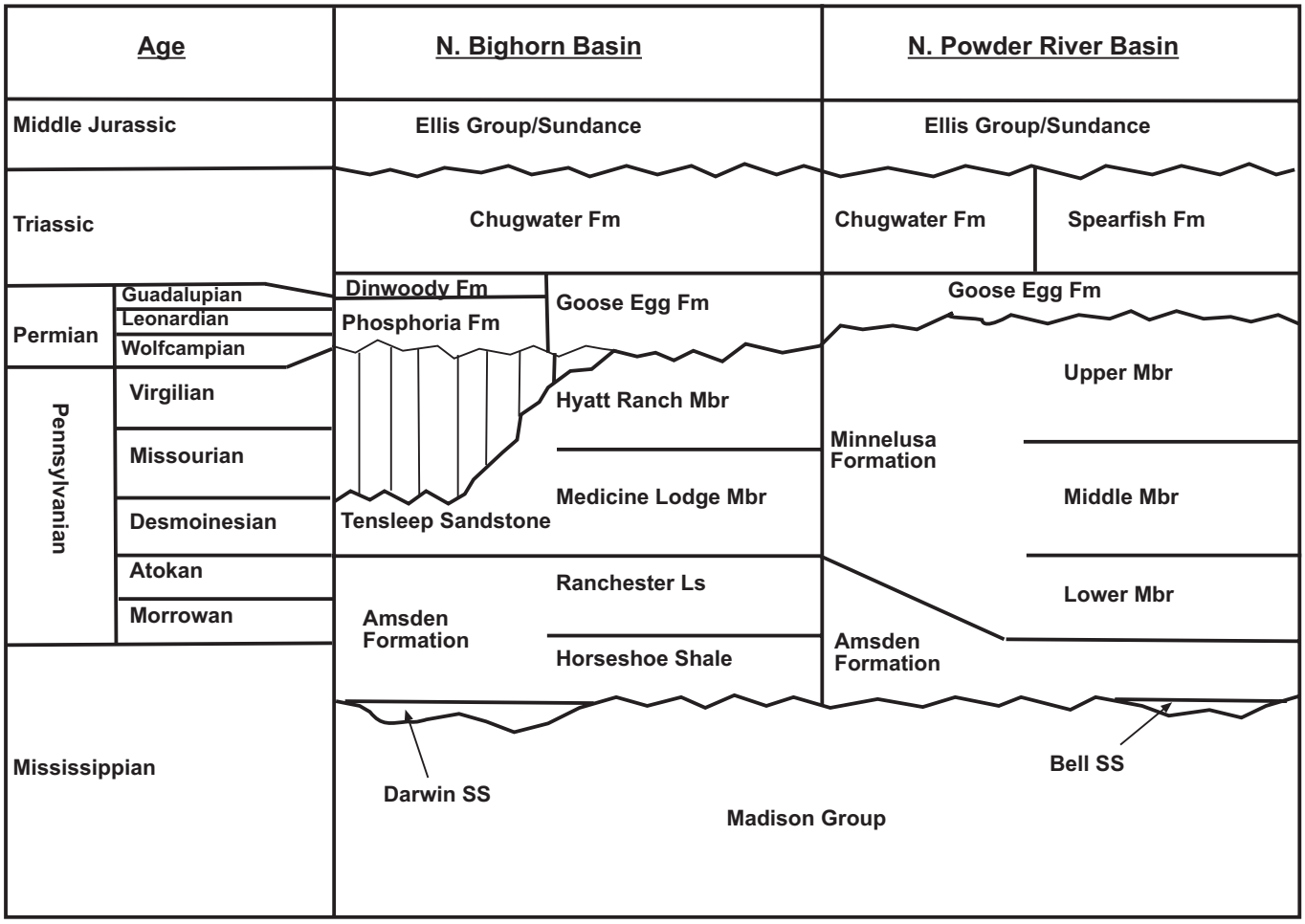

Figure 4. Stratigraphy in the project area, showing nomenclature used in the northern Bighorn Basin and northern Powder River Basin.

Tensleep Sandstone. Moore named the lower marine unit the Medicine Lodge Creek Member and the upper, eolian unit the Hyatt Ranch Member.

The lower Tensleep (Medicine Lodge Member) is considered to be supratidal sabkha flat deposits, consisting of interbedded marine sandstones and carbonate rocks interspersed with some discontinuous flooded and reworked eolian sandstones (Inden and others, 1996). These sediments are rich in dolomite and anhydrite cements. Along the east flank of the Bighorn Basin, the lower Tensleep outcrop along Tensleep Creek is composed of 58% dolomite, 25% sandstone, and 17% shale (Moore, 1984).

The upper Tensleep (Hyatt Ranch Member) is primarily eolian sandstone that contains thin, laterally continuous dolomite and dolomitic sandstone beds (Inden and others, 1996). These deposits represent hyper-saline ponds occurring in deflation hollows between dune ridges. The sandstone is well sorted and cemented with dolomite and calcite. A major unconformity at the top of the Tensleep has as much as 250 ft of local relief (Moore, 1984), causing the Tensleep to be highly variable in thickness throughout the basin (Lawson and Smith, 1966; Stone, 1967; Moore, 1984).

In the Powder River Basin the Permo-Pennsylvanian stratigraphy is similar but contains more near-shore facies than in the Bighorn Basin. The lower and upper Tensleep probably correlate to the middle member of the Minnelusa, although Moore (1984) suggests that they correlate with the middle and upper members of the Minnelusa based on log correlations. The Upper Minnelusa Formation of the Powder River Basin is Permian (Wolfcampian), consisting of a series of intercalated eolian and marine deposits. The eolian deposits are the preserved remnants of several episodes of off-shore progradation of eolian sand dunes into the evaporitic carbonate sedimentary environments (Fryberger, 1984).

The Middle Minnelusa Formation is Pennsylvanian Desmoinesian, Missourian, and Virgilian in age and consists of sandstone, dolomite, limestone, black shale, and evaporite deposits. Deposition of the Middle Minnelusa of the Powder River Basin took place in a carbonate sabkha environment, punctuated by transgressive periods that covered the region with a restricted shallow sea. The Middle Minnelusa in the northern area of the Powder River Basin is described as a coastal dune setting, representing the limit of these transgressive events (Desmond and others, 1984).

The distribution of Permo-Pennsylvanian rocks was controlled by a northeast-trending regional paleo-uplift in central Montana. This uplift was probably controlled by reactivation of faults that controlled the Central Montana Trough, a structural feature that was active repeatedly since at least Proterozoic time when rocks of the Belt Supergroup were deposited in the precursor Helena Embayment (Winston, 1986). Regionally, the Tensleep is beveled progressively down-section from south to north across the Bighorn Basin. An isopach of the Phosphoria to Madison (Permo-Pennsylvanian) interval by Lawson and Smith (1966) shows the overall thinning of this section into Montana due to this uplift. Lawson's Phosphoria isopach also shows a northward on-lapping and thinning onto a paleo-high in the area of south-central Montana. Farther north in the area of the Central Montana Trough, the entire Tensleep section is eroded to a zero edge.

The effect of this uplift and erosional truncation is the preservation of younger rocks progressively to the southeast (Fryberger, 1984; Mallory, 1972; Bailey and Baars, 1972). This resulted in the Wolfcampian Upper Minnelusa Formation being preserved only in a northeast-trending region southeast of the project area (Fryberger, 1984; Bailey and Baars, 1972). In south-central Montana the Tensleep is probably entirely Desmoinesian in age (Henbest, 1956; Inden and others, 1996), although Inden and others (1996) report the upper Tensleep in the Bighorn Basin is Missourian and Virgilian and only the lower part is Desmoinesian. This general regional wedge truncation pattern was altered locally by structurally controlled highs and lows; one such high developed in north-central Wyoming and extended northeast into the south-central edge of this project area in Montana (Mankiewicz and Steidtmann, 1979; Curry, 1984; Lawson and Smith, 1966; Inden and others, 1996). In the Big Horn Mountains in the project area this paleo-high is expressed as thinning of the Tensleep in the Lodge Grass Creek area, in the eastern part of Dry Head Canyon, and in the Bighorn Canyon area near the Wyoming border. North of this thin, the Tensleep thickens to 100 ft to locally over 200 ft, indicating a paleo-structural low was present in that area. These regional and local thickness patterns are illustrated in the isopach map of the Tensleep and in regional cross sections (Lopez and VanDelinder, 2006).

Shaly carbonates of the Permian Phosphoria Formation on-lapped the Tensleep unconformity in the central and western part of the Bighorn Basin; in the eastern and northern portion of the basin and in the Powder River Basin the laterally equivalent Goose Egg red beds and evaporites occupy this position. A major erosional unconformity is present at the top of the Permian rocks and indicates that the central Montana paleo-high was active at this time. The entire Permian section is absent in the north part of the project area due to a combination of non-deposition and erosion (Lopez and VanDelinder, 2006).

The Triassic Dinwoody and Goose Egg equivalents conformably overlap the Permo-Pennsylvanian sequence. They are composed primarily of anhydrite and dense dolomitic shale. Triassic red beds of the Chugwater or Spearfish Formations overlie this interval. The Triassic is unconformably overlain by the mid-Jurassic Ellis Group (Sundance). Due to this unconformity, no Lower Jurassic rocks are preserved in the northern Bighorn and northern Powder River Basins. Isopach mapping of the Triassic section shows a pronounced beveling from south to north across the region (plate 2; Thomas, 1965; MacLachlan, 1972). The Triassic is nearly 1,200 ft thick in the southern Bighorn Basin; it is about 600 ft thick near the southern part of the project area and is totally eroded out in the northern part of the project area (plate 2). These thickness patterns demonstrate that a regional high persisted in central Montana from Permian through Jurassic time (plate 2). Figure 5 diagrammatically illustrates these regional stratigraphic relationships.

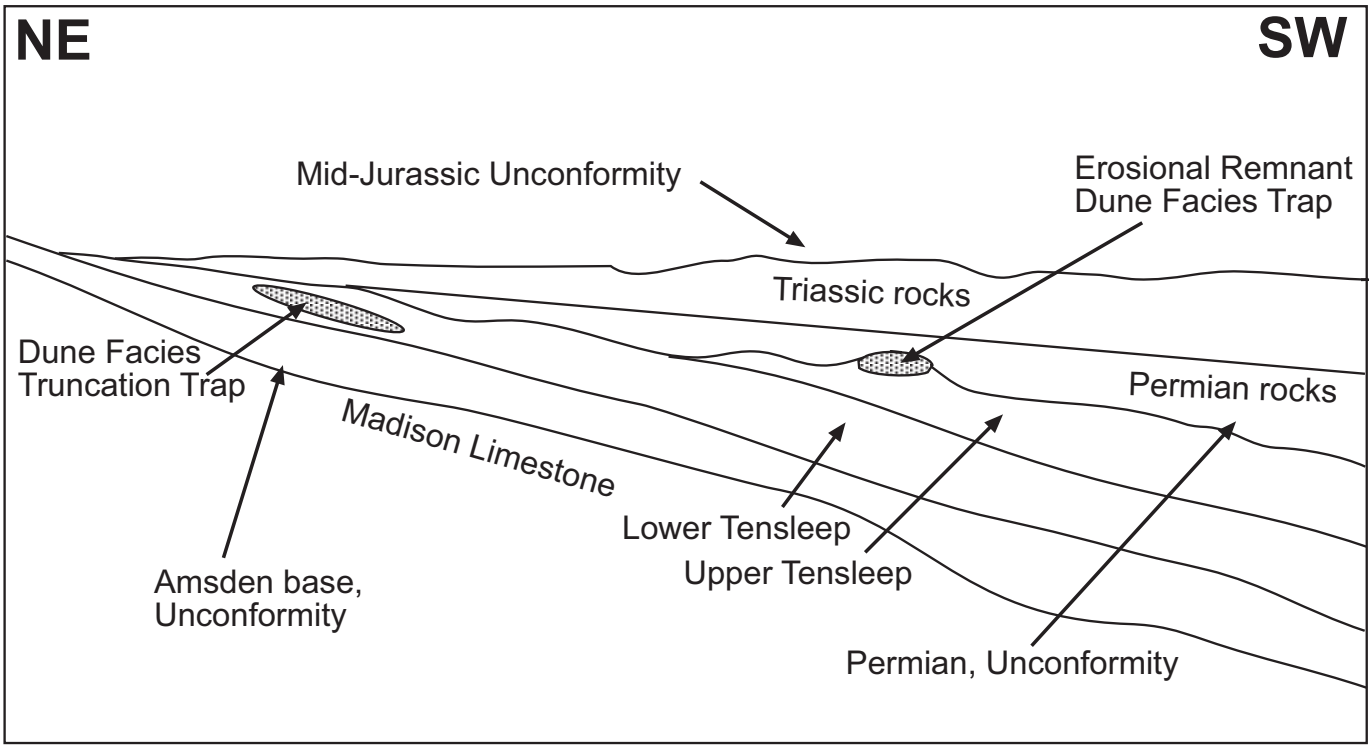

Figure 5. Simplified diagram illustrating regional stratigraphic relationships and reservoir development within the Permo-Pennsylvanian system.

Regional Paleogeography and Sequence Stratigraphy

During Permo-Pennsylvania deposition, the region was characterized by a broad shallow marine shelf on the eastern side of the deep foreland basin (Sublette Basin of Maughan, 1975) that formed inland of the Antler Orogenic Belt (Peterson, 1977; Inden and others, 1996; Maughan, 1975). The region is thought to have been just north of the equator in an arid climate within a belt of northeasterly winds (Andrews and Higgins, 1984; Mankiewicz and Steidtmann, 1979; Fryberger, 1984). The very shallow, nearly flat shelf resulted in a very wide shoreline zone of sand deposition (Fryberger, 1984).

The basal sequence boundary for the Permo-Pennsylvanian reservoir rocks of the Tensleep Sandstone is the erosional unconformity at the top of the Mississippian Madison Group. Gradual sea level rise and northeastward transgression resulted in deposition of the Mississippian–Pennsylvanian Amsden Formation, which grades from terrestrial deposits at the base to marine carbonate at the top. Deposition of the Tensleep occurred during the subsequent westward marine regression. Reservoir rocks in the Tensleep are associated with this migrating shoreline. Eolian sands are the main reservoir rocks deposited in a near-shore environment, where they are interbedded with near-shore marine and sabkha calcareous and dolomitic rocks. Within the Tensleep, numerous cycles occur characterized by basal marine or sabkha calcareous sandstone or dolomitic sandstone overlain by porous and permeable eolian sandstone, which in turn is capped by marine sandstone. The cycles represent the interplay of near-shore marine, sabkha, and eolian environments. Because of the very low shelf gradient, small changes in sea level resulted in repeated and apparently rapid marine incursions over eolian sand deposits. The sequence boundary at the top of the Tensleep is an erosional unconformity. Another sequence boundary occurs at the top of the Permian Phosphoria Formation; locally this unconformity cuts down into the top of the Tensleep Sandstone.

The most productive reservoirs in the Permo-Pennsylvanian system (Tensleep and Minnelusa Formations) are permeable and porous sandstone facies that were mainly deposited in eolian environments and that have not had porosity destroyed by

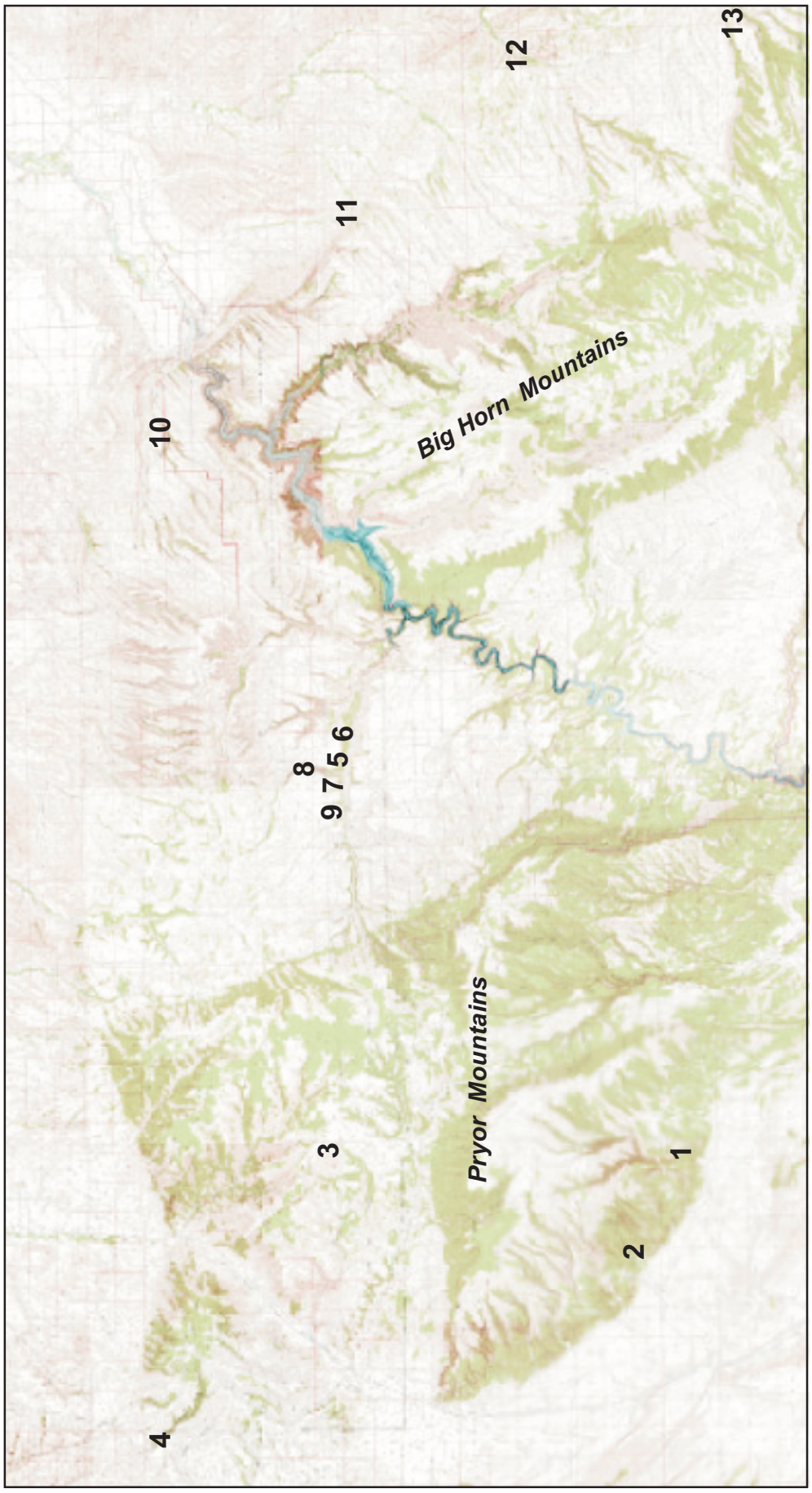

1: Bear Canyon
2: Stockman Trail
3: Crown Butte
4: Five-Mile Creek
5: DryHead #1
6: DryHead #2
7: DryHead #3
8: DryHead #4
9: Spring Creek
10: Grapevine Canyon
11: Soap Creek
12: Rotten Grass Creek
13: Lodge Grass Creek

Figure 6. Index map showing locations of Tensleep Sandstone measured sections in the Pryor and Big Horn Mountains.

precipitation of anhydrite or dolomite. These facies can be present in several stratigraphic positions within the Tensleep–Minnelusa interval and are controlled mainly by paleogeography. For example, favorable facies may be present in the upper Tensleep in one area, the lower Tensleep in another, or the upper or middle Minnelusa in other areas depending on the position within the depositional system relative to the shoreline at a particular time. The results of detailed stratigraphic field studies in the project area, discussed below, demonstrate these depositional patterns and cycles.

Tensleep Sandstone in South-Central Montana

Dramatic stratigraphic changes in the Tensleep occur across south-central Montana. To better understand these stratigraphic changes, 13 surface sections were measured and described in the Pryor and Big Horn Mountains (see Lopez and others, 2007). Locations of measured sections are shown in figure 6. The results are summarized in the following conclusions:

1. The upper Tensleep contact is unconformable, showing topographic relief of as much as 50 ft due to a combination of erosion and the presence or absence of dune sandstone intervals.

2. In the west, both upper and lower Tensleep are present. The lower is characterized by repeated cycles of marine sandstone, tens of feet thick, capped by very limey to dolomitic sandstone beds 1 to 5 ft thick. The upper Tensleep is characterized by cycles of eolian dune sandstone capped by marine limey to dolomitic sandstone. Dune sandstones can be as thick as 60 ft. The total Tensleep thickness in the western part of the area can be as much as 250 ft.

3. In the east and central parts of the area the upper Tensleep is absent and dune sandstones develop in the lower Tensleep. The vertical cycles are similar to those in the west. On the east side of the Big Horn Mountains the Tensleep thins to as little as 25 ft. These thickness patterns are shown diagrammatically in figure 7.

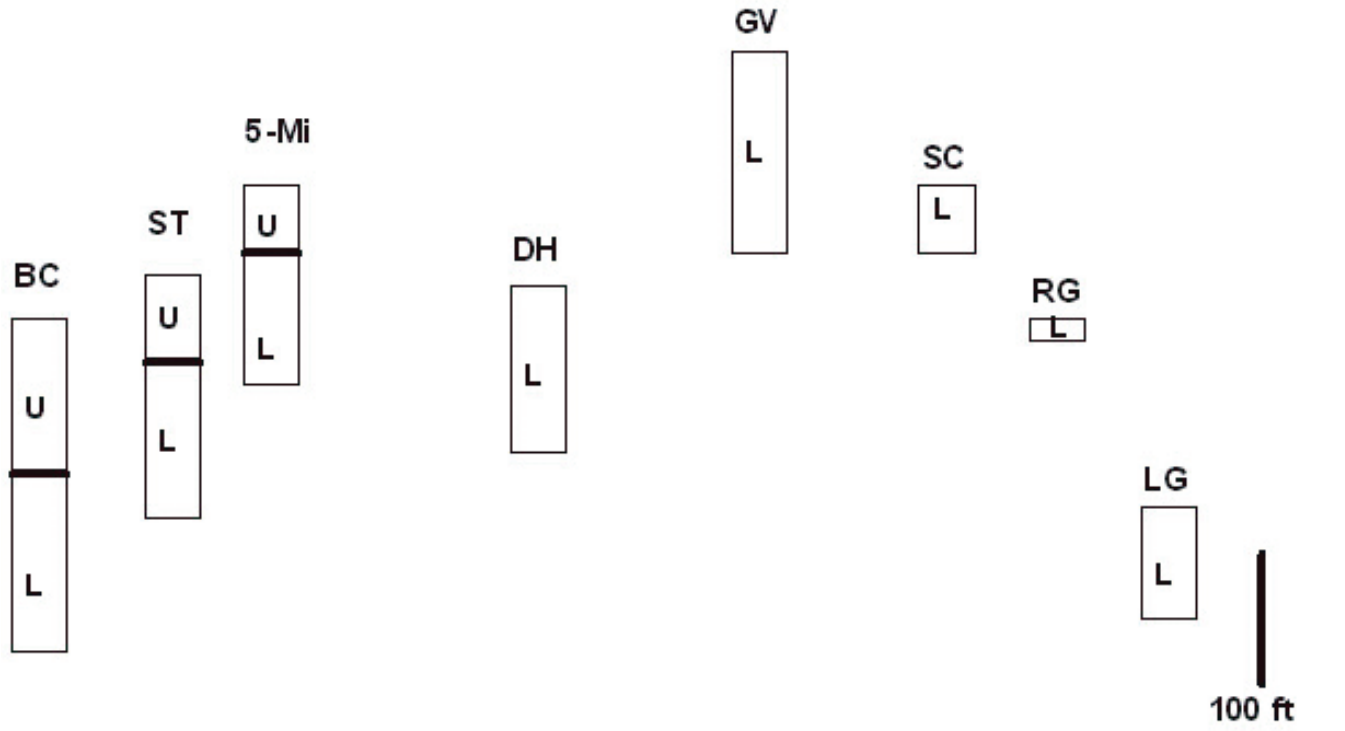

Figure 7. Thickness changes of Tensleep Sandstone across the project area shown diagrammatically. West is on the left, east on the right. BC, Bear Canyon; ST, Stockman Trail; 5-Mi, Five Mile Creek; DH, Dry Head Canyon; GV, Grapevine Canyon; SC, Soap Creek; RG, Rotten Grass Creek; LG, Lodge Grass Creek.

Figure 8. Sandy dolomite bed containing abundant chert nodules that marks the top of the lower Tensleep. Photo from Bear Canyon in western Pryor Mountains.

On the west side of the Pryor Mountains (Bear Creek, Stockman Trail, and Five-Mile Creek measured sections), both the lower and upper Tensleep are present and the total thickness reaches a maximum of about 240 ft in Bear Canyon (Lopez and others, 2007). In this area our observations confirm the work of Mankiewicz and Steidtmann (1979, p. 323), who described the lower Tensleep as being deposited in "supertidal, intertidal, and subtidal to lagoonal conditions" and described the upper Tensleep as deposits of "eolian and associated sabkha environments."

The lower Tensleep is 100 to 120 ft thick. It is a sequence of repeating cycles of limey shallow marine sandstone, sandy limestone, and sandy dolomite. The top of the lower Tensleep is marked by a widespread sandy dolomite bed 4–11 ft thick, with abundant chert nodules (fig. 8).

In the western part of the area, the upper Tensleep is generally characterized by cycles of sandy limestone or dolomite, overlain by light-colored eolian dune sandstone (fig. 9), which in turn is capped by marine limey sandstone (fig. 10). Eolian sandstones are very light gray, fine-grained, and noncalcareous, with high-angle planar and trough cross bedding with good

Figure 9. Typical character of dune facies, upper Tensleep. This dune interval is about 30 ft thick. Yellowish sandstone above is calcareous marine sandstone capping the light-colored dune sandstone.

Figure 10. Typical cycle in upper Tensleep. Toe of dune build up, above person's head, overlies light gray sandy dolomite and is capped by sandy dolomitic limestone.

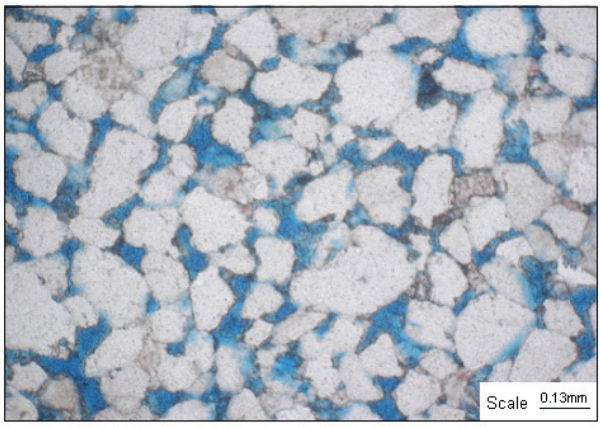

Figure 11. Tensleep, very fine to medium-grained sandstone at Bear Canyon (sample BC-1, Lopez and others, 2007) has good intergranular and secondary porosity. Original magnification was 63X with plane-polarized light. Brown areas at left center and upper left are minor dolomite cementation.

intergranular and secondary porosity (fig. 11). The dune sands are built out on shallow marine deposits of sandy limestones or dolomites in a regressive shoreline system. Rapid fluctuations of relative sea level must have occurred in order to produce the repeating cycles observed. Commonly eolian sandstone is capped by marine sandstone above a flooding surface. Burrows from the overlying marine sandstones commonly extend down into eolian sandstone for 3 to 4 ft (fig. 12). Individual dunes are limited in size, resulting in radically variable thicknesses of the upper Tensleep within small areas. For example, on the south side of Bear Creek the upper Tensleep is 72 ft thick, but on the north side, because an additional eolian cycle is preserved, 125 ft of upper Tensleep is present. This change occurs within a distance of about ¼ mile (see Bear Creek and Bear Creek 2 measured sections, Lopez and others, 2007).

In the central and eastern parts of the project area, only the lower Tensleep is present. During lower Tensleep time this area was characterized by a migrating shoreline, while in the west the area was offshore marine. For this reason eolian sandstones are present in cycles much like those in the west in the upper Tensleep (see measured sections in Lopez and others, 2007). The lower Tensleep is quite variable in thickness, ranging from about 25 ft at Rotten Grass Creek to 185 ft at Grapevine Dome (fig. 7; Lopez and others, 2007). In the subsurface in T. 3 S., R. 34 E., the lower Tensleep reaches a thickness of about 200 ft (plate 3). Eolian sandstones are very light gray,

Figure 12. Burrows extending into dune sandstone from overlying marine sandstone. Flooding surface is about 1 ft above the hammer; the flat-bedded sandstones above are very calcareous marine sandstone. Below the flooding surface, the sandstone is non-calcareous dune sandstone.

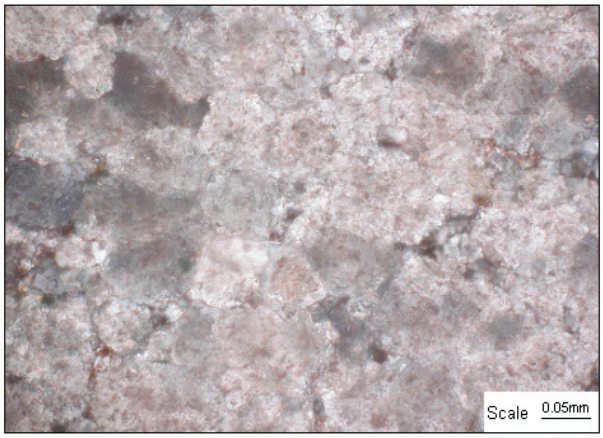

Figure 13. Lithofacies is interdune micritic sediment that was either subsequently dolomitized or contains syndepositional dolomite. There is sparse visible porosity in this sample. Dry Head measured section 4 sample 8 (Lopez and others, 2007). Original magnification was 160X with crossed nicols.

fine-grained, and non-calcareous, with high-angle planar and trough cross bedding. These sands occur in cycles underlain variably by either limey and dolomitic marine sandstones or by sandy, cherty limestone and dolomite (fig. 13). Dry Head Canyon (fig. 6) has excellent east–west exposures of the Tensleep Sandstone for a distance of about 10 miles, and a tributary to the north, Spring Creek, gives a third dimensional perspective (see four measured sections in Dry Head Canyon and Spring Creek section in Lopez and others, 2007). The repeated cycles of eolian and marine or sabkha deposits are clearly displayed in the canyon walls and illustrate the small areal extent of each dune on the order of ¼ square mile. These exposures also show building of dunes in an offsetting shingle pattern (fig. 14, foldout, next page). Individual dune sandstone intervals are as thick as 35 ft. Deposition of the cycles in the lower Tensleep is interpreted to have occurred in near-shore marine, sabkha, and eolian environments.

The highly variable thickness of the lower Tensleep is due to a combination of non-deposition, post-Permian erosion, or preservation of dunes at the top of the Tensleep. At Soap Creek, a dune is preserved at the top of the Tensleep in an area of only about 10 acres (fig. 15). A similar situation controls an oil accumulation at the top of the Tensleep in the Lodge Grass area (Mohl, 2006).

A regional cross section (plate 4) from the Bighorn Basin in the western part of the project area to the Powder River Basin in the east shows the stratigraphic and facies relationships described above and ties subsurface well data to surface observations described in Lopez and others (2007).

Figure 15. Tensleep Sandstone overlain by Chugwater Formation (red) in Upper Soap Creek. Note buildup of white eolian sandstone at the top of the Tensleep section in the right hand side of photograph that is absent on left half of photo.

Diagenesis in the Tensleep of South-Central Montana

Dolomite is the main diagenetic cement in both Tensleep outcrop and subsurface samples (fig. 16). This cement filled intergranular pores and is matrix in several samples (fig. 17). Leaching of dolomite cement or other cements like calcite (present but sparse) and anhydrite (not observed in outcrop or shallow Tensleep subsurface samples but reported in Minnelusa samples in the literature) produced large secondary pores (fig. 18). Enlargement and serration of individual detrital grains and grain edges is associated with this dissolution. Calcite is sparse in both outcrop and subsurface samples. Chert is also sparse and occurs as a replacement mineral in subsurface samples.

Tensleep eolian facies contain the best preserved intergranular and secondary porosity. Leaching of dolomite and calcite cement created large secondary pores with good interconnection (permeability). Subsurface samples also have good intergranular and secondary porosity and are local petroleum reservoirs (fig. 19).

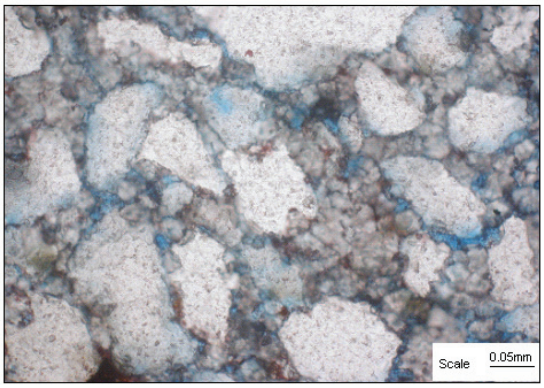

Figure 16. Dolomite is sparse to common in the Tensleep outcrop and subsurface samples. This outcrop image is from Crown Butte sample 2. Original magnification was 160X with plane-polarized light.

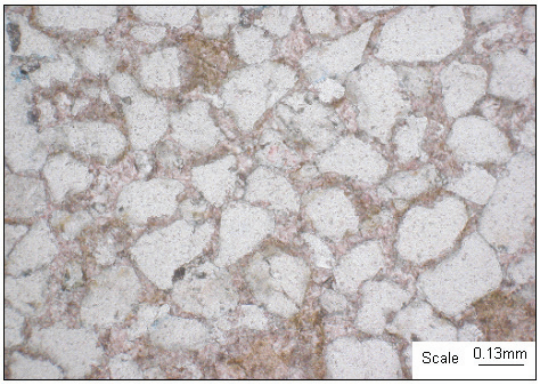

Figure 17. Dolomite forms a cement matrix in this Tensleep sample from the Five Mile Creek outcrop, sample 2. Sparse grain-to-grain contacts indicate early precipitation of the carbonate matrix. Original magnification was 63X with plane-polarized light.

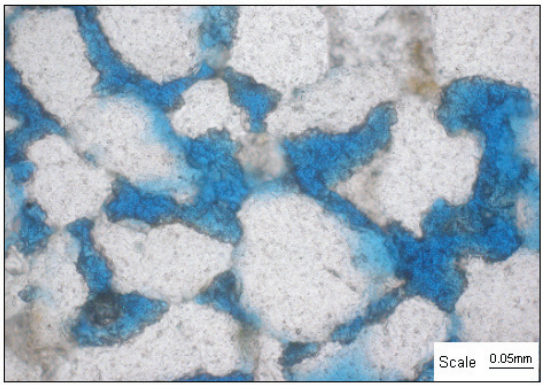

Figure 18. Large secondary pores are common in Tensleep samples. Removal of cement and/or matrix formed these large pores. Note the serrated grain edges that developed during leaching. Sample is from the Five Mile Creek outcrop, sample 2. Original magnification was 160X with plane-polarized light.

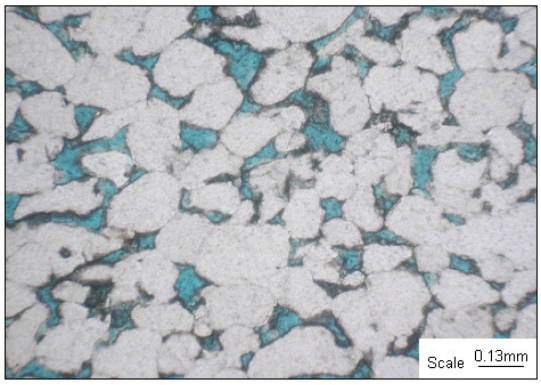

Figure 19. Residual oil lines intergranular and secondary pores in this Tensleep sample from the Barker Lawrence #1 Government test, 29-9S-33E. Original magnification was 63X with plane-polarized light.

PETROLEUM GENERATION AND MIGRATION HISTORY

Regional Petroleum System

Predicting the location of major hydrocarbon traps in the Permo-Pennsylvanian system is the main goal of this project. The stratigraphic relationships discussed above are extremely significant in determining when and where petroleum migration occurred. It is important to understand that hydrocarbon generation and migration in the Permo-Pennsylvanian petroleum system occurred before the formation of the Laramide Bighorn and Powder River Basins. Numerous workers have definitively typed the Permo-Pennsylvanian system hydrocarbon source to the organic-rich beds of the Phosphoria Formation (Brenneman and Smith, 1958; Sheldon, 1967; Momper and Williams, 1984, Claypool and others, 1984; Dennen and others, 2005). Stone (1967) provided the most comprehensive study of hydrocarbon generation, expulsion, and entrapment for the region. His ideas are summarized in the following four-part sequence:

1. End of Triassic: The Phosphoria Formation in the western Cordillera attained a burial depth sufficient for primary hydrocarbon generation; flush migration of oils into the Bighorn Basin was completed. Oil is accumulated in a regional stratigraphic trap created by the Phosphoria carbonate–red bed facies boundary. Oil expelled from the Phosphoria underwent long-range lateral migration into the Tensleep Sandstone and was entrapped in truncational unconformity traps.

2. End of Paleocene: Laramide folding caused spilling out and remigration of Tensleep stratigraphic oil traps into structural accumulations. Fractures and faults began spilling oil from regional Phosphoria stratigraphic traps into older Paleozoic formations on structural crests.

3. End of Eocene: Folding and crestal fracturing intensified, adjusting common-oil pools through fault communication, and a common-pool state with oil gravity density stratification across structural closures was created.

4. Recent: Development of present land surface and hydrodynamic environment resulting from basin erosion and fault leakage.

Evidence for early entrapment (early Jurassic or latest Triassic) of hydrocarbons has not only been documented by Stone (1967), but also was extensively investigated by Lawson and Smith (1966). Their paper focused on the evidence of partial or total stratigraphic entrapment of several structural Tensleep accumulations. A contrary view is Stone's conclusion that present-day Tensleep accumulations in the Bighorn Basin were all formed purely by structural entrapment. However, both studies recognized the presence of anomalously high oil gravities in several shallow outlying fields in the Bighorn Basin. These may be explained by early entrapment, which protected the crude from secondary migration degradation. However, based on modeling of burial history and thermal maturity, Roberts and others (2004, 2005) determined that peak oil generation from the Phosphoria in the southwestern Wyoming province began 85 million years ago (Ma) and continued until about 70 Ma. If this is true for the Bighorn Basin area, generation and migration had to have occurred before structural traps formed during the Laramide because of the anomalous relationships described by Stone (1967) and Lawson and Smith (1966). Roberts and others (2004, 2005) also indicated that in areas to the east the sedimentary section was thinner and oil generation should have been initiated later.

The accumulation at Frannie Field, along the Montana–Wyoming state line, provides the most compelling evidence for a structurally modified paleostratigraphic accumulation (fig. 20). The oil column at Frannie is irregular and does not correspond to the Laramide structural closure. Lawson and Smith (1966) attributed the irregular oil column at Frannie to a post-Tensleep channel scour on the west flank of the anticline. Their isopach map of the Phosphoria Formation depicting a dendritic channel pattern superimposed over the structure contour map of the top of the Phosphoria best explains the irregular oil column. Stone (1967) attributed the column dispersal to hydrodynamic tilting. However, the Tensleep pool does not have an active water drive and requires pressure maintenance due to a tar mat at the oil–water interface. Lawson and Smith (1966) suggest that Frannie is in part a 'frozen' early stratigraphic trap in the Tensleep that was later modified

by folding and uplift.

Further evidence that Frannie is a paleo-accumulation is also given in Stone (1967). The bubble-point pressures for Tensleep accumulations were calculated to determine a correlation with depth of overburden during emplacement. At Frannie Field, the bubble point–overburden computation agrees reasonably well with an Early Jurassic time of migration. Furthermore, the Tensleep crude does not appear to have been degraded much as a result of water washing (Stone, 1967).

On the Powder River Basin side of the project area, Soap Creek and Lodge Grass Fields produce from the Permo-Pennsylvanian system (fig. 20). In these two fields erosional remnants of eolian sandstone control the production, similar to the situation at Frannie Field. At Soap Creek, the trap is enhanced by structural closure. In the Lodge Grass area, Tensleep oil is trapped in preserved dunes in the footwall of a Laramide reverse fault (Mohl, 2006).

Overall, the evidence for early generation and truncation entrapment in the Tensleep is overwhelming. The Bighorn Basin is not consistent with traditional basin-sourced structural fill-up models. In fact, a general survey of the common-pool Paleozoic fields in the Bighorn Basin indicates that the majority of fields are filled to less than 50 percent of their trap capacity height (Stone, 1967). It is therefore necessary to have oils available to remigrate up-dip and between structures, because spill points in most of the down-dip fields have not been exceeded.

Petroleum Geochemistry of South-Central Montana

Samples of oil from Frannie Field in the Bighorn Basin, and Soap Creek and Lodge Grass Fields on the Powder River Basin side of the project area were analyzed to determine if the oils have the same genesis and to substantiate the hypothesis that the Tensleep production is all part of the same Permo-Pennsylvanian petroleum system. The analytical procedure by Geochem Laboratories, Inc. consisted of:

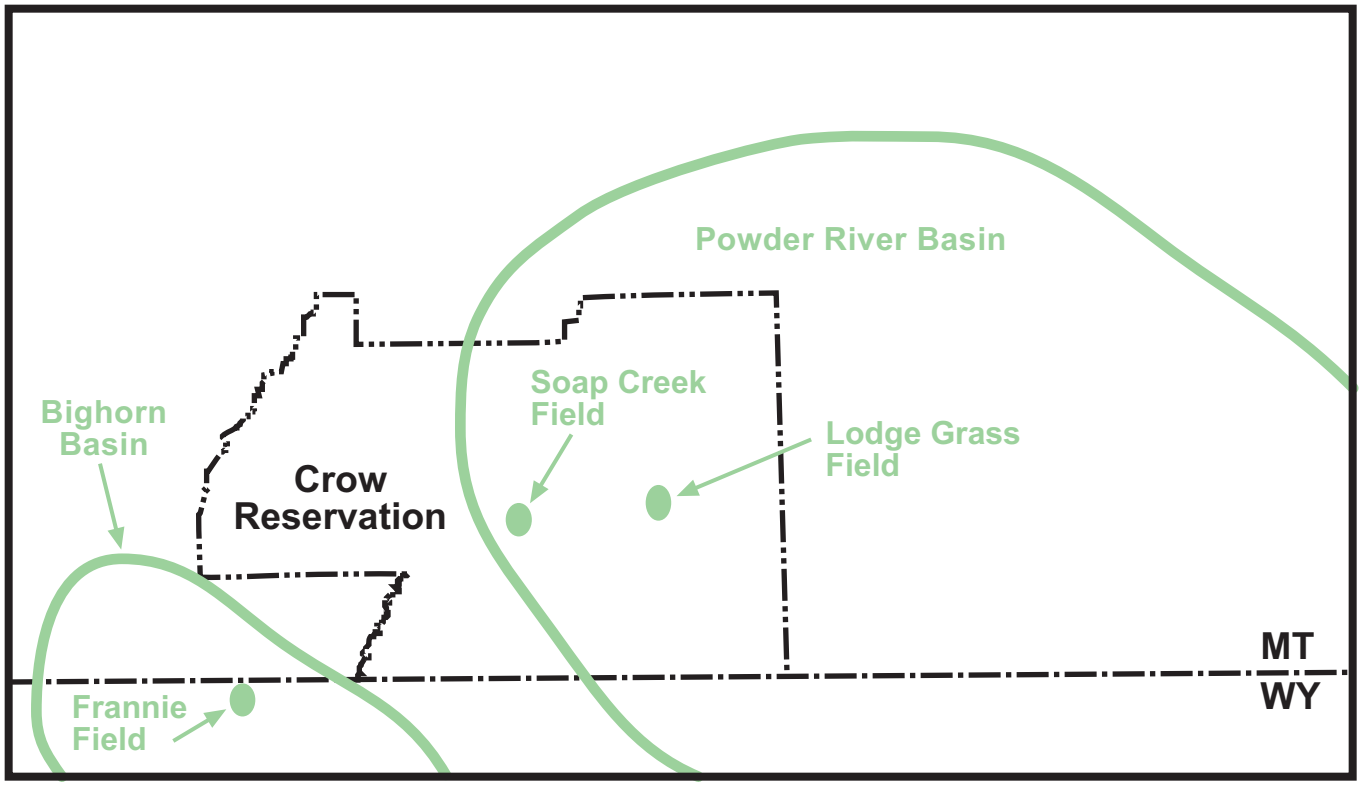

Figure 20. Project area index map showing locations of oil fields that produce from Tensleep reservoirs and were sampled for oil typing.

1. the separation of a small sample of each oil from the asphaltene and nitrogen-sulfur and oxygen (NSO) containing non-hydrocarbon components and analyzing the whole-oil paraffin-naphthene (P-N) and aromatic (AROM) hydrocarbon by gas chromatography. The 'finger print' chromatographic traces appear as figures 21–24.

2. the determination of a full-oil compositional analysis on each oil sample involving de-asphalteneing by pentane precipitation, followed by liquid chromatographic separation of the C15+ pentane soluble fraction into the C15+ P-N hydrocarbon, the AROM hydrocarbon, and the elutable NSO non-hydrocarbon fractions. The compositional data are reported in table 1.

Although all four oil samples had significant similarities, it was difficult to absolutely determine that the oils are all related because the samples were highly biodegraded to varying and significant degrees. Therefore, gas chromatographic mass spectrometric analysis of the tetra- and pentacyclic sterane and terpane biomarker components in the C15+ P-N fractions was conducted in order to compare the oils with greater confidence. The resultant chemical data clearly indicate a close agreement between all samples with respect to both thermal and maturity history, and a common organic source. All the analytical data and complete discussion of the analyses and results appear in the appendix.

The character of the oils indicates that all were from a Phosphoria source; figures 21–24 compare well with similar data for Phosphoria oil in the region (Dennen and others, 2005). There are no Phosphoria source rocks in the project area of south-central Montana; this requires that oil migrated from distant source areas, probably in central and southwestern Wyoming.

TENSLEEP PLAY DESCRIPTION AND CONTROLS, SOUTH-CENTRAL MONTANA

Exploration in the region for Tensleep oil accumulations has traditionally focused on Laramide structural features, although Lodge Grass Field has been recognized as a stratigraphic accumulation and has served as an analogue in that vicinity (see Mohl, 2006).

Regionally, oil shows and production in the

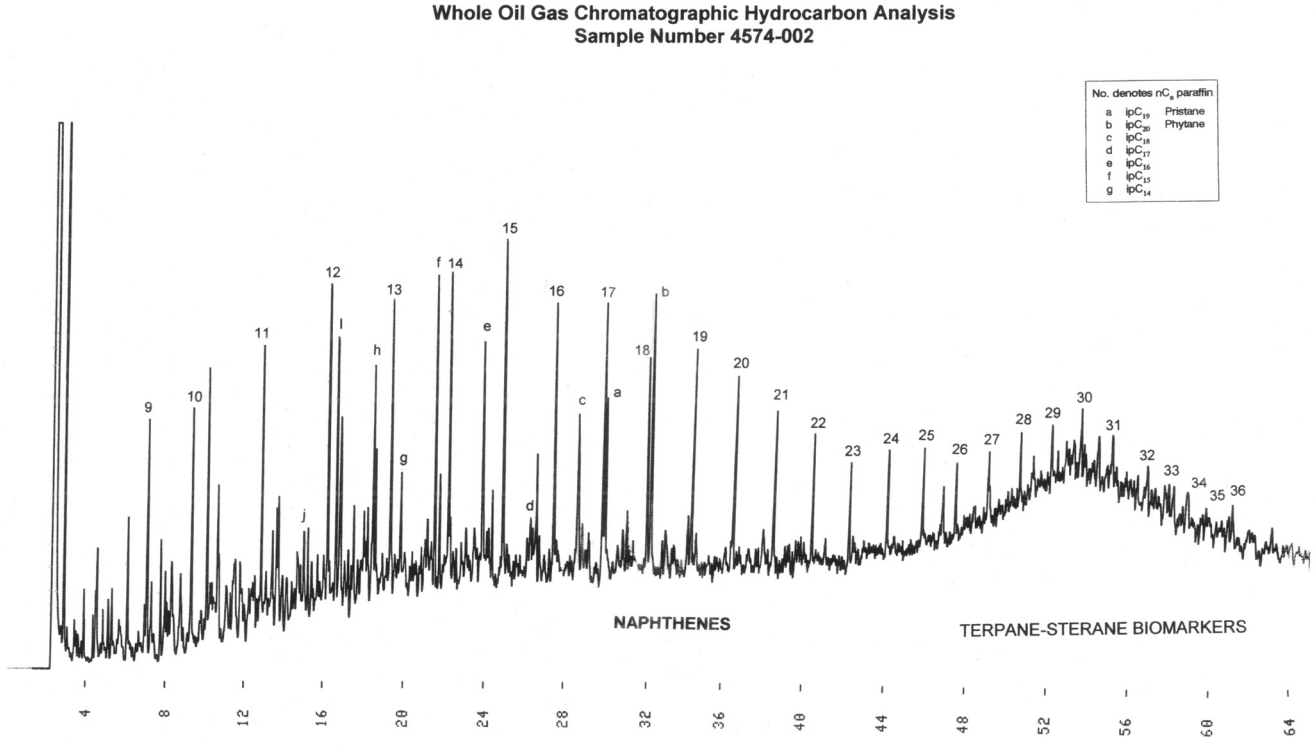

Figure 21. Chemical composition of oil from Soap Creek Oil Field.

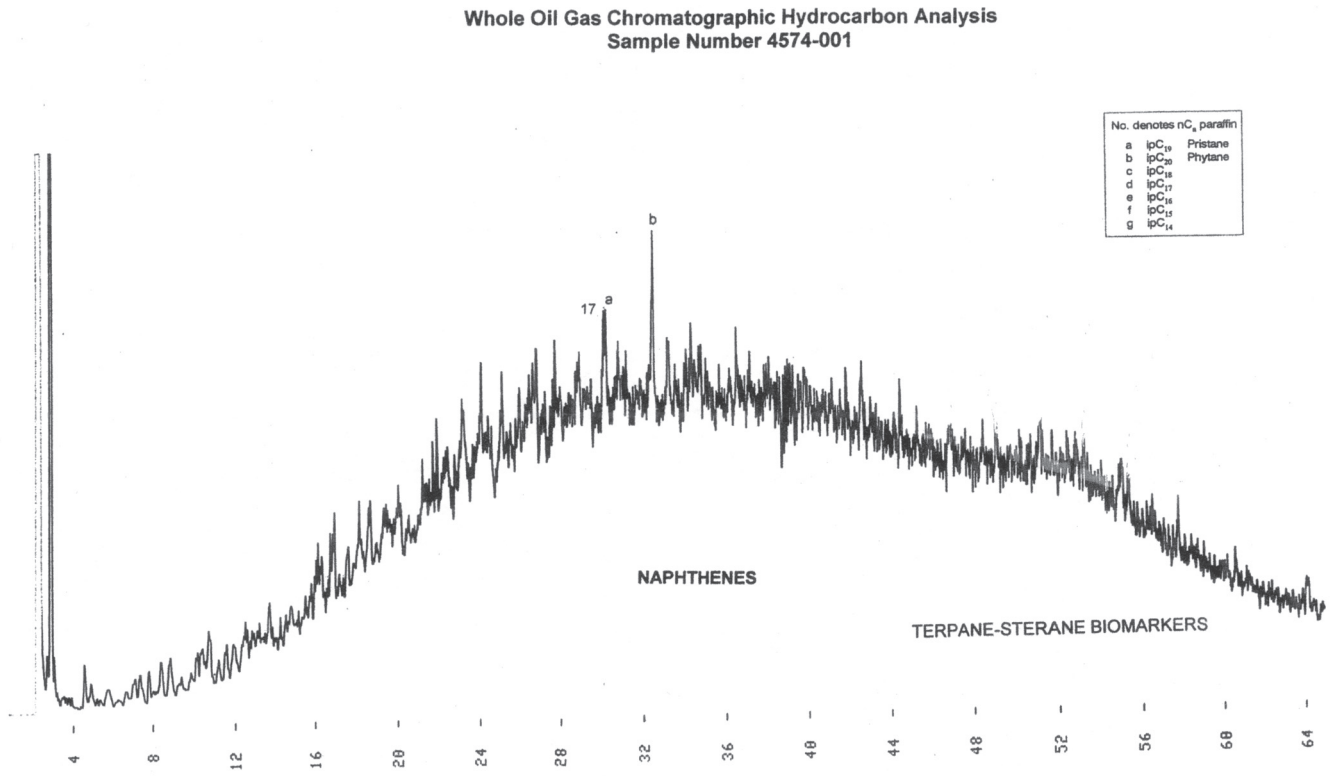

Figure 22. Chemical composition of oil from East Soap Creek Oil Field.

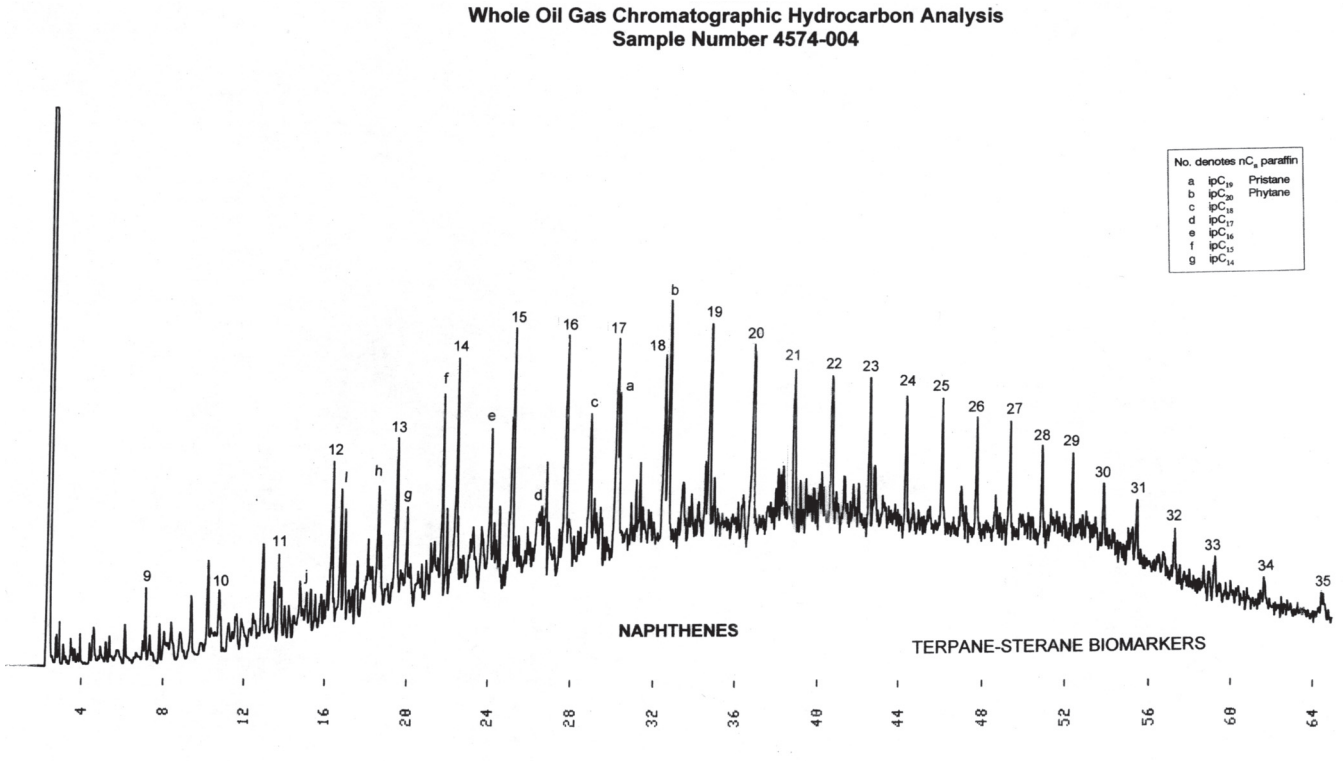

Figure 23. Chemical composition of oil from Lodge Grass Oil Field.

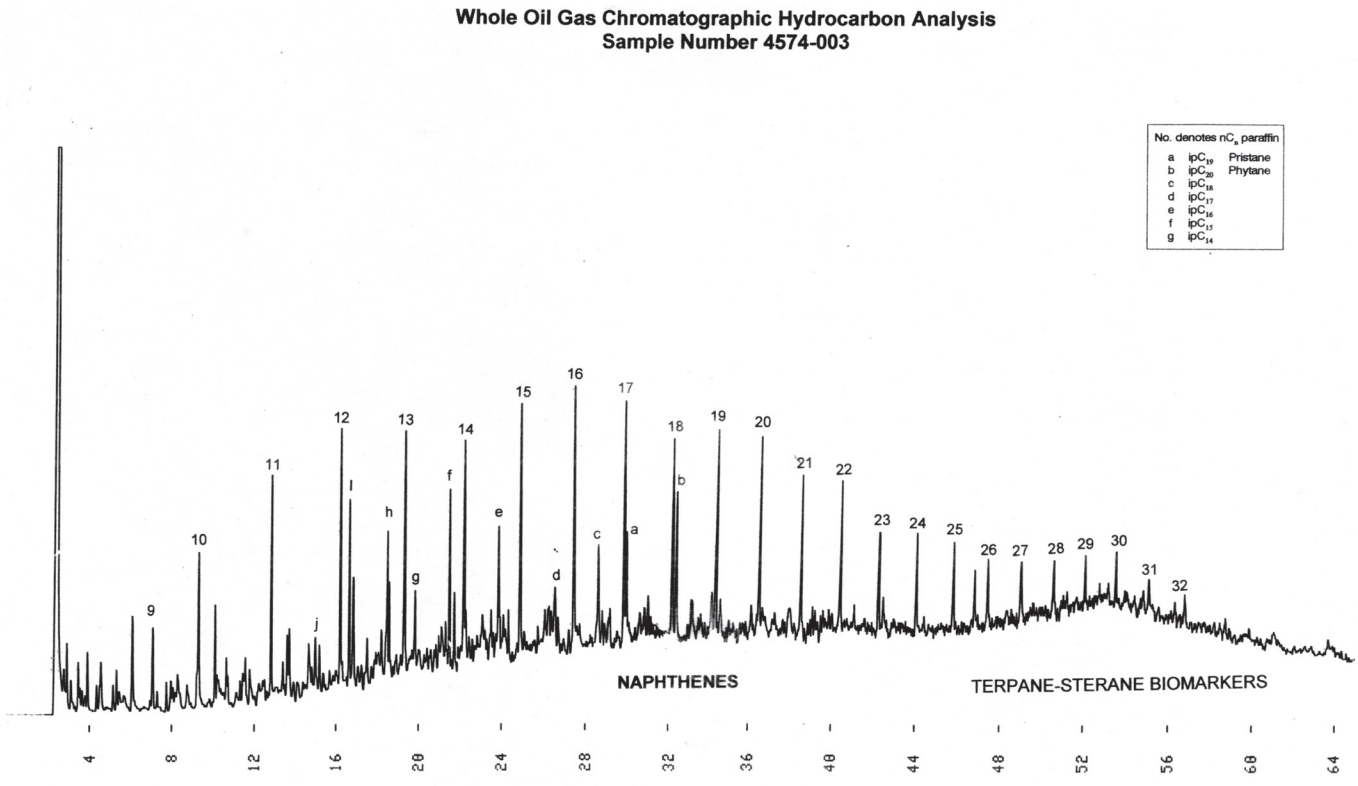

Figure 24. Chemical composition of oil from Frannie Oil Field.

Tensleep are absent in the northern part of the project area. Our regional mapping has determined that this absence is controlled by the merging of the top of the Tensleep Sandstone and the Jurassic unconformity (top of the Triassic Chugwater Formation). The zero contour line on the regional isopach map of the interval from the Jurassic unconformity to the top of the Tensleep (J-Penn isopach) defines where this merging occurs (plate 2). There are two possible explanations for the absence of Tensleep oil north of this line. If Stone's (1967) hypothesis of early oil migration in the Jurassic is correct, then the absence of oil is simply because the oil would have escaped to the atmosphere north of the zero edge where the Tensleep would have cropped out. However, Roberts and others (2005) proposed that peak generation from the Phosphoria did not occur until about 80 million years ago. In this case the absence of oil must be due to the lack of a top seal allowing migrating oil to move up-section out of the Tensleep. In either case, migration had to have occurred before Laramide deformation, because oil in the Tensleep in both the Bighorn Basin and the Powder River Basin has the same generation and migration history and has the same organic source in the Phosphoria Formation. Long-range migration of oil is also required because there are no Phosphoria source rocks present in south-central Montana, either because of non-deposition or post-Phosphoria erosion. These relationships indicate that there is potential for the discovery of oil in Tensleep stratigraphic traps or combination traps everywhere south of the J-Penn isopach zero contour, except where the Tensleep has been exposed by uplift and erosion (plate 2).

Known Tensleep fields in south-central Montana are generally small in area, which agrees with outcrop studies that show eolian dune sequences are generally quite small in lateral extent, on the order of 10 to 40 acres. However, they are very productive. Lodge Grass Field has cumulative production of nearly 400,000 barrels of oil (Montana Board of Oil and Gas Conservation); individual wells will probably make 300,000 to 500,000 barrels of oil (Keith Mohl, personal communication, 2007). There is the possibility of the discovery of larger fields, however, because large fields do exist nearby, such as Frannie Field at the southwest edge of the project area.

Table 1. Crude oil analyses: East Soap Creek Field , 4574-001; Soap Creek Field, 4574-002; Frannie Field, 4574-003; and Lodge Grass Field, 4574-004.

GeoChem Sample Number	4574-001	4574-002	4574-003	4574-004
Client Sample ID	#1	#2	#3	#4
GROSS OIL COMPOSITION				
<C15+	9.1	42.7	19.2	9.7
>C15+	90.9	57.3	80.8	90.3
DETAILED C15+ COMPOSITION				
ASPH	8.7	7.5	4.4	11.8
P-N HC	27.4	36.0	35.2	28.0
AROM HC	49.0	40.6	40.3	44.6
EL NSO	14.9	15.9	20.1	15.7
Non EL NSO	nm*	nm	nm	nm
WHOLE OIL COMPOSITION				
<C15+	9.1	42.7	19.2	9.7
Asphaltenes(ASPH) non HC	7.9	4.3	3.5	10.7
Paraffin-Naphthene(P-N) HC	24.9	20.6	28.5	25.3
Aromatic (AROM) HC	44.5	23.3	32.5	40.3
Eluted NSO non HC*	13.5	9.1	16.3	14.2
NonEluted NSO non HC	nm	nm	nm	nm
* Note No value was determined for the NonEluted NSO since this value may be an indeterminant mix of >C15+ HC and NonEluted NSO non HC				

Because of their relatively small size, exploration for Tensleep reservoirs is difficult and has usually been based on key exploration wells that have penetrated the Tensleep Sandstone with shows of oil. Isopach mapping is key to regional exploration. Producing fields like Soap Creek and Lodge Grass Fields correlate to local thin areas on the J-Penn isopach and where the underlying Tensleep is thickened by the presence of eolian sand buildup. Consequently, Tensleep gross isopach maps indicate that the Tensleep thickens in producing field areas. Seismic isochron mapping can be used to identify thinning of Triassic rocks and thick Tensleep sandstone intervals in prospective areas. Our work has shown that existing seismic data can be reprocessed to optimize isochron mapping and modeling of these thickness patterns. However, seismic data have not been used successfully to predict the presence of porous and permeable sandstone because the velocity contrast between porous and permeable sandstone and tight limey or dolomitic sandstone is too small.

In the project area, hydrodynamic considerations are important. All the existing Tensleep fields have active water drives. In many cases, the reservoir pressure today is as it was when initially discovered. In areas of high structural complexity, such as the Lodge Grass–Crow Agency fault and the Lake Basin fault zone, significant structural closure may be necessary to trap oil because of the strong hydrodynamic influence exerted by the underlying Madison Formation aquifer. Numerous wells near these features have revealed oil-saturated Tensleep sands, only to recover fresh water on drill stem tests. This is most likely evidence of paleo trap breaching due to vertical fracture/fault fluid conduits or proximal fault juxtaposition to a major aquifer causing hydrodynamic destruction of irreducible water saturations

in the oil column.

Farther away from prominent tectonic elements, stratigraphic traps in the Tensleep are more likely to be protected from flushing. However, like many of the Minnelusa fields in the Powder River Basin, these reservoirs may require secondary pressure maintenance to recover a significant portion of their reserves.

Significant formation water salinity variations, like those found between Soap Creek [resistivity of water (Rw) of 3.5 ohms] and East Soap Creek (Rw of 0.65 ohms), along with integration of potentiometric maps relative to prominent structural elements, should prove useful in quantifying trap type and potential when investigating specific areas for exploration.

SUMMARY AND CONCLUSIONS

The Permo-Pennsylvanian stratigraphic section in the Bighorn and Powder River Basins is the most prolific oil-producing system in the central Rocky Mountain Region. These reservoirs have produced in excess of 2 billion barrels of oil in the Bighorn Basin and in excess of 525 million barrels of oil in the Powder River Basin. The Tensleep–Minnelusa play is part of the much more extensive regional petroleum system sourced from the Permian Phosphoria Formation. Reservoir facies were controlled by eastward change from marine to coastal depositional environments in combination with erosional wedging in the Permian and Jurassic. Eolian sands, the main reservoir rocks, were deposited in a near-shore environment where they are interbedded with near-shore marine and sabkha calcareous and dolomitic rocks. Within the Tensleep, numerous cycles occur that are characterized by basal marine or sabkha calcareous sandstone or dolomitic sandstone overlain by porous and permeable eolian sandstone, which in turn is capped by marine sandstone. The cycles represent the interplay of near-shore marine, sabkha, and eolian environments.

On the west side of the project area, both the lower and the upper Tensleep are present, and the total thickness reaches a maximum of about 240 ft. The lower Tensleep is 100 to 120 ft thick and is a sequence of repeating cycles of limey shallow marine sandstone, sandy limestone, and sandy dolomite. The top of the lower Tensleep is marked by a widespread sandy dolomite bed 4–11 ft thick with abundant chert nodules. The upper Tensleep is generally characterized by cycles of sandy limestone or dolomite overlain by light-colored eolian dune sandstone, which in turn is capped by marine limey sandstone.

In the central and eastern parts of the project area, only the lower Tensleep is present. Here eolian sandstones are present in cycles much like those in the west in the upper Tensleep. The lower Tensleep is quite variable in thickness, ranging from about 25 ft to over 200 ft.

The oil accumulations in the Tensleep are best described as structurally modified paleostratigraphic accumulation. At Frannie Field the irregular oil column can be explained by a post-Tensleep channel scour on the west flank of the anticline. On the Powder River Basin side of the project area, Soap Creek and Lodge Grass Fields produce from the Permo-Pennsylvanian system. In these two fields, erosional remnants of eolian sandstone control the production, similar to the situation at Frannie Field. At Soap Creek, the trap is enhanced by structural closure. In the Lodge Grass area, Tensleep oil is trapped in preserved dunes in the footwall of a Laramide reverse fault (Mohl, 2006). Oil generation and migration were early; two hypotheses have been presented, either before mid-Jurassic erosion that produced a major regional unconformity or migration during late Cretaceous, about 82 Ma. Migration occurred prior to the Laramide separation of the basins, because oil in both the Bighorn Basin and the Powder River Basin is part of the same petroleum system. Geochemical analysis of oils from producing fields across the region shows that the oils are all similar and have the same source and generation history, which confirms our original hypothesis that they are all part of one petroleum system. No Phosphoria source rocks exist in the project area of south-central Montana, which would require that oil migrated from distant source areas, probably in central and southwestern Wyoming.

Oil shows and production in the Tensleep are absent in the northern part of the project area. This

appears to be controlled by the merging of the top of the Tensleep Sandstone and the Jurassic unconformity (top of the Triassic Chugwater Formation). There are two possible explanations for the absence of Tensleep oil north of this line. If oil migration occurred in the Jurassic time, then the absence of oil is simply because the oil would have escaped to the atmosphere north of the zero edge where the Tensleep would have cropped out. However, if generation from the Phosphoria did not occur until about 82 Ma, the absence of oil must be due to the lack of a top seal allowing migrating oil to move up-section out of the Tensleep. There should be potential for the discovery of oil in Tensleep stratigraphic traps or combination structural-stratigraphic traps everywhere south of the J-Penn isopach zero contour, except where the Tensleep has been exposed by uplift and erosion.

Known Tensleep fields in south-central Montana are generally small in area, which agrees with outcrop studies that show eolian dune sequences are generally quite small in lateral extent, on the order of 10 to 40 acres. Although existing fields are small in area, they are very productive; individual wells will probably make 300,000 to 500,000 barrels of oil.

Hydrodynamic considerations are also important since existing Tensleep fields in the study area have water drives. In many cases, the reservoir pressure today is as it was when initially discovered. In areas of high structural complexity, such as the Lodge Grass–Crow Agency fault and the Lake Basin fault zone, significant structural closure may be necessary to trap oil because of the strong hydrodynamic influence exerted by the underlying Madison Formation aquifer. Farther away from prominent tectonic elements, stratigraphic traps in the Tensleep are more likely to be protected from flushing. However, like many of the Minnelusa fields in the Powder River Basin, these reservoirs may require secondary pressure maintenance to recover a significant portion of their reserves.

ACKNOWLEDGMENTS

Access to the Crow Indian Reservation was a key element in the outcrop studies as critical stratigraphic changes occur there. Because of relationships developed with the Crow Tribe by the P.I. during previous DOE-funded research, access has been granted by the Tribe; we thank the Tribe for that access. We also thank the Dry Head Ranch for their hospitality and access to private lands. Technical reviews and suggestions for improvement by Ed Deal, Phyllis Hargrave, Keith Mohl, and Vince Larson are greatly appreciated. This final product would not have been possible without the excellent editing and layout by Susan Barth and graphic design and cartography by Susan Smith.

REFERENCES CITED

Alpha, A.G., and Fanshawe, J.R., 1954, Tectonics of northern Bighorn Basin area and adjacent south-central Montana: Billings Geological Society, Fifth Annual Field Conference Guidebook, p. 72–79.

Andrews, Sarah, and Higgins, L.S., 1984, Influence of depositional facies on hydrocarbon production in the Tensleep Sandstone, Big Horn Basin, Wyoming: A working hypothesis: Wyoming Geological Association, The Permian and Pennsylvanian Geology of Wyoming; 35th Annual Field Conference Guidebook, p. 183–197.

Bailey, Rascoe, Jr., and Baars, D.L., 1972, Permian System, *in* Geologic atlas of the Rocky Mountain region: Rocky Mountain Association of Geologists, p. 143–165.

Brenneman, M.C., and Smith, P.V., 1958, The chemical relationships between crude oils and their source rocks, *in* Habitat of oil: American Association of Petroleum Geologists, p. 818–849.

Chamberlin, R.T., 1945, Basement control in Rocky Mountain deformation: American Journal of Science, vol. 243A, p. 98–116.

Claypool, G.E, Love, A. H., and Maughan, E.K., 1984, Organic geochemistry, incipient metamorphism, and oil generation in black shale members of Phosphoria Formation, Western interior United States, *in* Demaison, G., and Murris, R.J., eds., Petroleum geochemistry and basin evaluations: American Association of Petroleum Geologists Memoir 35, p. 181–191.

Curry, W.H.,III, 1984, Paleotopography at the top of the Tensleep Formation, Bighorn Basin, Wyoming, *in* Goolsby, Jim, and Morton, Doug, eds., The Permian and Pennsylvanian geology of Wyoming: Wyoming Geological Association 35th Annual Field Conference Guidebook, p. 199–211.

Dennen, Kristin, Burns, William, Burruss, Robert, and Hatcher, Kendra, 2005, Geochemical analyses of oils and gases, Naval Petroleum Reserve No. 3, Teapot Dome Field, Natrona County, Wyoming: U.S. Geological Survey Open-File Report 2005-1275, 63 p.

Desmond, R.J., Steidtmann, J.R., and Cardinal, D.F., 1984, Stratigraphy and depositional environments of the Middle Member of the Minnelusa Formation, Central Powder River Basin, Wyoming, *in* Goolsby, Jim, and Morton, Doug, eds., The Permian and Pennsylvanian geology of Wyoming: Wyoming Geological Association 35th Annual Field Conference Guidebook, p. 213–239.

Foose, R.M., Wise, D.U., and Garbarini, G.S., 1961, Structural geology of the Beartooth Mountains, Montana, and Wyoming: Geological Society of America, vol. 72, p. 1143–1172.

Fryberger, S.G., 1984, The Permian Upper Minnelusa Formation, Wyoming: ancient example of an offshore-prograding eolian sea with geomorphic facies, and system-boundary traps for petroleum, *in* Goolsby, Jim, and Morton, Doug, eds., The Permian and Pennsylvanian geology of Wyoming: Wyoming Geological Association 35th Annual Field Conference Guidebook, p. 241–271.

Hancock, E.T., 1919, Geology and oil and gas prospects of the Lake Basin Field, Montana: U.S. Geological Survey Bulletin 691, p. 101–147.

Hancock, E.T., 1920, Geology and oil and gas prospects of the Huntley Field, Montana: U.S. Geological Survey Bulletin 711, p. 105–148.

Henbest, L.G., 1956, Foraminifera and correlation of the Tensleep Sandstone of Pennsylvanian age in Wyoming: Wyoming Geological Association, 11th Annual Field Conference Guidebook, p. 58–63.

Hoppin, R.A., 1974, Lineaments: Their role in tectonics of Central Rocky Mountains: American Association of Petroleum Geologists Bulletin, vol. 58, p. 2260–2273.

Inden, R.F., Horne, J.C., Coalson, Edward, and Oesleby, Tom, 1996, Tectonic and stratigraphic influences on Phosphoria, Tensleep, and Madison Reservoirs: Wyoming Geologic Association Field Trip Guide.

Johnson, E.A., 2005, Geologic assessment of undiscovered oil and gas resources in the Phosphoria total petroleum system, southwestern Wyoming Province, Wyoming, Colorado, and Utah, *in* Petroleum systems and geologic assessment of oil and gas in the southwestern Wyoming Province, Wyoming, Colorado, and Utah, ch 4: U.S. Geological Survey Digital Data Series DDS-69-D.

Lawson, D.E., and Smith J.R., 1966, Pennsylvanian and Permian influence on the Tensleep oil accumulation, Bighorn Basin, Wyoming: American Association of Petroleum Geologists Bulletin, vol.

55, p. 2197–2220.

Lopez, D.A., 1995, Field guide to the northern Pryor-Bighorn structural block, south-central Montana: Montana Bureau of Mines and Geology Open-File Report 330, 26 p.

Lopez, D.A., 1996, Structural geology of the northern Pryor-Bighorn Uplift, south-central Montana [Abs]: American Association of Petroleum Geologists Bulletin, vol. 80, p. 974–975.

Lopez, D.A., 2000a, Geologic map of the Bridger quadrangle, Montana: Montana Bureau of Mines and Geology Geologic Map 58, scale 1:100,000.

Lopez, D.A., 2000b, Geologic map of the Billings 30' x 60' quadrangle, Montana: Montana Bureau of Mines and Geology Geologic Map 59, 1 sheet, 1:100,000.

Lopez, D.A., 2000c, Greybull Sandstone petroleum potential on the Crow Indian Reservation of south-central Montana: Montana Bureau of Mines and Geology: Report of Investigation 9, 90 p., 5 plates.

Lopez, D.A., and VanDelinder, S.W., 2006, Regional stratigraphic log cross sections of the Tensleep Formation, Powder River Basin, Bighorn Basin: Montana Bureau of Mines and Geology Open-File Report 547, 3 sheets.

Lopez, D.A., VanDelinder, S.W., Hendricks, M.L., Reddish-Kuzara, S., Schwartz, C.W., and Bear Claw, D.C., 2007, Measured sections of the Pennsylvanian Tensleep Sandstone, Pryor and Big Horn Mountains, Montana: Montana Bureau of Mines and Geology Open-File Report 553, 55 p.

Luebking, G.A., 1985a, Soap Creek East Field, Big Horn County, Montana, *in* Montana oil and gas fields, 2006, Montana Geological Society (CD).

Luebking, G.A., 1985b, Marcus Snyder Field, Big Horn County, Montana, *in* Montana oil and gas fields, 2006, Montana Geological Society (CD).

MacLachlan, M.E., 1972, Triassic System, *in* Rocky Mountain Association of Geologists, Geologic atlas of the Rocky Mountain Region, p. 166–176.

Mallory, W.M., 1972, Pennsylvanian system, regional synthesis, *in* Rocky Mountain Association of Geologists, Geologic atlas of the Rocky Mountain Region, p. 111–127.

Mankiewicz, D., and Steidtmann, J.R., 1979, Depositional environments and diagenesis of the Tensleep Sandstone, eastern Bighorn Basin, Wyoming: Society for Sedimentary Geology Special Publication 26, p. 319–336.

Maughan, E.K., 1975, Organic carbon in shale beds of the Permian Phosphoria Formation of eastern Idaho and adjacent states—A summary report: Wyoming Geological Association 27th Annual Field Conference Guidebook, p. 107–115.

McConnell, D.A, 1994, Fixed-hinge, basement-involved fault-propagation folds, Wyoming: Geological Society of America Bulletin, vol. 106, p. 813–894.

Mohl, K.L., 2006, Lodge Grass Field, Big Horn County, Montana, *in* Montana oil and gas fields, 2006, Montana Geological Society (CD).

Momper, J.A., and Williams, J.A., 1984, Geochemical exploration in the Powder River Basin, *in* Demaison, G., and Murris, R.J., eds., Petroleum geochemistry and basin evaluations: American Association of Petroleum Geologists Memoir 35, p. 181–191.

Moore, D.A., 1984, The Tensleep Formation of the Southeastern Bighorn Basin, Wyoming, *in* Goolsby, Jim, and Morton, Doug, eds., The Permian and Pennsylvanian geology of Wyoming: Wyoming Geological Association 35th Annual Field Conference Guidebook, p. 273–279.

Peterson, J.A., 1977, Paleozoic shelf-margins and marginal basins, western Rocky Mountains-Great Basin, United States: Wyoming Geological Association, Montana Geological Society, and Utah Geological Society, Rocky Mountain Thrust Belt Geology and Resources Guidebook, p. 135–153.

Roberts, L.N.R., Lewan, M.D., and Finn, T.M., 2004, Timing of oil and gas generation of petroleum systems in the southwestern Wyoming province: The Mountain Geologist, vol. 41, p. 87–118.

Roberts, L.N.R., Lewan, M.D., and Finn, T.M., 2005, Burial history, thermal maturity, and oil and gas generation history of petroleum systems in the southwestern Wyoming province, Wyoming, Colorado, and Utah, *in* Petroleum systems and geologic assessment of oil and gas in the southwestern Wyoming Province, Wyoming, Colorado, and Utah, ch 4: U.S. Geological Survey Digital Data Series DDS-69-D, 25 p.

Sheldon, R.P., 1967, Long-distance migration of oil in Wyoming: The Mountain Geologist, vol. 4., p. 53–65.

Smith, J.G., 1965, Fundamental transcurrent faulting in northern Rocky Mountains: American Association of Petroleum Geologists Bulletin vol. 49, p. 1398–1409.

Stone, D.S., 1967, Theory of Paleozoic oil and gas accumulations in Bighorn Basin, Wyoming: American Association of Petroleum Geologists Bulletin, vol. 51, p. 2056–2114.

Thom, W.T., 1923, The relation of deep-seated faults to the surface structural features of central Montana: American Association of Petroleum Geologists Bulletin, vol. 7, p. 1–13.

Thomas, L., 1965, Sedimentation and structural development of Bighorn Basin: American Association of Petroleum Geologists Bulletin, vol. 49, p. 1867–1877.

Vuke, S.M., Heffern, E.L., Bergantino, R.N., and Colton, R.B., 2001, Geologic map of the Lame Deer 30' x 60' quadrangle, eastern Montana: Montana Bureau of Mines and Geology Open-File Report 428, 1 sheet, 1:100,000.

Vuke, S.M., Wilde, E.M., Lopez, D.A., and Bergantino, R.N., 2000, Geologic map of the Lodge Grass Quadrangle, Montana: Montana Bureau of Mines and Geology Geologic Map 56, scale, 1:100,000.

Wilson, C.W., 1936, Geology of the Nye-Bowler Lineament, Stillwater and Carbon Counties, Montana: American Association of Petroleum Geologists Bulletin, vol. 20, p. 1161–1188.

Winston, D., 1986, Sedimentation and tectonics of the Middle Proterozoic Belt Basin and their influence on the Phanerozoic compression and extension in western Montana and northern Idaho, *in* Peterson, J.A., Paleotectonics and sedimentation in the Rocky Mountain Region, United States: American Association of Petroleum Geologists Memoir 41, p. 87–118.

Wise, D.U., 2000, Laramide structures in basement and cover of the Beartooth Uplift near Red Lodge, Montana: American Association of Petroleum Geologists Bulletin vol. 84, no. 3, p. 360–375.

APPENDIX

Organic Geochemistry of Tensleep Oils

Dr. Geoffrey Bayliss, of Geochem Laboratories, Inc., conducted the analyses and is responsible for the discussion and conclusions presented herein. The oil samples from producing Tensleep oil fields Soap Creek East, Soap Creek, Frannie, and Lodge Grass were assigned sample numbers 4574-001, 4574-002, 4574-003, and 4574-004, respectively. Data in this discussion are referenced to these sample numbers.

The analytical program carried out entailed:

1. the separation of a small sample of each oil from the asphaltene and nitrogen sulfur and oxygen (NSO) containing non-hydrocarbon components and analyzing the whole-oil paraffin-naphthene (P-N) and aromatic (AROM) hydrocarbon by gas chromatography. The 'fingerprint' chromatographic traces appear in the report text as figures 21–24.

2. the determination of a full oil compositional analysis on each oil sample involved de-asphalteneing by pentane precipitation, followed by liquid chromatographic separation of the C15+ pentane soluble fraction into the C15+ P-N hydrocarbon, the AROM hydrocarbon, and the elutable NSO non-hydrocarbon fractions. The compositional data is reported in table 1 of the main text.

The gas chromatic analytical data have been computed from measurements made on the gas chromatograms presented in figures 21–24 and are shown as a normalized normal paraffin hydrocarbon (n-C_9 through n-C_{36}) and isoprenoid hydrocarbon (ip-C_{11} through ip-C_{20}; j through b) distribution in table 1. The gross composition and significant ratios are shown as percentages in tables A-1 and A-2 for normal paraffins, isoprenoid hydrocarbons, and unresolved naphthenic cyclic hydrocarbons. The pristane ip-C_{19} (a) *I* phytane ip-C_{20} (b) ratio and the Carbon Preference Index A and B are also shown.

Compositional analytical data and whole-oil gas chromatographic analyses indicate significant similarities between the four oils. It is apparent, however, that the four oils have all been subjected to varying degrees of biodegradation. In fact, sample 4574-001 has been so extensively degraded that it is extremely difficult to characterize it to the other three oils. Therefore, in order to compare the oils with a degree of confidence, gas chromatographic mass spectrometric (GCMS) analyses were conducted of the tetra- and penta-cyclic sterane and terpane biomarker components, present in the C15+ P-N hydrocarbon fractions previously isolated in the liquid chromatographic phase of the study, carried out on all four samples.

GCMS analysis is one of the most current techniques available to the geochemist. However, in most cases the data are complex to interpret and require an extensive understanding of organic chemistry. As a tool for source rock determination and crude oil correlation, however, significant ratios and notable differences and similarities can be derived from GCMS data; these values are closely related to and dependent upon geological processes relative to the entrapment, preservation, and thermal degradation of organic matter in sediments with increasing depth of burial.

Included in this report are the biomarker compounds identified by the various GCMS *m/z* fragment ions *m/z* 217, 218, 231, 259, 191, and 177 (figs. A-1–A-8). The individual biomarker compounds have been identified alphabetically for convenience of peak identification against the tabulated sterane and terpane hydrocarbons identified by their generic chemical names.

The two sets of peak identities also need clarification. The A, B, C, and D set (figs. A-1–A-4) was that originally used previously by GeoChem Labs for biomarker geochemistry (note the reassignment in B and D) and is included herein, should one wish to compare these data with previously generated, older data. The A* set (fig. A-5) is the current amended identification listing that has been used in this report.

The basic GCMS data for the four samples are recorded in tables A-3 and A-4, titled Biomarker Abundances-Steranes (peak areas) and Biomarker Abundances-Terpanes (peak areas), respectively.

A summation of the Biomarker Molecular Ratios

is shown in table A-5 for the four samples identified by *m/z*, peak ratio formulae, biomarker identity ,and the ratio values for each sample. The code in column 4 indicates what that specific ratio relates to, i.e., Maturity or Source Material.

In this case, the comparison of the sample data, 4575-001,-002, -003, and -004, clearly indicates a close agreement between all samples from both a thermal maturity history and a common organic source origin. One can make these observations without having to know the relative significance of the actual values determined. To assist further in interpreting these data, a summary of the basic data is included in table A-6 along with re-computed significant ratios and percentages. These values are recorded in table A-6 with an explanation for each of the ratios for each sample presented in the GCMS Data Quantitative Review sheets that follow table A-6. Once again, the data consistently indicate that these four oils are derived from the same source-rock facies. Note the detailed distributional compositions of the steranes, the terpanes, the percentage composition for the steranes and terpanes and the ratios for almost all of the source- and maturity-related values. The high terpane percentage versus the low sterane content is consistent with these oils having been sourced from a dominantly terrestrial organic matter source. As a consequence, these oils originally would have had a dominant paraffin oil character. Similarly, the oils are thermally mature, as is shown by Ratio 5, 7, 8, 9, 15, and 16, and also by the close-to-unity CPI A and CPI B values shown in table A-4. Note also, in the chromatographic traces presented in figures 21–24, the distinctive isoprenoid hydrocarbon distributions in samples 4574-002,-003, and -004 (a,b,c,d,e,f,g,h,i, and j; table A-3). This parameter is again indicative of a common organic matter source facies. The oil sample, 4574¬-001, also belongs to this oil system but has been severely biodegraded with the bulk of the originally in-place normal paraffins and lower molecular isoprenoid hydrocarbons removed. However, pristane (ip-C_{19}) and phytane (ip-C_{20}) still remain in this oil, as well as probably small quantities of the normals and other isoprenoids which have not been identified.

Based on the gas chromatographic traces, the order of biodegradation in these oils, from extensive biodegradation to lesser degrees of biodegradation, is 4574-001, 4574-004, 4574-003, and 4574-002; this order would be suggested from the Ratio 12 values shown for the GCMS data. Finally, the absence of 18(H)-oleanane in any of these oils would suggest that these four oils are from a Lower Cretaceous or older source rock, which would be consistent with a Phosphoria source.

Included at the end of this appendix, following the GCMS data quantitative review sheets, are GCMS fragmentation traces for all the oil samples.

Table A-1

WHOLE OIL GC PARAFFIN-NAPHTHENE (P-N) ANALYSIS

Sample #	4574-001	4574-002	4574-003	4574-004
C9		3.8	1.7	1.5
C10		3.9	3.4	1.9
C11		4.5	4.8	1.9
j		1.1	1.1	0.8
C12		5.1	5.5	3.2
i		4.3	4.0	3.4
h		3.9	3.1	2.4
C13		4.7	5.1	3.4
g		1.7	1.5	1.7
f		5.0	3.6	3.9
C14		4.9	4.6	4.7
e		3.5	2.8	2.9
C15		5.4	5.4	5.3
d		0.7	1.0	0.8
C16		4.5	5.8	4.7
c		2.6	2.1	2.8
C17		4.5	5.4	4.7
a		2.8	1.9	3.0
C18		3.5	4.3	3.9
b		4.5	3.3	4.5
C19		3.5	4.4	4.2
C20		3.1	4.2	3.9
C21		2.6	3.5	3.2
C22		2.1	3.2	3.2
C23		1.7	2.3	3.4
C24		1.8	2.2	3.0
C25		1.6	1.9	2.8
C26		1.2	1.5	2.6
C27		1.3	1.3	2.6
C28		1.2	1.3	2.1
C29		1.0	1.2	1.9
C30		1.1	1.2	1.3
C31		0.7	0.8	1.3
C32		0.6	0.7	1.1
C33		0.4	0.0	0.9
C34		0.6	0.0	0.6
C35		0.3	0.0	0.4
C36		0.6	0.0	0.0

Table A-2

WHOLE OIL GC PARAFFIN-NAPHTHENE (P-N) ANALYSIS

Sample #	4574-001	4574-002	4574-003	4574-004
Normal Paraffins %	0.9est.	49.09	59.25	43.24
Isoprenoid HC's %	0.4est.	4.49	6.11	4.73
Naphthenes %	98.7est	46.42	34.64	52.03
CPI A		0.96	0.95	1.09
CPI B		0.91	0.86	1.14
ipC19/ipC20	0.52	0.63	0.58	0.66

Biomarker Compound Identification

Figure A-1

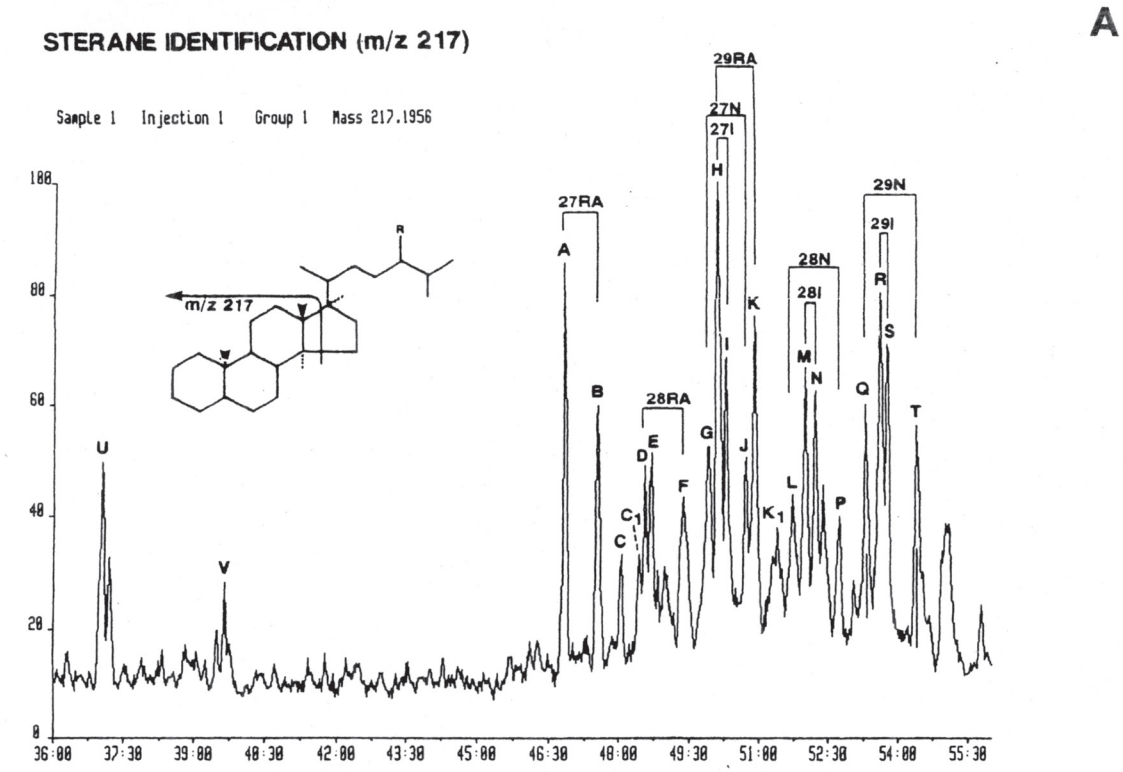

N(normal) = $\alpha\alpha\alpha$ STERANES I (iso) = $\alpha\beta\beta$ STERANES RA (rearranged) = $\beta\alpha$ STERANES

	Compound	Code
A	13β(H), 17α(H) - diacholestane 20S	$C_{27}H_{48}$ 27RA
B	13β(H), 17α(H) - diacholestane 20R	$C_{27}H_{48}$ 27RA
C	13α(H), 17β(H) - diacholestane 20S	$C_{27}H_{48}$
C^1	13α(H), 17β(H) - diacholestane 20R	$C_{27}H_{48}$
D	13β(H), 17α(H) - 24 - methyl-diacholestane 20S (24S)	$C_{28}H_{50}$ 28RA
E	13β(H), 17α(H) - 24 - methyl-diacholestane 20S (24R)	$C_{28}H_{50}$ 28RA
F	13β(H), 17α(H) - 24 - methyl-diacholestane 20R (24R+S)	$C_{28}H_{50}$ 28RA
G	5α(H), 14α(H), 17α(H) - cholestane 20S	$C_{27}H_{48}$ 27N
	13α(H), 17β(H) - 24 - methyl-diacholestane 20S (24S+R)	$C_{28}H_{50}$
H	5α(H), 14β(H), 17β(H) - isocholestane 20R	$C_{27}H_{48}$ 27I
	13β(H), 17α(H), - 24 - ethyl-diacholestane 20S (24R+S)	$C_{29}H_{52}$ 29RA
I	5α(H), 14β(H), 17β(H) - isocholestane 20S	$C_{27}H_{48}$ 27I
	13α(H), 17β(H), - 24 - methyl-diacholestane 20R	$C_{28}H_{50}$
J	5α(H), 14α(H), 17α(H) - cholestane 20R	$C_{27}H_{48}$ 27N
K	13β(H), 17α(H), - 24 - ethyl-diacholestane 20R (24S+R)	$C_{29}H_{52}$ 29RA
K^1	13α(H), 17β(H), - 24 - ethyl-diacholestane 20S (24S+R)	$C_{29}H_{52}$
L	5α(H), 14α(H), 17α(H) - 24 - methyl-cholestane 20S (24S+R)	$C_{28}H_{50}$ 28N
L^1	13α(H), 17β(H) - 24 - ethyl-diacholestane 20R (24S+R)	$C_{29}H_{52}$
M	5α(H), 14β(H), 17β(H) - 24 - methyl-isocholestane 20R (24S+R)	$C_{28}H_{50}$ 28I
N	5α(H), 14β(H), 17β(H) - 24 - methyl-isocholestane 20S (24S+R)	$C_{28}H_{50}$ 28I
P	5α(H), 14α(H), 17α(H) - 24 - methyl-cholestane 20R (24S+R)	$C_{28}H_{50}$ 28N
Q	5α(H), 14α(H), 17α(H) - 24 - ethyl-cholestane 20S (24S+R)	$C_{29}H_{52}$ 29N
R	5α(H), 14β(H), 17β(H) - 24 - ethyl-isocholestane 20R (24S+R)	$C_{29}H_{52}$ 29I
S	5α(H), 14β(H), 17β(H) - 24 - ethyl-isocholestane 20S (24S+R)	$C_{29}H_{52}$ 29I
T	5α(H), 14α(H), 17α(H) - 24 - ethyl-cholestane 20R (24S+R)	$C_{29}H_{52}$ 29N
U	5α(H) - pregnane	$C_{21}H_{36}$
V	5α(H) - bisnorcholane	$C_{22}H_{38}$

Figure A-2

B

STERANE IDENTIFICATION (m/z 218)

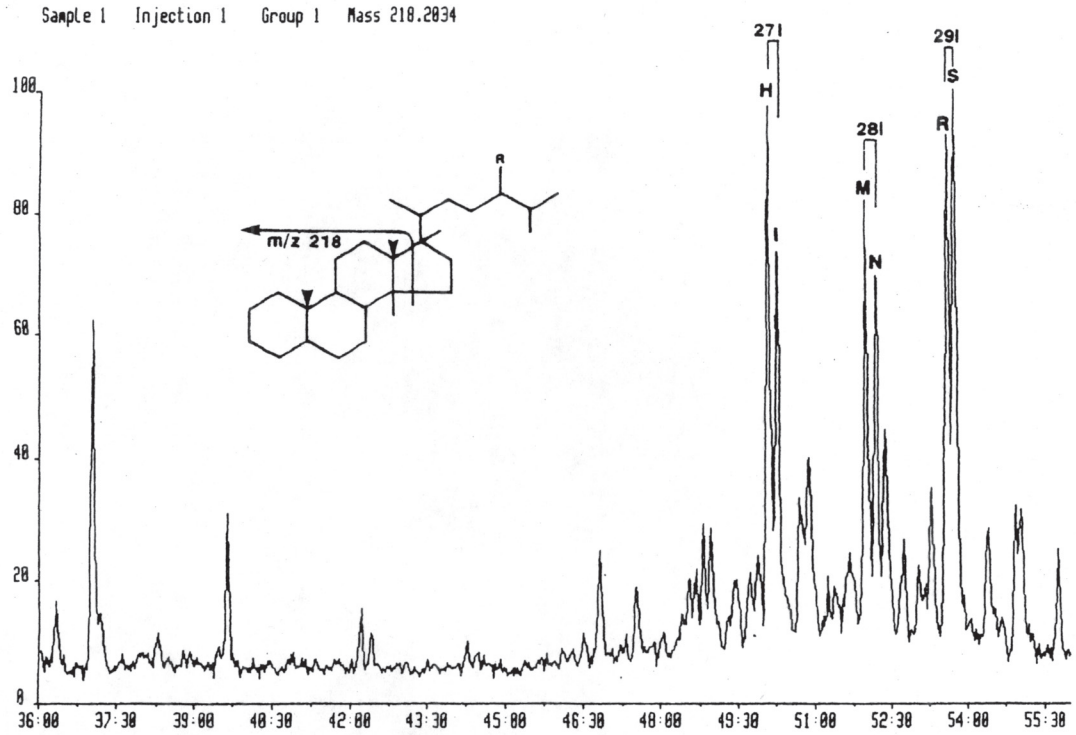

I (iso) = $\alpha\beta\beta$ STERANES

Old Ident		Compound		Code
A	H	5α(H), 14β(H), 17β(H) - cholestane 20R	$C_{27}H_{48}$	27I
B	I	5α(H), 14β(H), 17β(H) - cholestane 20S	$C_{27}H_{48}$	27I
C	M	5α(H), 14β(H), 17β(H) - 24-methyl-cholestane 20R	$C_{28}H_{50}$	28I
D	N	5α(H), 14β(H), 17β(H) - 24-methyl-cholestane 20S	$C_{28}H_{50}$	28I
E	R	5α(H), 14β(H), 17β(H) - 24-ethyl-cholestane 20R	$C_{29}H_{52}$	29I
F	S	5α(H), 14β(H), 17β(H) - 24-ethyl-cholestane 20S	$C_{29}H_{52}$	29I

Figure A-3

C

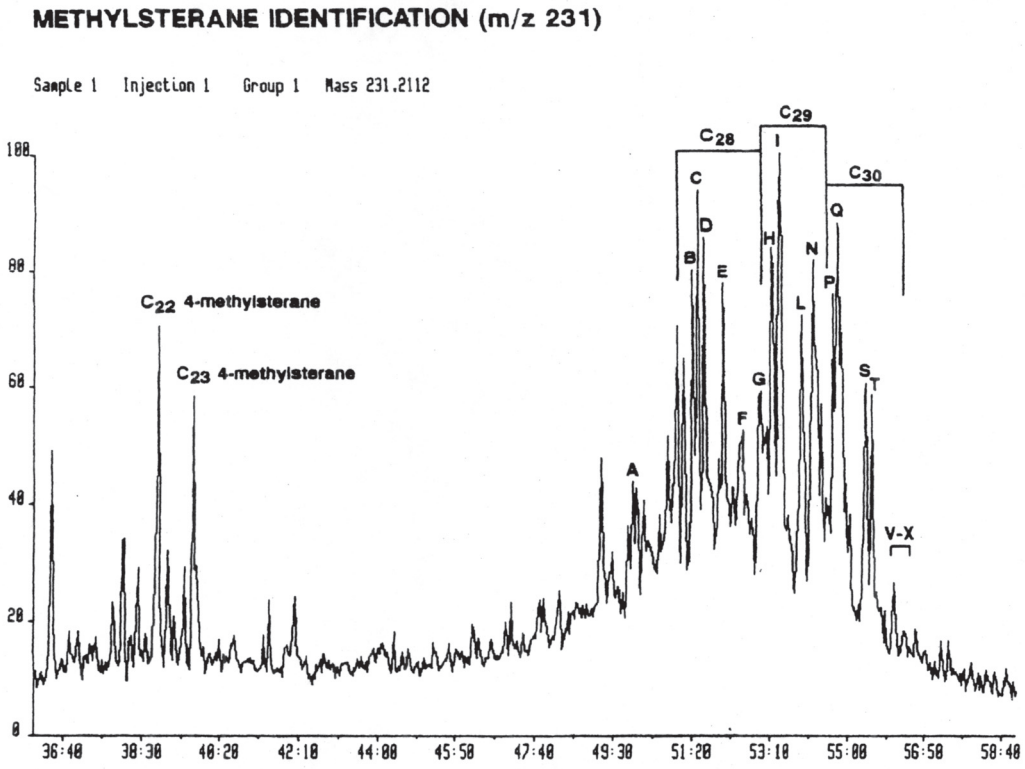

Compound*

A	5β, 14α, 17α(H)-cholestane 20R	C_{27}
B	5β, 14α, 17α(H)-4α-methylcholestane 20S	C_{28}
C	5α, 14α, 17α(H)-3β-methylcholestane 20R	C_{28}
E	5β, 14α, 17α(H)-24-methylcholestane 20R	C_{28}
F	5α, 14α, 17α(H)-4α-methylcholestane 20R	C_{28}
G	5α, 14α, 17α(H)-4β-methylcholestane 20R	C_{28}
H	5β, 14α, 17α(H)-4α,24-dimethylcholestane 20R	C_{29}
I	5α, 14α, 17α(H)-24-ethylcholestane 20S	C_{29}
J	5α, 14α, 17α(H)-3β,24-dimethylcholestane 20R	C_{29}
K	5β, 14α, 17α(H)-24-ethylcholestane 20R	C_{29}
L	5α, 14α, 17α(H)-4α,24-dimethylcholestane 20R	C_{29}
M	5β, 14α, 17α(H)-4α,24-dimethylcholestane 20R	C_{29}
N	5α, 14α, 17α(H)-4β,24-dimethylcholestane 20R	C_{29}
P	5α, 14α, 17α(H)-3β-methyl-24-ethylcholestane 20R	C_{30}
Q	5α, 14α, 17α(H)-4α,23,24-trimethylcholestane 20R	C_{30}
R	5β, 14α, 17α(H)-4α,23,24-trimethylcholestane 20R	C_{30}
S	5α, 14α, 17α(H)-4α-methyl-24-ethylcholestane 20R	C_{30}
	5α, 14α, 17α(H)-4α,23,24-trimethylcholestane 20R	C_{30}
T	5α, 14α, 17α(H)-4α,23,24-trimethylcholestane 20R	C_{30}
U	5α, 14α, 17α(H)-4β,23,24-trimethylcholestane 20R	C_{30}
V	5α, 14α, 17α(H)-4β,23,24-trimethylcholestane 20R	C_{30}
W	5α, 14α, 17α(H)-4β,23,24-trimethylcholestane 20R	C_{30}
X	5α, 14α, 17α(H)-4β,23,24-trimethylcholestane 20R	C_{30}
Y	5α, 14α, 17α(H)-3β,24-diethylcholestane 20R	C_{31}

* tentative assignments after Hollander et al, 1993.

Figure A-4

D

REARRANGED STERANE IDENTIFICATION (m/z 259)

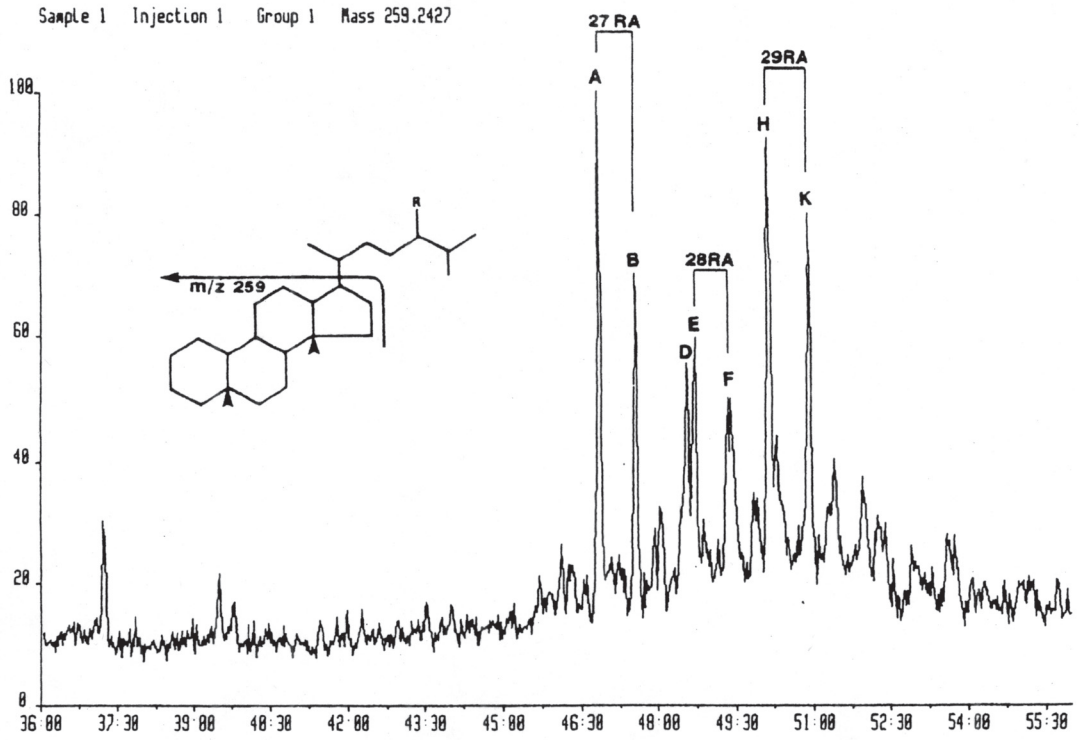

RA (rearranged) = $\beta\alpha$ STERANES

Old Ident		Compound		Code
A	A	13β(H), 17α(H) - diacholestane 20S	$C_{27}H_{48}$	27RA
B	B	13β(H), 17α(H) - diacholestane 20R	$C_{27}H_{48}$	27RA
C	E	13β(H), 17α(H) - 24-methyl-diacholestane 20S	$C_{28}H_{50}$	28RA
D	F	13β(H), 17α(H) - 24-methyl-diacholestane 20R	$C_{28}H_{50}$	28RA
F	H	13β(H), 17α(H) - 24-ethyl-diacholestane 20S	$C_{29}H_{52}$	29RA
G	K	13β(H), 17α(H) - 24-ethyl-diacholestane 20R	$C_{29}H_{52}$	29RA

Figure A-5

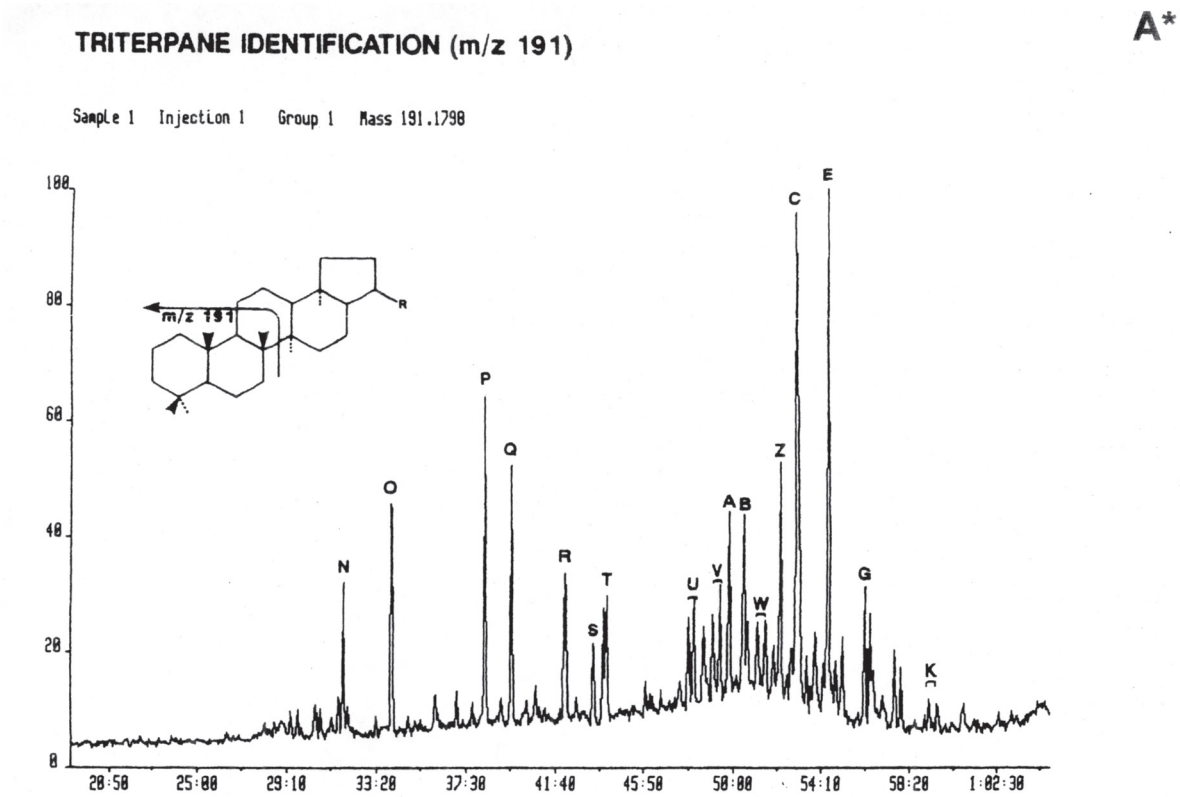

	Compound	
A	18α (H), 21β (H) -22, 29, 30- trisnorneohopane (Ts)	C_{27}
B	17α (H), 21β (H) -22, 29, 30- trisnorhopane (Tm)	C_{27}
Z	17α (H), 18α (H), 21β (H) -28, 30- bisnorhopane	C_{28}
C	17α (H), 21β (H) - 30- norhopane	C_{29}
C_1	18α (H) - 30- norneohopane	C_{29}
X	15α - methyl- 17α (H) -27 - norhopane	C_{30}
D	17β (H), 21α (H) -30 - normoretane	C_{29}
E	17α (H), 21β (H) - hopane	C_{30}
F	17β (H), 21α (H) - 30 - moretane	C_{30}
G	17α (H), 21β (H) - homohopane (22S)	C_{31}
H	17α (H), 21β (H) - homohopane (22R)	C_{31}
G_1	Gammacerane	C_{30}
I	17β (H), 21α (H) - homomoretane	C_{31}
J	17α (H), 21β (H) - bishomohopane (22S and 22R)	C_{32}
K	17α (H), 21β (H) - trishomohopane (22S and 22R)	C_{33}
L	17α (H), 21β (H) - tetrakishomohopane (22S and 22R)	C_{34}
M	17α (H), 21β (H) - pentakishomohopane (22S and 22R)	C_{35}

N	C_{20} Tricyclic Terpane
O	C_{21} Tricyclic Terpane
P	C_{23} Tricyclic Terpane
Q	C_{24} Tricyclic Terpane
R	C_{25} Tricyclic Terpane
S	C_{24} Tetracyclic Terpane
T	C_{26} Tricyclic Terpane
U	C_{28} Tricyclic Terpane
V	C_{29} Tricyclic Terpane
W	C_{30} Tricyclic Terpane

Figure A-6

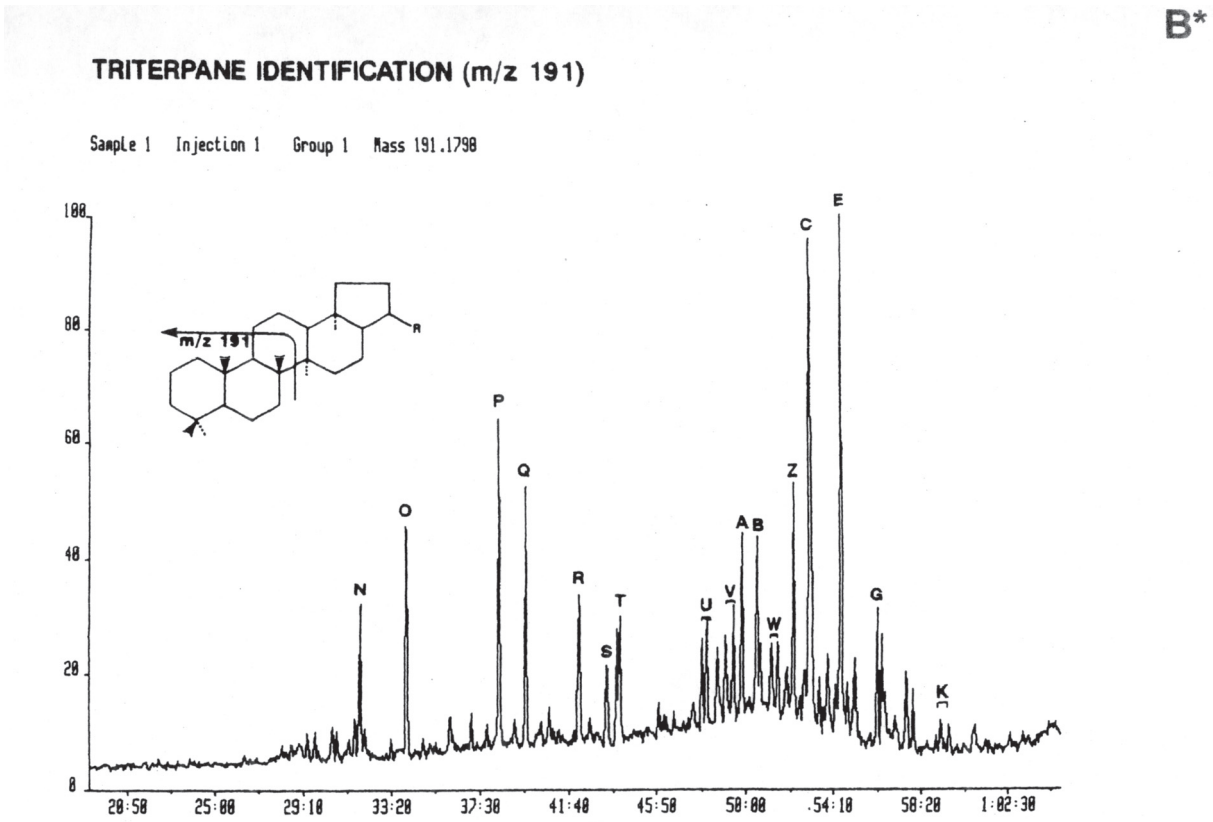

	Compound	
A	18α (H), 21β (H) -22, 29, 30- trisnorneohopane (Ts)	C_{27}
B	17α (H), 21β (H) -22, 29, 30- trisnorhopane (Tm)	C_{27}
Z	17α (H), 18α (H), 21β (H) -28, 30- bisnorhopane	C_{28}
C	17α (H), 21β (H) - 30- norhopane	C_{29}
C_1	18α (H) - 30- norneohopane	C_{29}
X	15α - methyl- 17α (H) -27 - norhopane	C_{30}
D	17β (H), 21α (H) -30 - normoretane	C_{29}
E	17α (H), 21β (H) - hopane	C_{30}
F	17β (H), 21α (H) - 30 - moretane	C_{30}
G	17α (H), 21β (H) - homohopane (22S)	C_{31}
H	17α (H), 21β (H) - homohopane (22R)	C_{31}
G_1	Gammacerane	C_{30}
I	17β (H), 21α (H) - homomoretane	C_{31}
J	17α (H), 21β (H) - bishomohopane (22S and 22R)	C_{32}
K	17α (H), 21β (H) - trishomohopane (22S and 22R)	C_{33}
L	17α (H), 21β (H) - tetrakishomohopane (22S and 22R)	C_{34}
M	17α (H), 21β (H) - pentakishomohopane (22S and 22R)	C_{35}

N	C_{20} Tricyclic Terpane
O	C_{21} Tricyclic Terpane
P	C_{23} Tricyclic Terpane
Q	C_{24} Tricyclic Terpane
R	C_{25} Tricyclic Terpane
S	C_{24} Tetracyclic Terpane
T	C_{26} Tricyclic Terpane
U	C_{28} Tricyclic Terpane
V	C_{29} Tricyclic Terpane
W	C_{30} Tricyclic Terpane

Figure A-7

C*

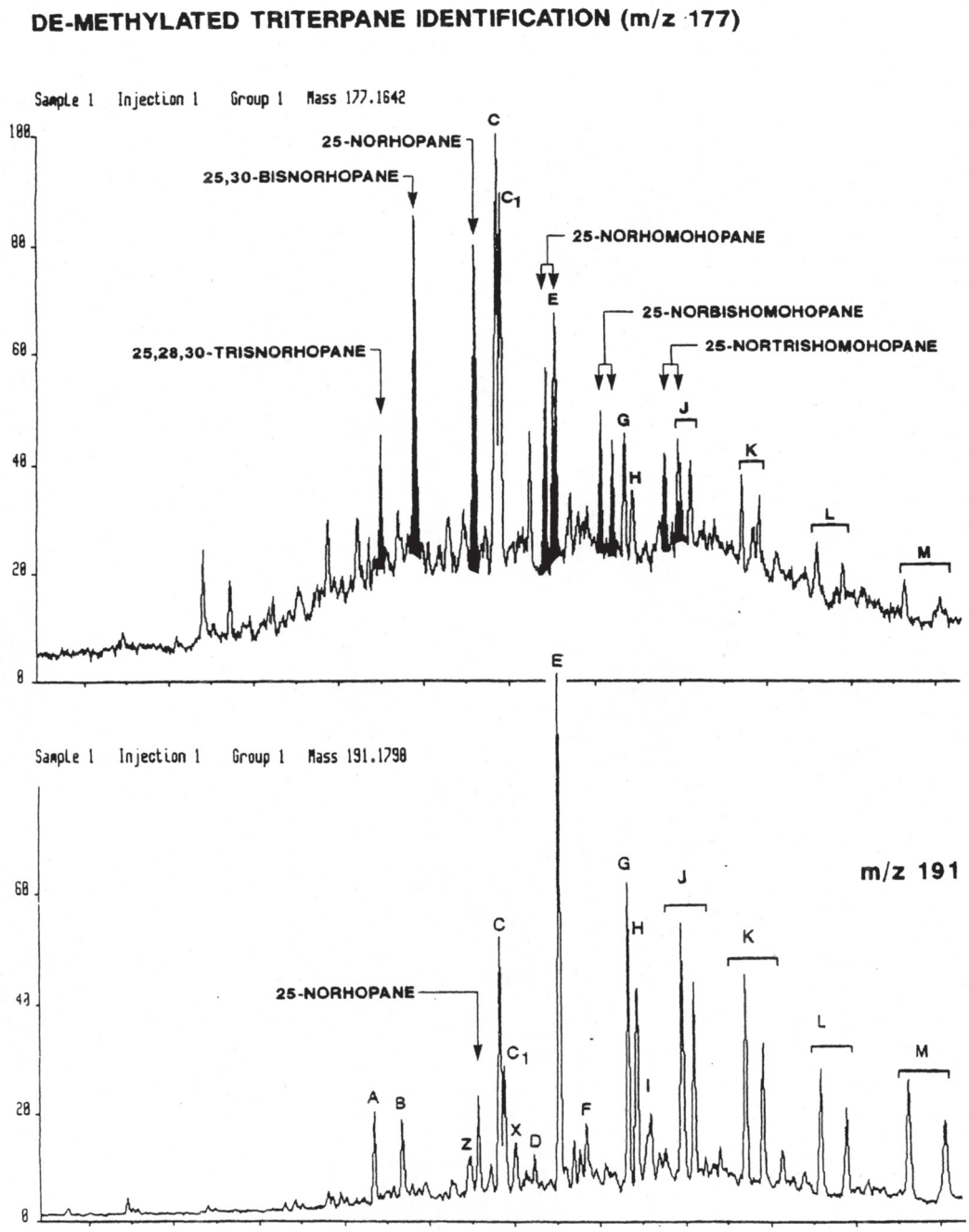

PEAKS 'A' THROUGH 'Z' IDENTIFIED ON M/Z 191 STANDARD MASS FRAGMENTOGRAM

ALL OF 25-NORHOPANES POSSESS 17α(H), 21β(H) CONFIGURATION

Figure A-8

D*

TRITERPANE IDENTIFICATION (m/z 191)

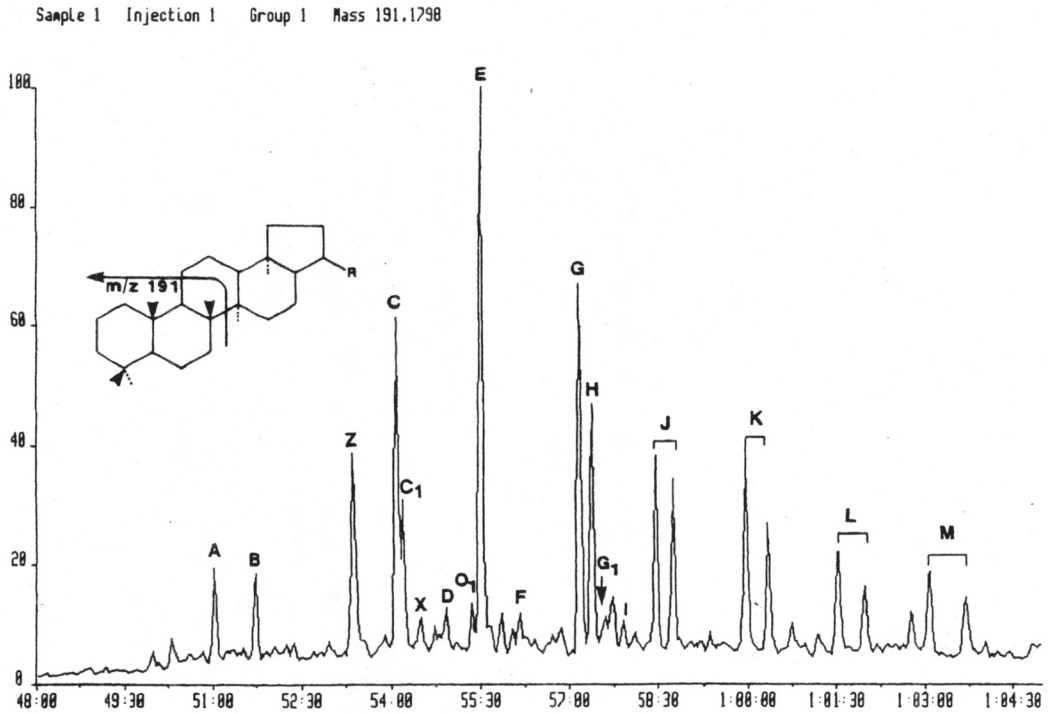

	Compound	Code	
A	18α (H), 21β (H) -22, 29, 30 - trisnorneohopane (Ts)	C_{27}	
B	17α (H), 21α (H) -22, 29, 30 - trisnorhopane (Tm)	C_{27}	
W	17α (H), 25, 30 - bisnorhopane	C_{28}	
Z	17α (H), 18α (H), 21β(H) -28, 30 - bisnorhopane	C_{28}	
Y	17α (H) - 25 - norhopane	C_{29}	
C	17α (H), 21β (H) - 30 - norhopane	C_{29}	
C^1	18α (H) - 30 - norneohopane	C_{29}	"C_{29} Ts"
X	15α - methyl - 17α (H) - 27 - norhopane	C_{30}	"diahopane"
D	17β (H), 21α (H) - 30 - normoretane	C_{29}	
O^1	18α (H) - oleanane	C_{30}	
E	17α (H), 21β (H) - hopane	C_{30}	
	17β (H), 21β (H) - 30 - norhopane	C_{29}	
F	17β (H), 21α (H) - 30 - moretane	C_{30}	
G	17α (H), 21β (H) - homohopane (22S)	C_{31}	
H	17α (H), 21β (H) - homohopane (22R)	C_{31}	
G^1	Gammacerane	C_{30}	
	17β (H), 21β (H) - hopane	C_{30}	
I	17β (H), 21α (H) - homomoretane	C_{31}	
J	17α (H), 21β (H) - bishomohopane (22S and 22R)	C_{32}	
	17β (H), 21β (H) - methylhopane	C_{31}	
K	17α (H), 21β (H) - trishomohopane (22S and 22R)	C_{33}	
	17β (H), 21β (H) - ethylhopane	C_{32}	
L	17α (H), 21β (H) - tetrakishomohopane (22S and 22R)	C_{34}	
M	17α (H), 21β (H) - pentakishomohopane (22S and SSR)	C_{35}	

Sample Biomarker Composition
Steranes
Terpanes

Table A-3

Biomarker Abundances -- Steranes (peak areas)

GEOCHEM SAMPLE NUMBER		05/15544-001A	05/15544-002A	05/15544-003A	05/15544-004A
WELL NAME					
DEPTH / IDENTITY		4574-001	4574-002	4574-003	4574-004
M/Z	Peak				
217	U	2715	1898	2233	1723
	V	1627	1111	1166	1064
	A	646	561	460	473
	B	187	137	158	126
	C	139	149	94	98
	D	668	481	467	446
	E	295	194	202	182
	F	231	122	189	164
	TOTAL	6507	4654	4969	4277
	G	1718	1171	1020	1289
	H	2271	1593	1453	1616
	I	2015	1376	1260	1443
	J	2029	1295	1262	1505
	K	463	296	288	322
	L	509	379	365	353
	M	1193	774	810	896
	N	999	659	695	765
	P	805	556	597	636
	Q	1275	869	833	883
	R	1503	1048	1039	1184
	S	1296	828	880	977
	T	1130	778	650	764
	TOTAL	17207	11623	11151	12632
	GRAND TOTAL	23714	16277	16120	16908
	G+J+L+P+Q+T	7466	5049	4727	5429
218	H	3628	2382	2202	2525
	I	3392	2156	2046	2384
	M	1717	1162	1262	1241
	N	1677	1089	1197	1197
	R	2380	1467	1630	1789
	S	2239	1423	1529	1594
259	A	275	222	182	215
	B	162	121	127	117
	D	211	133	120	96
	E	75	111	52	105
	F	78	45	42	40
	H	380	268	240	304
	K	154	91	109	121

Table A-4

Biomarker Abundances -- Terpanes (peak areas)

GEOCHEM SAMPLE NUMBER		05/15544-001A	05/15544-002A	05/15544-003A	05/15544-004A
WELL NAME					
DEPTH / IDENTITY		4574-001	4574-002	4574-003	4574-004
M/Z	Peak				
191	A	904	670	725	714
	B	3769	2488	2716	2569
	Z	1090	757	892	773
	C	8291	5682	6628	6000
	C1	809	517	648	589
	X	156	75	75	90
	D	459	332	333	322
	E	6857	4631	4518	4989
	F	532	304	263	336
	G	3434	2244	2215	2509
	H	2594	1707	1693	1875
	G1	379	275	169	279
	I	654	481	575	557
	J	3696	2441	2388	2721
	K	2026	1353	1320	1570
	L	1099	722	737	872
	M	1362	922	949	1104
	TOTAL	38110	25600	26844	27868
	N	2610	1814	2224	1653
	O	4150	2645	3425	2709
	P	19310	12730	15874	12934
	Q	5469	3493	4650	3633
	R	4913	3153	4086	3253
	S	1637	1128	1482	1095
	T	1821	1206	1532	1225
	U	0	0	0	0
	V	0	0	0	0
	W	0	0	0	0
	TOTAL	39910	26168	33272	26502
	GRAND TOTAL	78019	51769	60116	54370

Table A-5

Biomarker Molecular Ratios

GEOCHEM SAMPLE NUMBER				05/15544-001A	05/15544-002A	05/15544-003A	05/15544-004A
WELL NAME							
DEPTH / IDENTITY				4574-001	4574-002	4574-003	4574-004
M/Z	PEAKS *	IDENTITY	CODE				
191	B/A	Tm/Ts	M1	4.17	3.71	3.75	3.60
191	G/(G+H)	C_{31} hH-S/R	M2	0.57	0.57	0.57	0.57
191	X/E	DiaH	M3	0.02	0.02	0.02	0.02
191	C/C1	NorH/C_{29} Ts	M4	10.25	10.99	10.23	10.19
178 192	1.5(2+3/P+1+9)	MPI Index 1	M5				
178 192	3(2/P+1+9)	MPI Index 2	M6				
168	3/2	Mebiphenyl	M7				
231	A/(A+E+G)	TA St	M8				
198	4/1	Medibzthio	M9				
217	Q/T	C_{29} αα St	M10	1.13	1.12	1.28	1.16
217	(R+S)/(Q -> T)	C_{29} St	M11	0.54	0.53	0.56	0.57
191	C/E	NorH	S1	1.21	1.23	1.47	1.20
191	Z/E	BisnorH	S2	0.16	0.16	0.20	0.15
191	hH/(A,B,C,E)	hH/H	S3	0.72	0.70	0.64	0.75
191	M/(G+H+J+K+L+M)	hH Index	S4	0.10	0.10	0.10	0.10
191	M/L	C_{35} /C_{34} hH	S5	1.24	1.28	1.29	1.27
191	G1/G	Gamma	S6	0.11	0.12	0.08	0.11
191	(N -> W)/(A,B,C,E)	Tricyclics	S7	2.01	1.94	2.28	1.86
191	S/P	C_{24} /C_{23}	S8	0.08	0.09	0.09	0.08
191	S/T	C_{24} /C_{26}	S9	0.90	0.93	0.97	0.89
259 217	(A -> F,H,K)/(A -> T)	DiaSt	S10	0.07	0.07	0.07	0.07
217	(L+M+N+P)/(Q+R+S+T)	C_{28} /C_{29} St	S11	0.67	0.67	0.73	0.70
218	H+I:M+N:R+S	ββ St	S12	47:23:31	47:23:30	43:25:32	46:23:32
191 217	(A,B,C,E)/A -> T	H/St	S13	1.02	1.02	1.15	1.01
198 178	4/p	Medibzthio/phen	S14				
191	A+B+C+E	ppm H	S15				
217	A -> T	ppm St	S16				

* Peak Identification on Standard Fragmentograms CODE: M = maturity S = source
bzthio = benzothiophenes Gamma = Gammacerane hH = Homohopanes H = Hopanes Me = methyl
MN = methylnaphthalenes MP = methylphenanthrenes Rg = regular St = Steranes TA = triaromatic

Table A-6

GCMS DATA

	Sample Number 4574-001	Sample Number 4574-002	Sample Number 4574-003	Sample Number 4574-004
Steranes				
C27	46.2	47.3	44.2	44.4
C28	23.6	22.8	24.5	24.1
C29	30.2	29.9	31.3	31.5
Terpanes				
C27	12.26	12.34	12.82	11.78
C28	2.86	2.96	3.32	2.77
C29	25.08	25.51	28.35	24.8
C30	20.79	20.64	18.72	20.43
C31	17.53	17.31	16.7	17.73
C32	9.7	9.53	8.9	9.76
C33	5.32	5.28	4.92	5.63
C34	2.88	2.82	2.75	3.13
C35	3.57	3.6	3.54	3.96
Sterane %	19.6	19.7	18.6	19.8
Terpanes %	80.4	80.3	81.4	80.2
Significant Ratios				
3	0.052	0.055	0.048	0.051
4	0.57	0.56	0.56	0.57
5	1.08	1.05	1.05	1.06
6	nd	nd	nd	nd
7	4.17	3.71	3.74	3.6
8	6.92	7.28	7.58	7.58
9	62.80%	61.90%	62.70%	62.30%
10	1.13	1.13	1.13	1.14
11	0.93	0.84	0.97	1.01
12	0.29	0.24	0.34	0.27
13	0.052	0.056	0.036	0.053
14	0.54	0.55	0.55	0.57
15	0.57	0.57	0.57	0.57
16	0.93	0.94	0.94	0.94
17	absent	absent	absent	absent

GCMS Quantitative Reviews

GCMS DATA

QUANTATIVE REVIEW
SAMPLE 4574-001

1 Relative Composition of Tri- and Pentacyclic Terpanes and Steranes by Carbon Number

Steranes (m/z 218)		Tri- and Pentacyclic Terpanes (m/z 191)	
	%		%
C27	46.20	C27	12.26
C28	23.60	C28	2.86
C29	30.20	C29	25.08
	100.00	C30	20.79
		C31	17.53
		C32	9.70
		C33	5.32
		C34	2.88
		C35	3.57
			100.00

2 Relative Percentages of Steranes and Terpanes calculated using m/z 217 and m/z 191

	%
Steranes	19.6
Terpanes	80.4

3 Maturity Ratio- Ratio of 17β(H) Normoretane to the sum of (17β(H) Normoretane + 17β(H) norhopane)

Ratio 0.052

4 Maturity Ratio-Ratio of 17α(H) 22S Homohopane to the sum of (17α(H) 22S Homohopane + 17α(H) 22R Homohopane)

Ratio 0.57

5 Maturity Ratio-Ratio of the 22S/22R Epimers of the 17α(H),21β(H)-Hopanes reaches equilibrium at approximately 60/40 ratio(1.50) in a Mature Oil. Immature Oils are lower.

Ratio 1.08

6 Maturity Ratio-Ratio of Primary/Secondary Terpanes approaches one(decreases) as Maturity increases

Ratio nd

7 Maturity and Migration Ratio-Ratio of 17α(H)-22, 29, 30-Trisnorhopane to 18α(H)-22, 29, 30-Trisnorhopane II decreases as Maturity increases and Migration occurs.

Ratio 4.17

8 Maturity Ratio-Ratio of 17α(H), 21β(H)-Hopane to (17β(H)-Moretane + 17β, 21α(H)-30-Normoretane) increases as Maturity increases.

9 Maturity and Migration Ratio-Percent of C29 20S-Steranes to total C29 -20S and -20R Steranes increases.

Percenta 62.8

10 Source Character Ratio-Ratio of C29 Cholestane (20S & 20R) to C29 Isocholestane (20S & 20) : (Internal Ratio of 5a-Steranes)

Ratio 1.13

11 Maturation and Source Character Ratio-Ratio of 5α C28 Steranes / 5α C29 Steranes is insensitive to Maturation.

Ratio 0.93

12 Biodegradation Ratio-Ratio of 13β(H),17α(H)(20R) C27 Sterane to 13β(H),17α(H)(20S) C27 Sterane increases with increasing biodegradation.

Ratio 0.29

13 Source Character Ratio-Ratio of Gammacerane to the sum of (Gammacerane + 17α(H),21β Hopane)

Ratio 0.052

14 Maturation Ratio-Ratio of 5α(H),14β(H),17β(H) C29 Sterane to sum of (5α(H),14β(H),17β C29 Sterane+ 5α(H),14α(H),17α(H) C29 Sterane) increases with increasing Maturation

Ratio 0.54

15 Maturation Ratio-Ratio of 22S 17α(H),21β(H) C32 Hopanes to sum of (22S 17α(H),21β(H) C32 Hopanes + 22R 17β(H),21α(H), C32 Hopanes) reaches an equilibrium value of 0.55 to 0.60 with increasing Maturation.

Ratio 0.57

16 Temperature Maturation Ratio-Ratio of 17α(H),21β(H) C30 Hopane to (17α(H),21β(H) C30 Hopane + 17β(H),21α C30 Hopane) increases with increasing temperature of Maturation.

Ratio 0.93

17 Oleanane-Presence or absence of Oleanane can indicate the age of a rock (bitumen) or a reservoired crude oil as being Mid Cretaceous or younger (Oleanane present) or Lower Cretaceous or older (Oleanane absent).

O' 18α(H)- Oleanane

GCMS DATA

QUANTATIVE REVIEW
4574-002

1 Relative Composition of Tri- and Pentacyclic Terpanes and Steranes by Carbon Number

Steranes (m/z 218)		Tri- and Pentacyclic Terpanes (m/z 191)	
	%		%
C27	47.30	C27	12.34
C28	22.80	C28	2.96
C29	29.90	C29	25.51
	100.00	C30	20.64
		C31	17.31
		C32	9.53
		C33	5.28
		C34	2.82
		C35	3.60
			100.00

2 Relative Percentages of Steranes and Terpanes calculated using m/z 217 and m/z 191

	%
Steranes	19.7
Terpanes	80.3

3 Maturity Ratio- Ratio of 17β(H) Normoretane to the sum of (17β(H) Normoretane + 17β(H) norhopane)

Ratio 0.055

4 Maturity Ratio-Ratio of 17α(H) 22S Homohopane to the sum of (17α(H) 22S Homohopane + 17α(H) 22R Homohopane)

Ratio 0.56

5 Maturity Ratio-Ratio of the 22S/22R Epimers of the 17α(H),21β(H)-Hopanes reaches equilibrium at approximately 60/40 ratio(1.50) in a Mature Oil. Immature Oils are lower.

Ratio 1.05

6 Maturity Ratio-Ratio of Primary/Secondary Terpanes approaches one(decreases) as Maturity Increases

Ratio

7 Maturity and Migration Ratio-Ratio of 17α(H)-22, 29, 30-Trisnorhopane to 18α(H)-22, 29, 30-Trisnorhopane II decreases as Maturity increases and Migration occurs.

Ratio 3.71

8 Maturity Ratio-Ratio of 17α(H), 21β(H)-Hopane to (17β(H)-Moretane + 17β, 21α(H)-30-Normoretane) increases as Maturity increases.

Ratio 7.28

9 Maturity and Migration Ratio-Percent of C29 20S-Steranes to total C29 -20S and -20R Steranes increases.

Percenta 61.9

10 Source Character Ratio-Ratio of C29 Cholestane (20S & 20R) to C29 Isocholestane (20S & 20) : (Internal Ratio of 5a-Steranes)

Ratio 1.13

11 Maturation and Source Character Ratio-Ratio of 5α C28 Steranes / 5α C29 Steranes is insensitive to Maturation.

Ratio 0.89

12 Biodegradation Ratio-Ratio of 13β(H),17α(H)(20R) C27 Sterane to 13β(H),17α(H)(20S) C27 Sterane increases with increasing biodegradation.

Ratio 0.24

13 Source Character Ratio-Ratio of Gammacerane to the sum of (Gammacerane + 17α(H),21β Hopane)

Ratio 0.056

14 Maturation Ratio-Ratio of 5α(H),14β(H),17β(H) C29 Sterane to sum of (5α(H),14β(H),17β C29 Sterane+ 5α(H),14α(H),17α(H) C29 Sterane) increases with increasing Maturation

Ratio 0.55

15 Maturation Ratio-Ratio of 22S 17α(H),21β(H) C32 Hopanes to sum of (22S 17α(H),21β(H) C32 Hopanes + 22R 17β(H),21α(H), C32 Hopanes) reaches an equilibrium value of 0.55 to 0.60 with increasing Maturation.

Ratio 0.57

16 Temperature Maturation Ratio-Ratio of 17α(H),21β(H) C30 Hopane to (17α(H),21β(H) C30 Hopane + 17β(H),21α C30 Hopane) increases with increasing temperature of Maturation.

Ratio 0.94

17 Oleanane-Presence or absence of Oleanane can indicate the age of a rock (bitumen) or a reservoired crude oil as being Mid Cretaceous or younger (Oleanane present) or Lower Cretaceous or older (Oleanane absent).

O' 18α(H)- Oleanane

GCMS DATA

QUANTATIVE REVIEW
4574-003

1 Relative Composition of Tri- and Pentacyclic Terpanes and Steranes by Carbon Number

Steranes (m/z 218)		Tri- and Pentacyclic Terpanes (m/z 191)	
	%		%
C27	44.20	C27	12.82
C28	24.50	C28	3.32
C29	31.30	C29	28.35
	100.00	C30	18.72
		C31	16.70
		C32	8.90
		C33	4.92
		C34	2.75
		C35	3.54
			100.00

2 Relative Percentages of Steranes and Terpanes calculated using m/z 217 and m/z 191

	%
Steranes	18.6
Terpanes	81.4

3 Maturity Ratio- Ratio of 17β(H) Normoretane to the sum of (17β(H) Normoretane + 17β(H) norhopane)

Ratio 0.048

4 Maturity Ratio-Ratio of 17α(H) 22S Homohopane to the sum of (17α(H) 22S Homohopane + 17α(H) 22R Homohopane)

Ratio 0.56

5 Maturity Ratio-Ratio of the 22S/22R Epimers of the 17α(H),21β(H)-Hopanes reaches equilibrium at approximately 60/40 ratio(1.50) in a Mature Oil. Immature Oils are lower.

Ratio 1.05

6 Maturity Ratio-Ratio of Primary/Secondary Terpanes approaches one(decreases) as Maturity Increases

Ratio

7 Maturity and Migration Ratio-Ratio of 17α(H)-22, 29, 30-Trisnorhopane to 18α(H)-22, 29, 30-Trisnorhopane II decreases as Maturity increases and Migration occurs.

Ratio 3.74

8 Maturity Ratio-Ratio of 17α(H), 21β(H)-Hopane to (17β(H)-Moretane + 17β, 21α(H)-30-Normoretane) increases as Maturity increases.

Ratio 7.58

9 Maturity and Migration Ratio-Percent of C29 20S-Steranes to total C29 -20S and -20R Steranes increases.

Percenta 62.7

10 Source Character Ratio-Ratio of C29 Cholestane (20S & 20R) to C29 Isocholestane (20S & 20) : (Internal Ratio of 5a-Steranes)

Ratio 1.13

11 Maturation and Source Character Ratio-Ratio of 5α C28 Steranes / 5α C29 Steranes is insensitive to Maturation.

Ratio 0.97

12 Biodegradation Ratio-Ratio of 13β(H),17α(H)(20R) C27 Sterane to 13β(H),17α(H)(20S) C27 Sterane increases with increasing biodegradation.

Ratio 0.34

13 Source Character Ratio-Ratio of Gammacerane to the sum of (Gammacerane + 17α(H),21β Hopane)

Ratio 0.036

14 Maturation Ratio-Ratio of 5α(H),14β(H),17β(H) C29 Sterane to sum of (5α(H),14β(H),17β C29 Sterane+ 5α(H),14α(H),17α(H) C29 Sterane) increases with increasing Maturation

Ratio 0.55

15 Maturation Ratio-Ratio of 22S 17α(H),21β(H) C32 Hopanes to sum of (22S 17α(H),21β(H) C32 Hopanes + 22R 17β(H),21α(H), C32 Hopanes) reaches an equilibrium value of 0.55 to 0.60 with increasing Maturation.

Ratio 0.57

16 Temperature Maturation Ratio-Ratio of 17α(H),21β(H) C30 Hopane to (17α(H),21β(H) C30 Hopane + 17β(H),21α C30 Hopane) increases with increasing temperature of Maturation.

Ratio 0.94

17 Oleanane-Presence or absence of Oleanane can indicate the age of a rock (bitumen) or a reservoired crude oil as being Mid Cretaceous or younger (Oleanane present) or Lower Cretaceous or older (Oleanane absent).

O' 18α(H)- Oleanane

GCMS DATA

QUANTATIVE REVIEW
4574-004

1 Relative Composition of Tri- and Pentacyclic Terpanes and Steranes by Carbon Number

Steranes (m/z 218)		Tri- and Pentacyclic Terpanes (m/z 191)	
	%		%
C27	44.40	C27	11.78
C28	24.10	C28	2.77
C29	31.50	C29	24.80
	100.00	C30	20.43
		C31	17.73
		C32	9.76
		C33	5.63
		C34	3.13
		C35	3.96
			100.00

2 Relative Percentages of Steranes and Terpanes calculated using m/z 217 and m/z 191

	%
Steranes	19.8
Terpanes	80.2

3 Maturity Ratio- Ratio of 17β(H) Normoretane to the sum of (17β(H) Normoretane + 17β(H) norhopane)

Ratio 0.051

4 Maturity Ratio-Ratio of 17α(H) 22S Homohopane to the sum of (17α(H) 22S Homohopane + 17α(H) 22R Homohopane)

Ratio 0.57

5 Maturity Ratio-Ratio of the 22S/22R Epimers of the 17α(H),21β(H)-Hopanes reaches equilibrium at approximately 60/40 ratio(1.50) in a Mature Oil. Immature Oils are lower.

Ratio 1.06

6 Maturity Ratio-Ratio of Primary/Secondary Terpanes approaches one(decreases) as Maturity Increases

Ratio

7 Maturity and Migration Ratio-Ratio of 17α(H)-22, 29, 30-Trisnorhopane to 18α(H)-22, 29, 30-Trisnorhopane II decreases as Maturity increases and Migration occurs.

Ratio 3.60

8 Maturity Ratio-Ratio of 17α(H), 21β(H)-Hopane to (17β(H)-Moretane + 17β, 21α(H)-30-Normoretane) increases as Maturity increases.

Ratio 7.58

9 Maturity and Migration Ratio-Percent of C29 20S-Steranes to total C29 -20S and -20R Steranes increases.

Percent: 62.3

10 Source Character Ratio-Ratio of C29 Cholestane (20S & 20R) to C29 Isocholestane (20S & 20) : (Internal Ratio of 5a-Steranes)

Ratio 1.14

11 Maturation and Source Character Ratio-Ratio of 5α C28 Steranes / 5α C29 Steranes is insensitive to Maturation.

Ratio 1.01

12 Biodegradation Ratio-Ratio of 13β(H),17α(H)(20R) C27 Sterane to 13β(H),17α(H)(20S) C27 Sterane increases with increasing biodegradation.

Ratio 0.27

13 Source Character Ratio-Ratio of Gammacerane to the sum of (Gammacerane + 17α(H),21β Hopane)

Ratio 0.053

14 Maturation Ratio-Ratio of 5α(H),14β(H),17β(H) C29 Sterane to sum of (5α(H),14β(H),17β C29 Sterane+ 5α(H),14α(H),17α(H) C29 Sterane) increases with increasing Maturation

Ratio 0.57

15 Maturation Ratio-Ratio of 22S 17α(H),21β(H) C32 Hopanes to sum of (22S 17α(H),21β(H) C32 Hopanes + 22R 17β(H),21α(H), C32 Hopanes) reaches an equilibrium value of 0.55 to 0.60 with increasing Maturation.

Ratio 0.57

16 Temperature Maturation Ratio-Ratio of 17α(H),21β(H) C30 Hopane to (17α(H),21β(H) C30 Hopane + 17β(H),21α C30 Hopane) increases with increasing temperature of Maturation.

Ratio 0.94

17 Oleanane-Presence or absence of Oleanane can indicate the age of a rock (bitumen) or a reservoired crude oil as being Mid Cretaceous or younger (Oleanane present) or Lower Cretaceous or older (Oleanane absent).

O' 18α(H)- Oleanane

Sample GCMS Fragmentation Traces

```
File       : C:\MSDCHEM\1\DATA\155441S.D
Operator   :
Acquired   : 24 Oct 2005  20:33     using AcqMethod BIOMARK
Instrument :   Instrumen
Sample Name: 15544-001 SATS
Misc Info  : 4574-001
Vial Number: 3
```

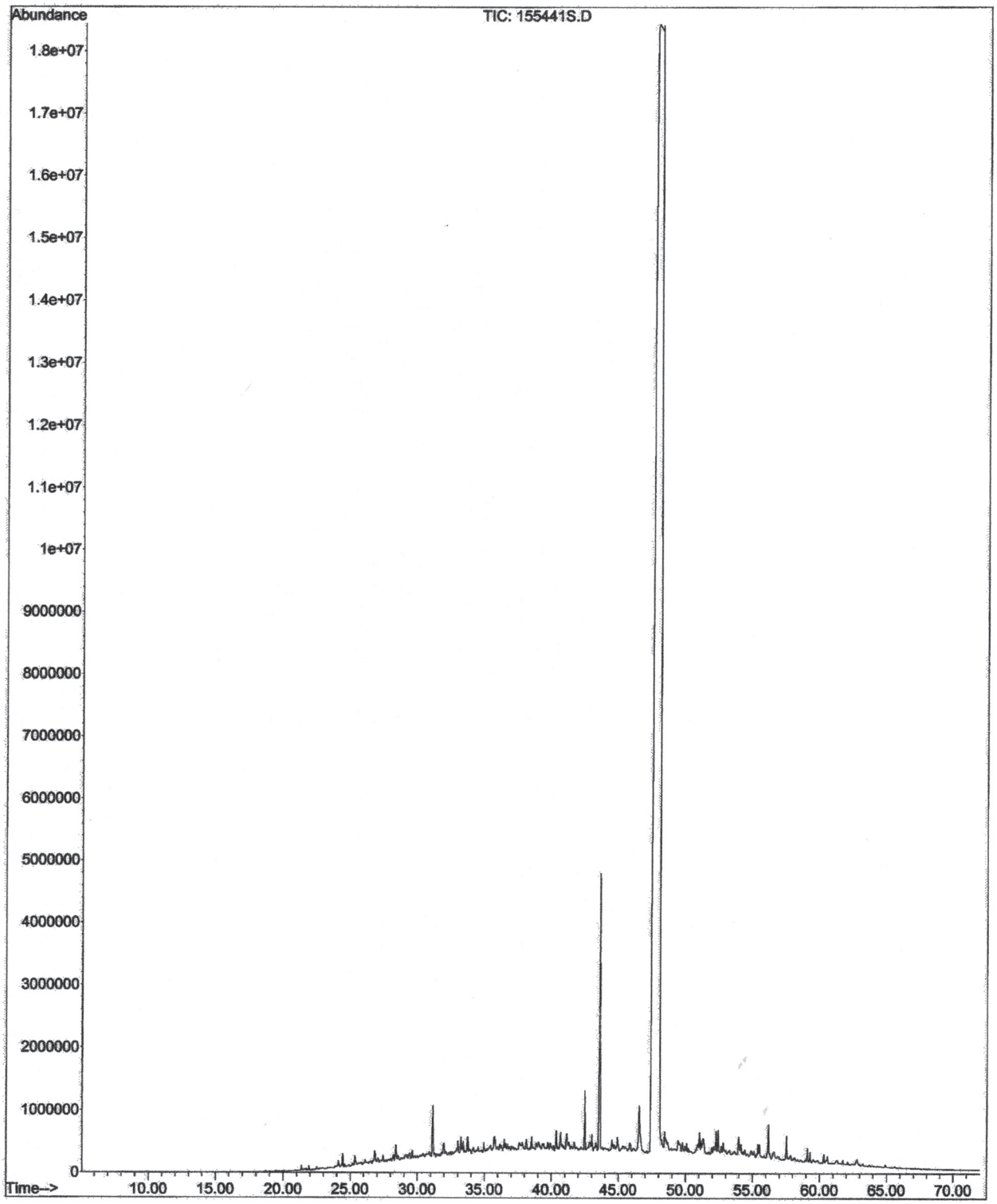

```
File        : C:\MSDCHEM\1\DATA\155441S.D
Operator    :
Acquired    : 24 Oct 2005  20:33      using AcqMethod BIOMARK
Instrument :   Instrumen
Sample Name: 15544-001 SATS
Misc Info   : 4574-001
Vial Number: 3
```

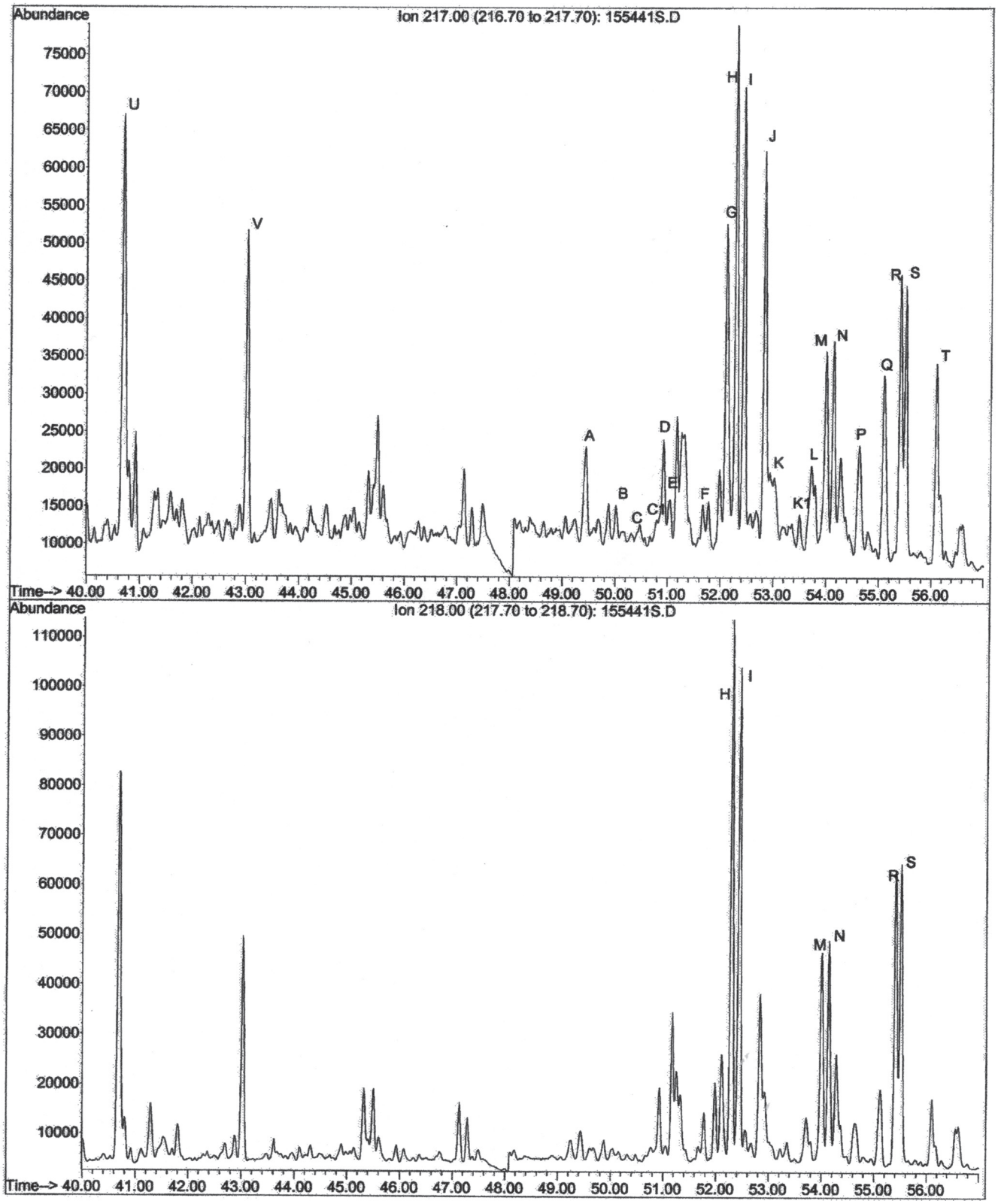

```
File       : C:\MSDCHEM\1\DATA\155441S.D
Operator   :
Acquired   : 24 Oct 2005  20:33     using AcqMethod BIOMARK
Instrument :   Instrumen
Sample Name: 15544-001 SATS
Misc Info  : 4574-001
Vial Number: 3
```

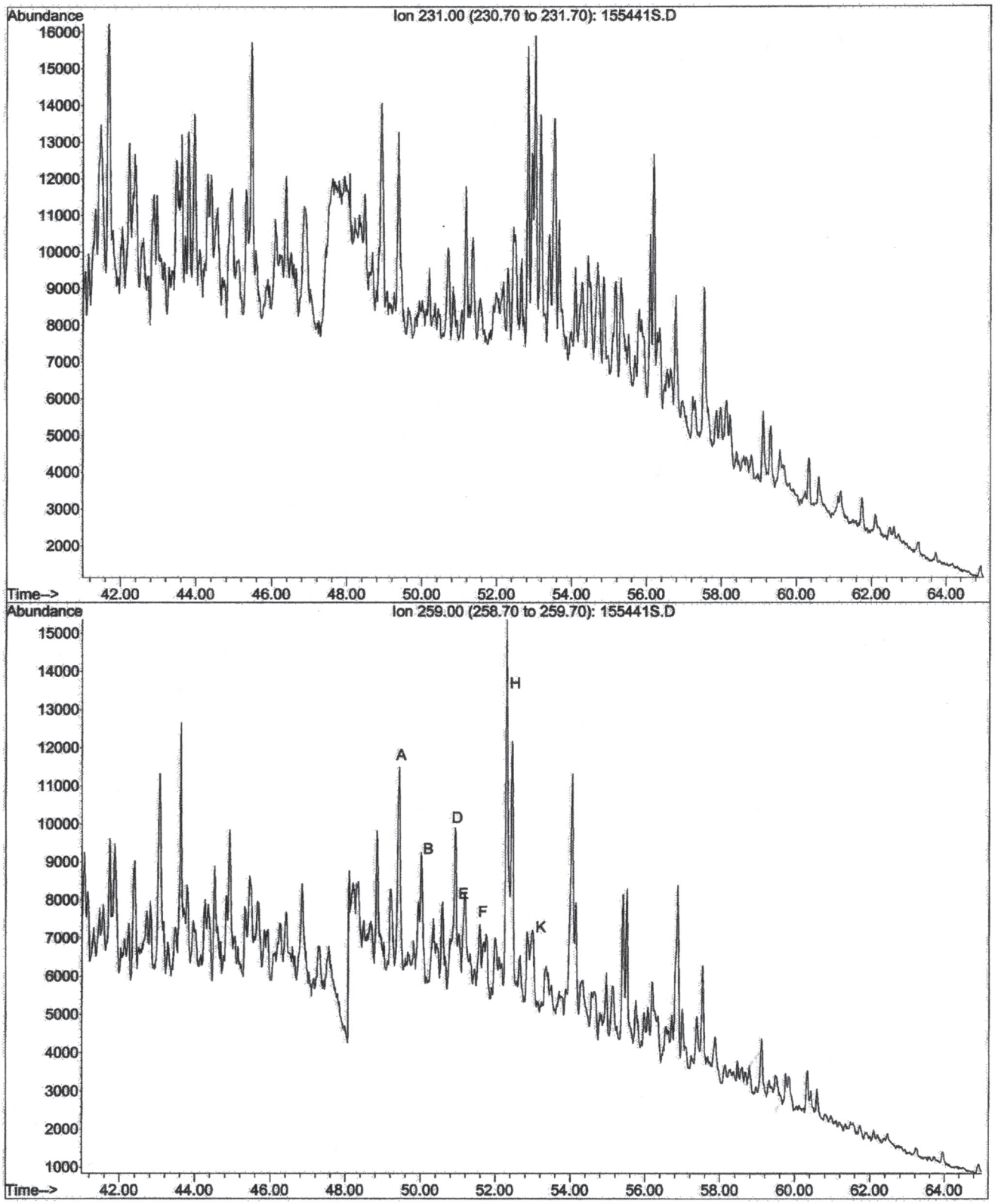

```
File        : C:\MSDCHEM\1\DATA\155441S.D
Operator    :
Acquired    : 24 Oct 2005  20:33     using AcqMethod BIOMARK
Instrument :   Instrumen
Sample Name: 15544-001 SATS
Misc Info   : 4574-001
Vial Number: 3
```

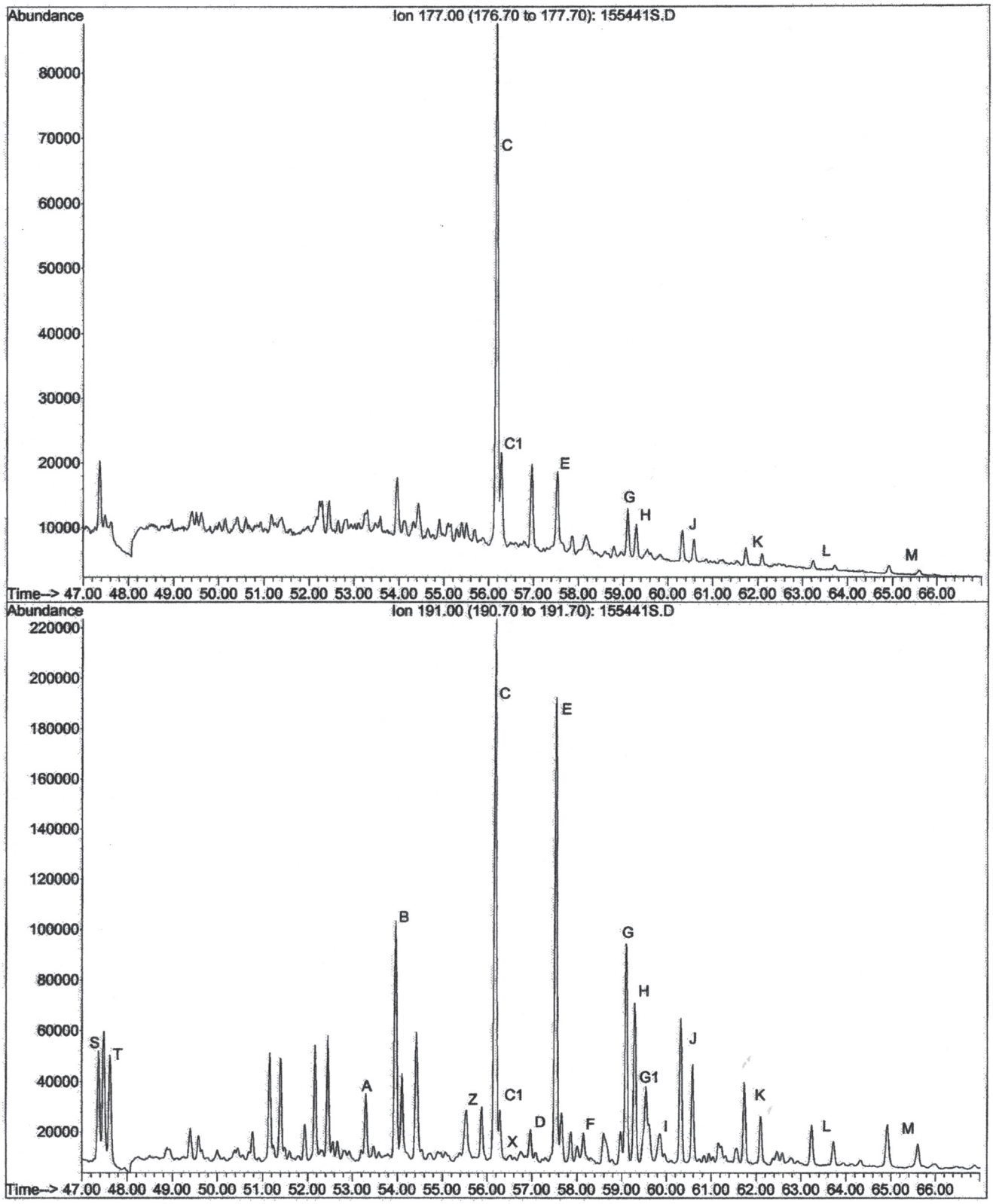

```
File        : C:\MSDCHEM\1\DATA\155441S.D
Operator    :
Acquired    : 24 Oct 2005  20:33      using AcqMethod BIOMARK
Instrument :   Instrumen
Sample Name: 15544-001 SATS
Misc Info   : 4574-001
Vial Number: 3
```

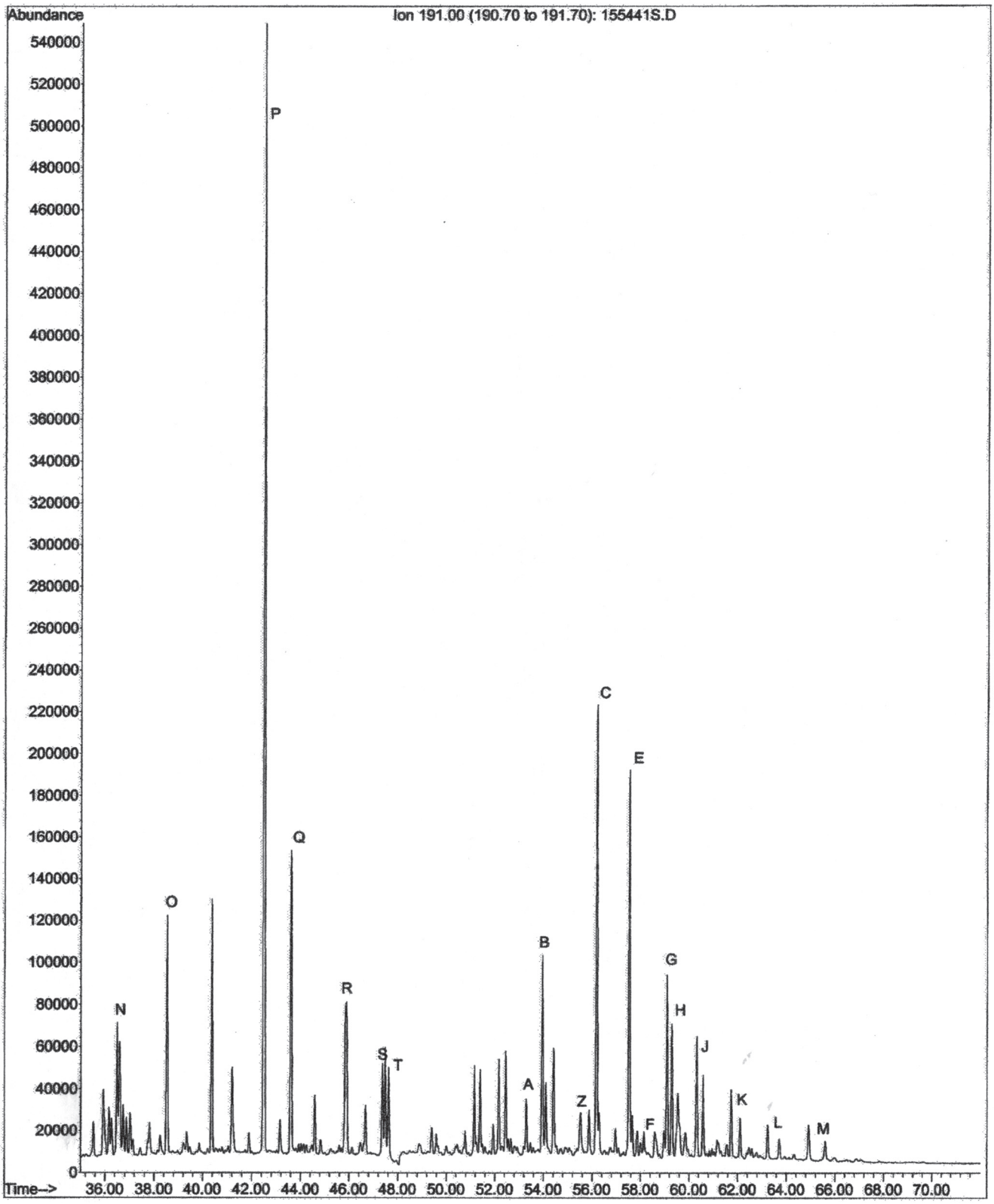

```
File        : C:\MSDCHEM\1\DATA\155441S.D
Operator    :
Acquired    : 24 Oct 2005  20:33     using AcqMethod BIOMARK
Instrument :   Instrumen
Sample Name: 15544-001 SATS
Misc Info   : 4574-001
Vial Number: 3
```

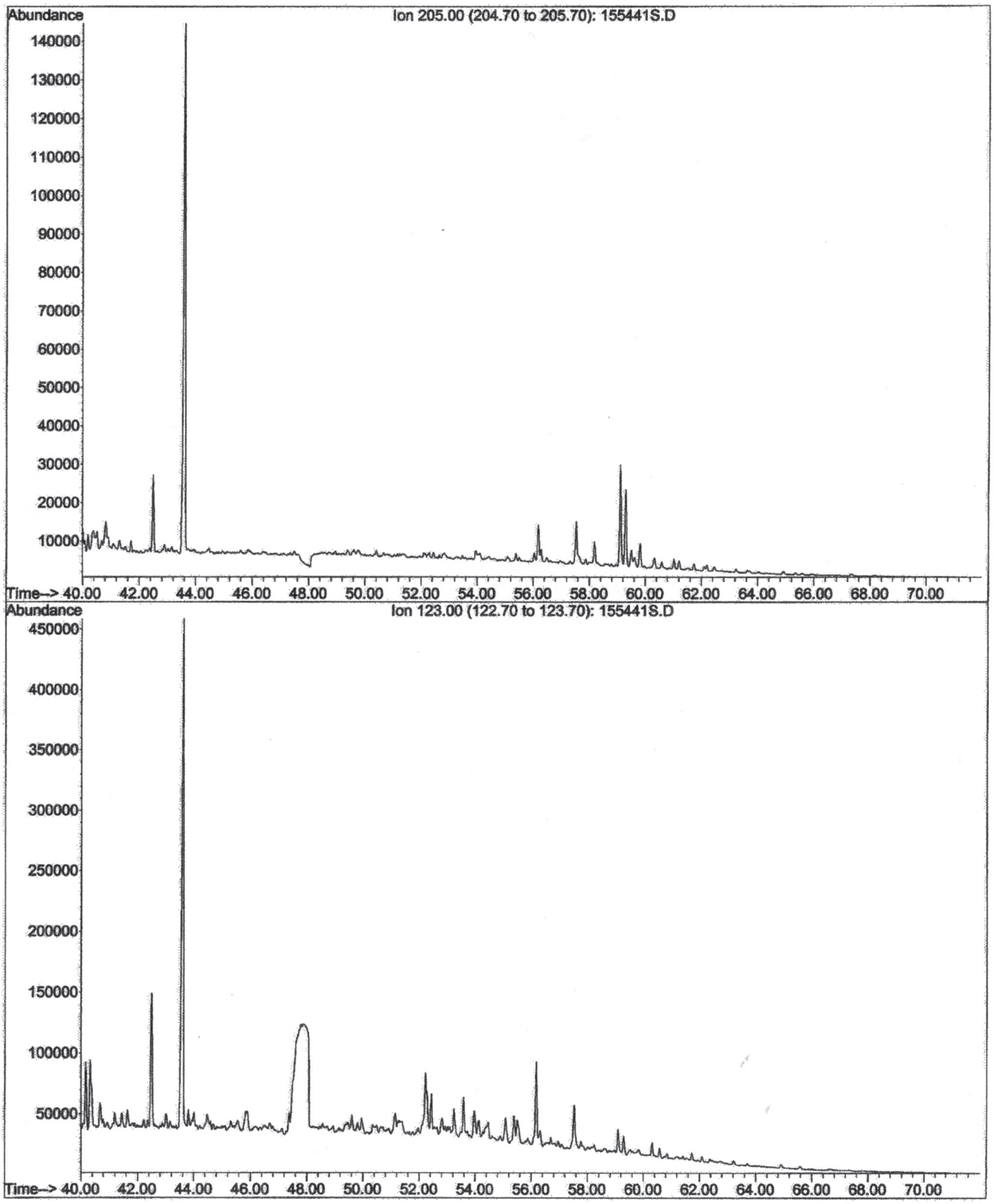

```
File        : C:\MSDCHEM\1\DATA\155442S.D
Operator    :
Acquired    : 24 Oct 2005  21:53      using AcqMethod BIOMARK
Instrument :   Instrumen
Sample Name: 15544-002 SATS
Misc Info   : 4574-002
Vial Number: 4
```

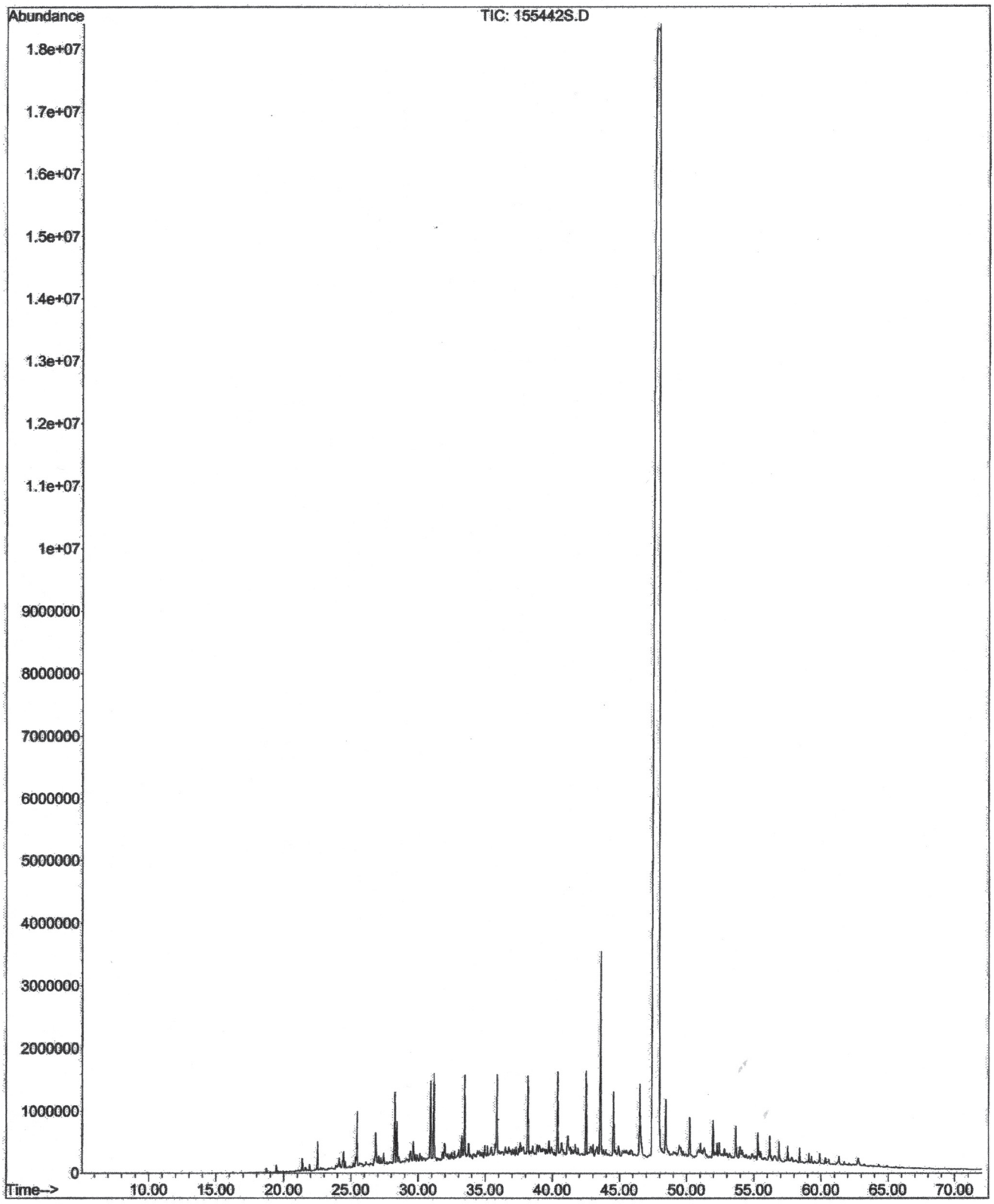

```
File        : C:\MSDCHEM\1\DATA\155442S.D
Operator    :
Acquired    : 24 Oct 2005  21:53      using AcqMethod BIOMARK
Instrument :   Instrumen
Sample Name: 15544-002 SATS
Misc Info   : 4574-002
Vial Number: 4
```

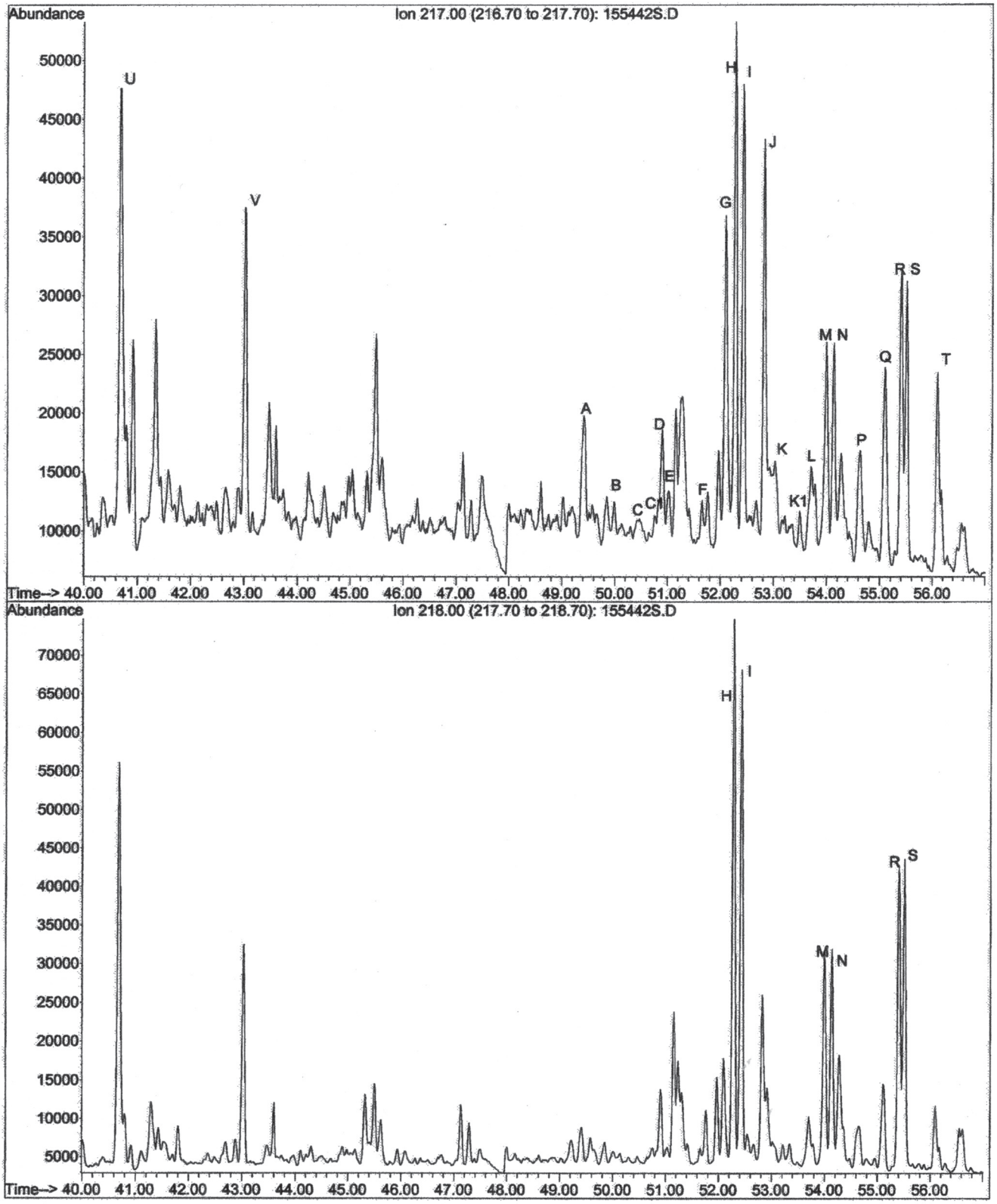

```
File       : C:\MSDCHEM\1\DATA\155442S.D
Operator   :
Acquired   : 24 Oct 2005  21:53     using AcqMethod BIOMARK
Instrument :   Instrumen
Sample Name: 15544-002 SATS
Misc Info  : 4574-002
Vial Number: 4
```

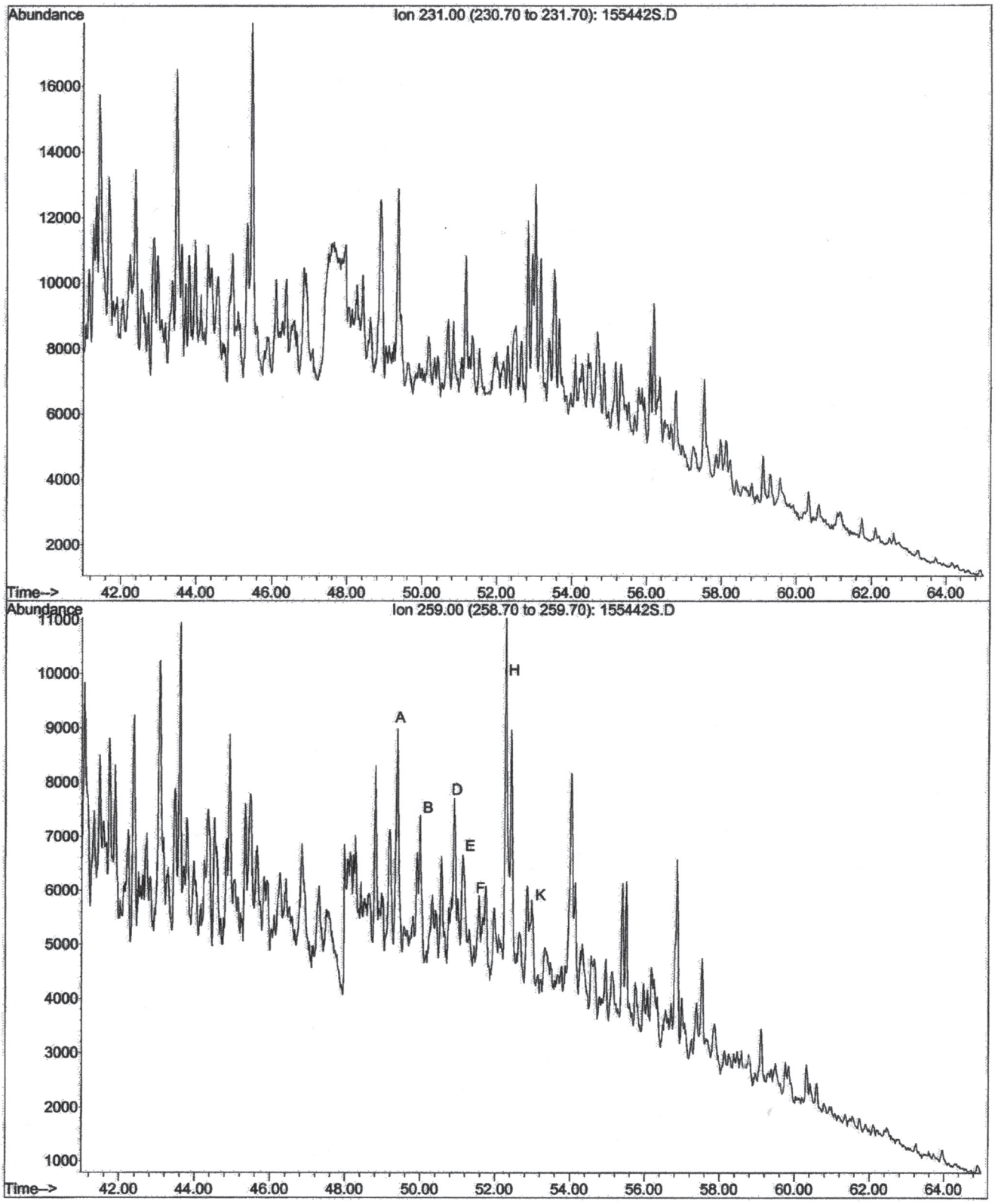

```
File        : C:\MSDCHEM\1\DATA\155442S.D
Operator    :
Acquired    : 24 Oct 2005  21:53      using AcqMethod BIOMARK
Instrument :   Instrumen
Sample Name: 15544-002 SATS
Misc Info   : 4574-002
Vial Number: 4
```

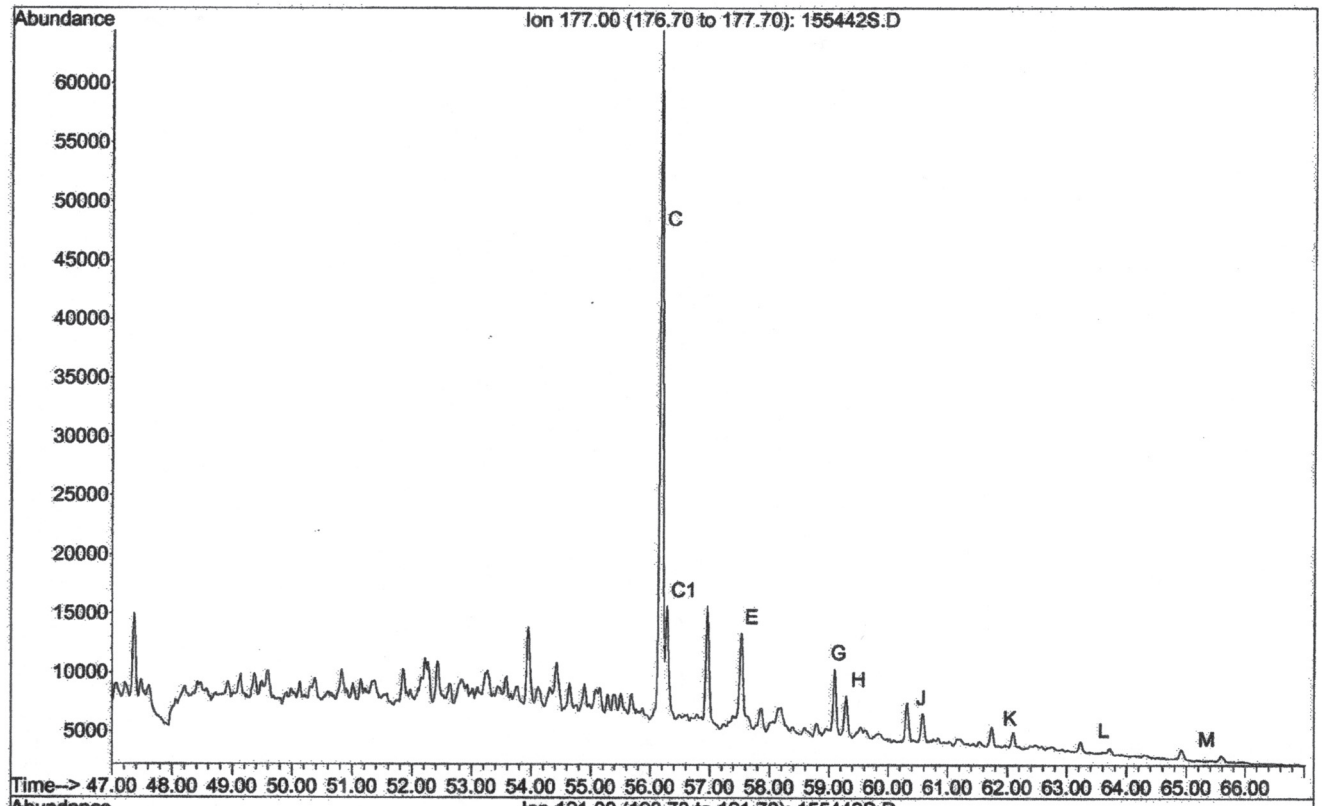

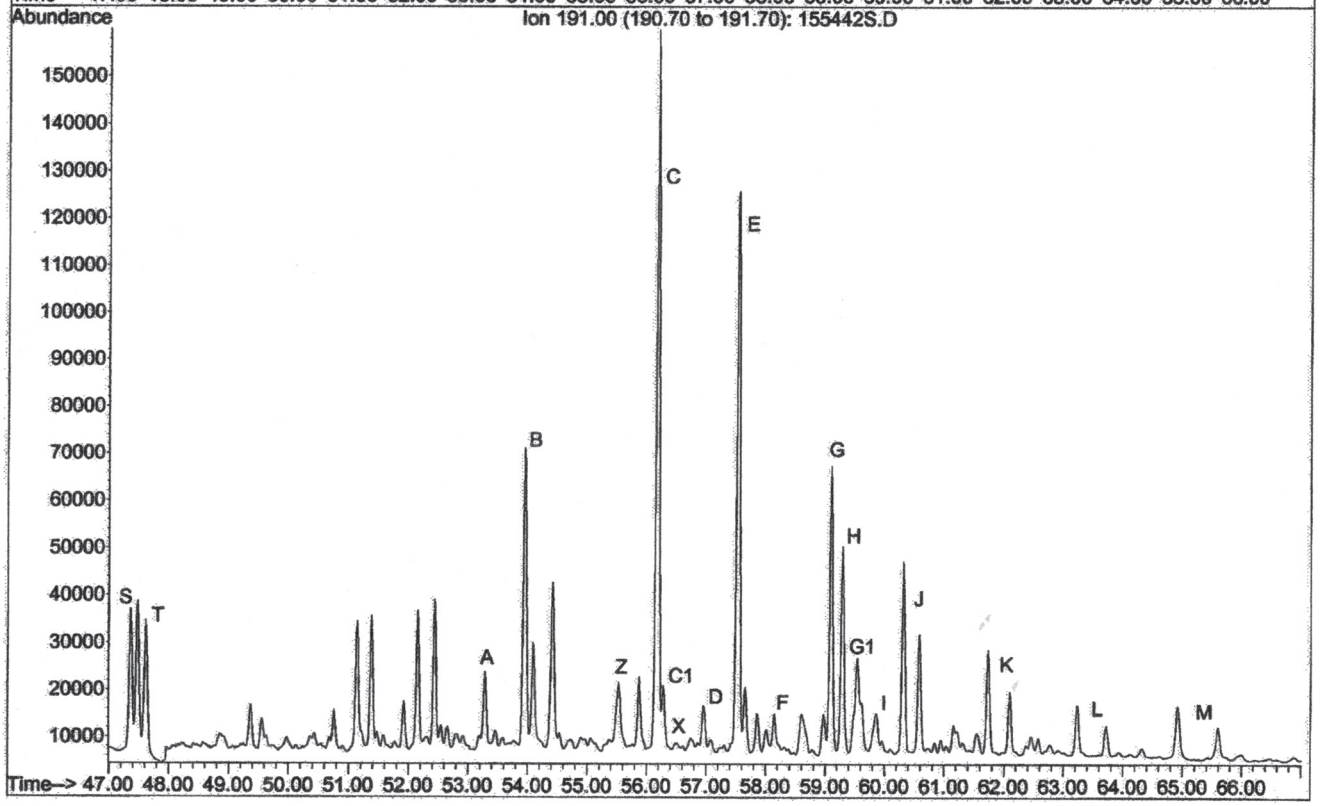

```
File        : C:\MSDCHEM\1\DATA\155442S.D
Operator    :
Acquired    : 24 Oct 2005  21:53      using AcqMethod BIOMARK
Instrument :   Instrumen
Sample Name: 15544-002 SATS
Misc Info   : 4574-002
Vial Number: 4
```

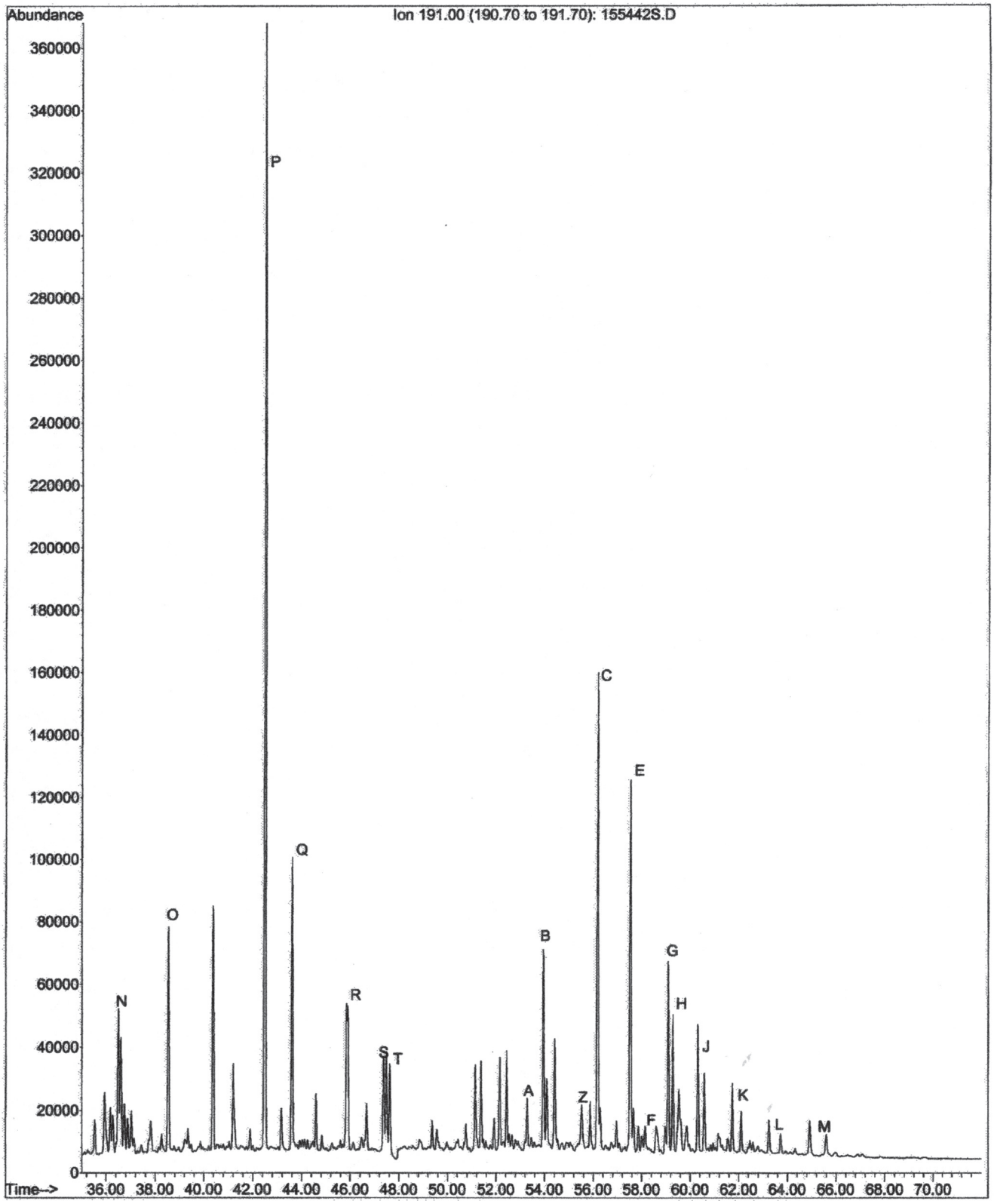

```
File        : C:\MSDCHEM\1\DATA\155442S.D
Operator    :
Acquired    : 24 Oct 2005  21:53      using AcqMethod BIOMARK
Instrument :   Instrumen
Sample Name: 15544-002 SATS
Misc Info   : 4574-002
Vial Number: 4
```

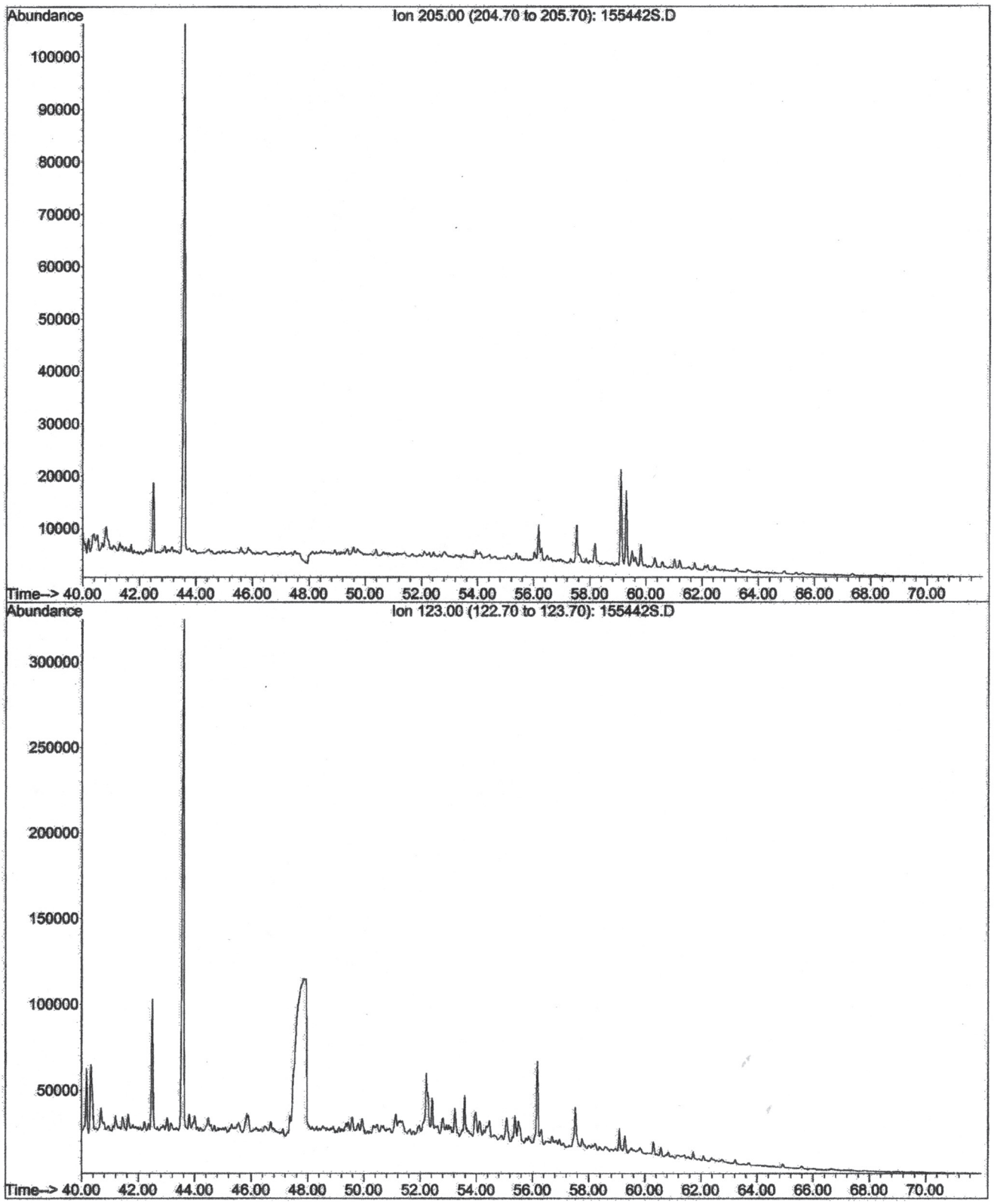

```
File        : C:\MSDCHEM\1\DATA\155443S.D
Operator    :
Acquired    : 24 Oct 2005  23:13     using AcqMethod BIOMARK
Instrument :   Instrumen
Sample Name: 15544-003 SATS
Misc Info   : 4574-003
Vial Number: 5
```

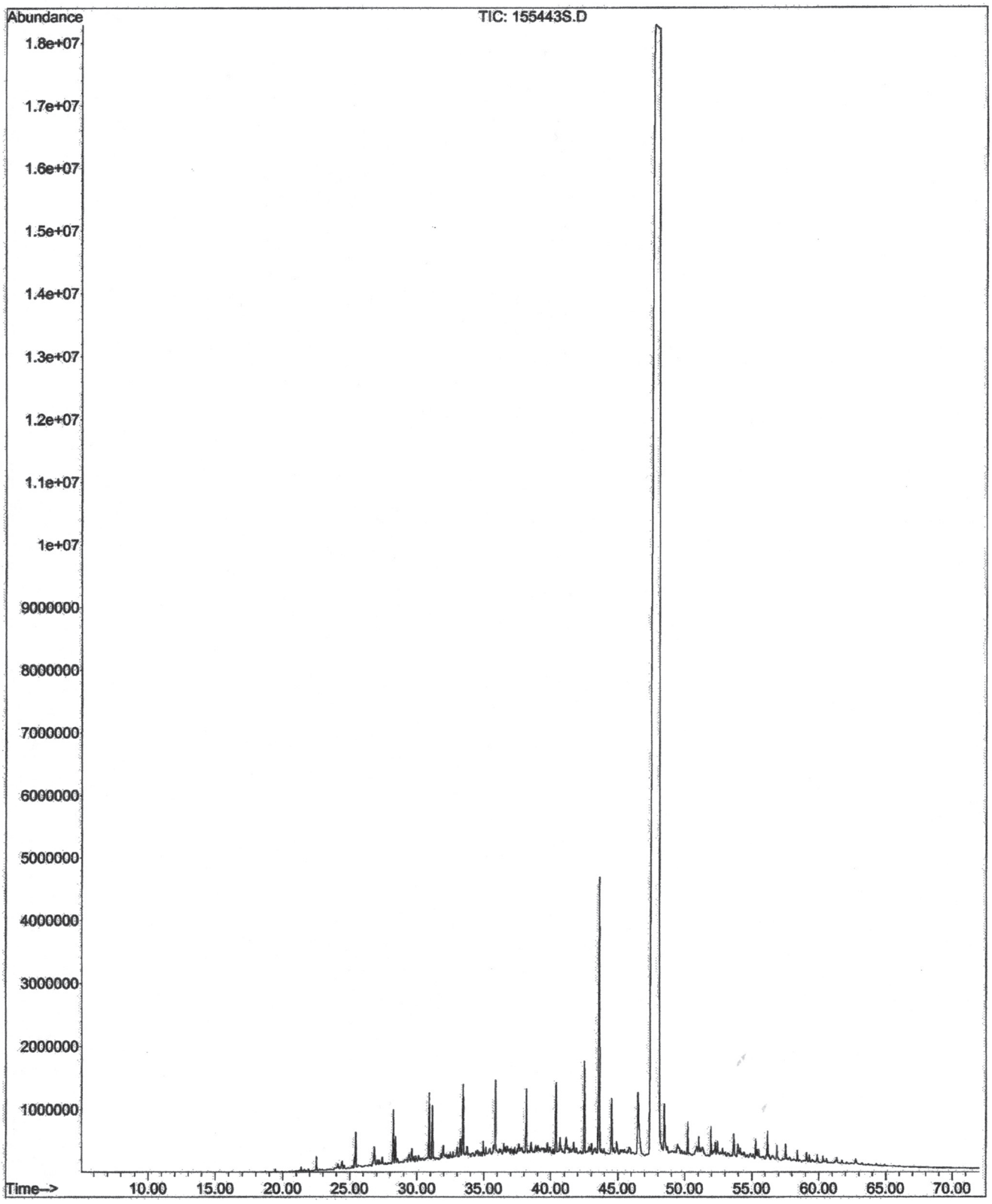

```
File        : C:\MSDCHEM\1\DATA\155443S.D
Operator    :
Acquired    : 24 Oct 2005  23:13      using AcqMethod BIOMARK
Instrument :   Instrumen
Sample Name: 15544-003 SATS
Misc Info   : 4574-003
Vial Number: 5
```

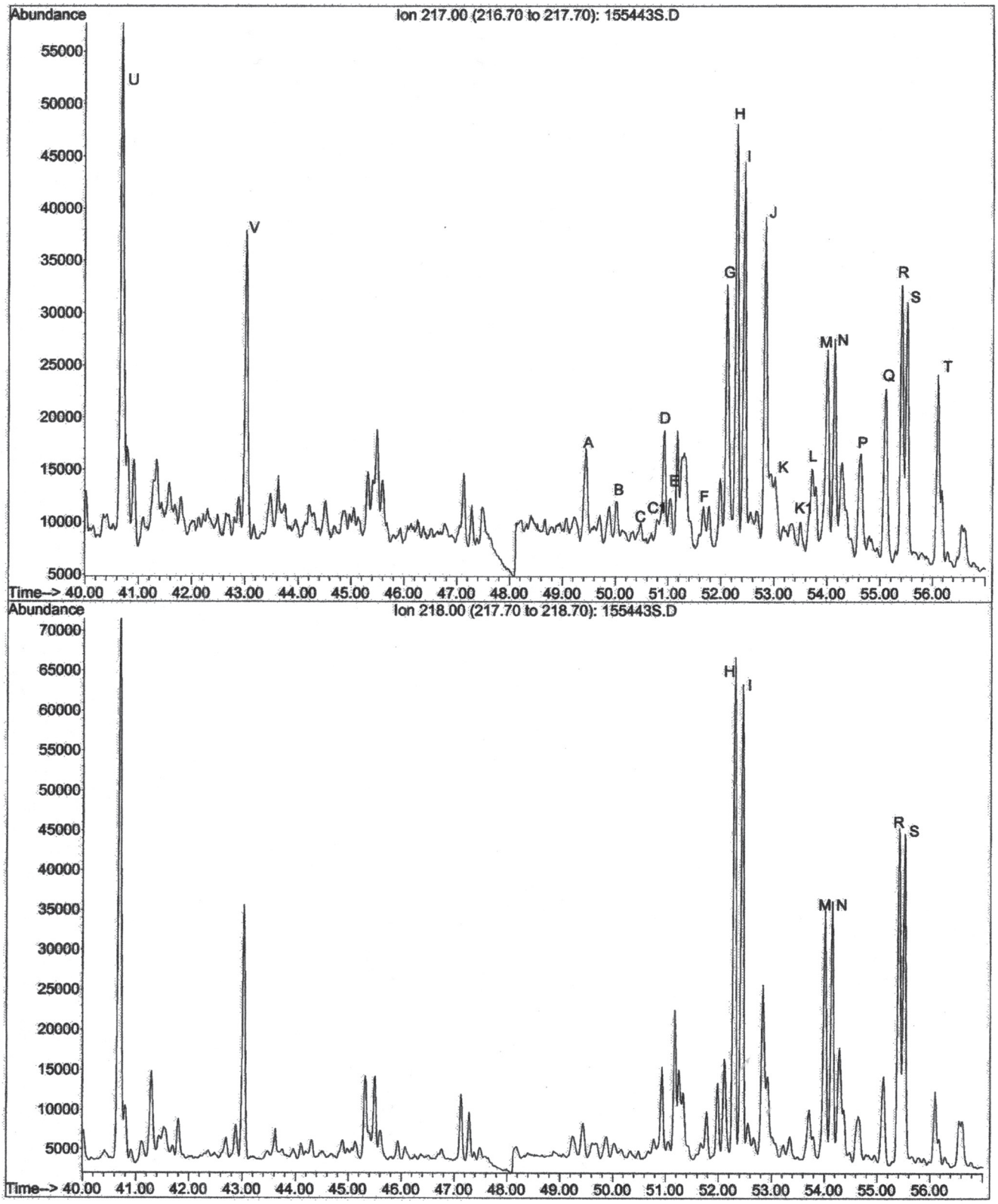

```
File        : C:\MSDCHEM\1\DATA\155443S.D
Operator    :
Acquired    : 24 Oct 2005  23:13     using AcqMethod BIOMARK
Instrument :   Instrumen
Sample Name: 15544-003 SATS
Misc Info   : 4574-003
Vial Number: 5
```

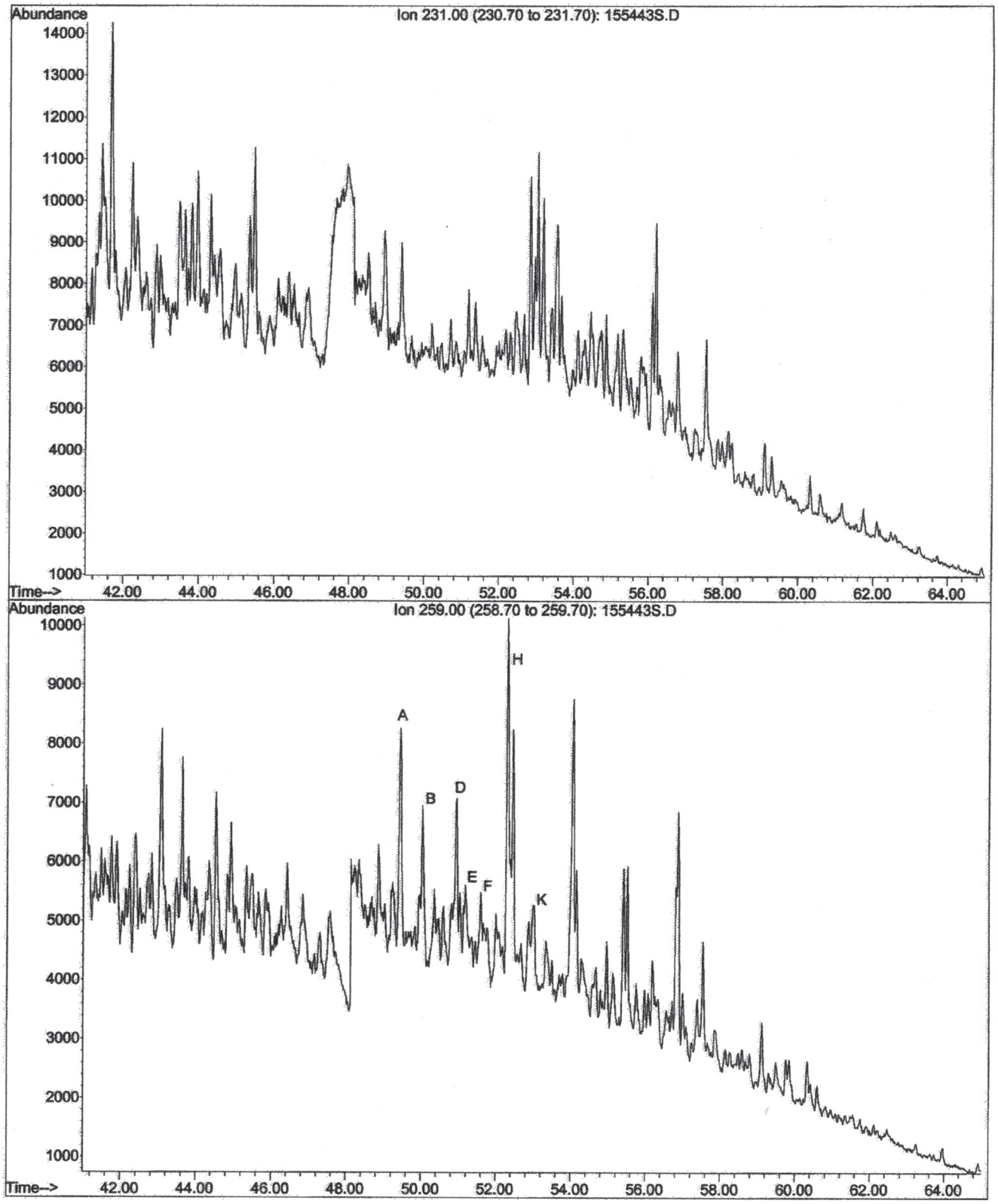

```
File       : C:\MSDCHEM\1\DATA\155443S.D
Operator   :
Acquired   : 24 Oct 2005  23:13     using AcqMethod BIOMARK
Instrument :   Instrumen
Sample Name: 15544-003 SATS
Misc Info  : 4574-003
Vial Number: 5
```

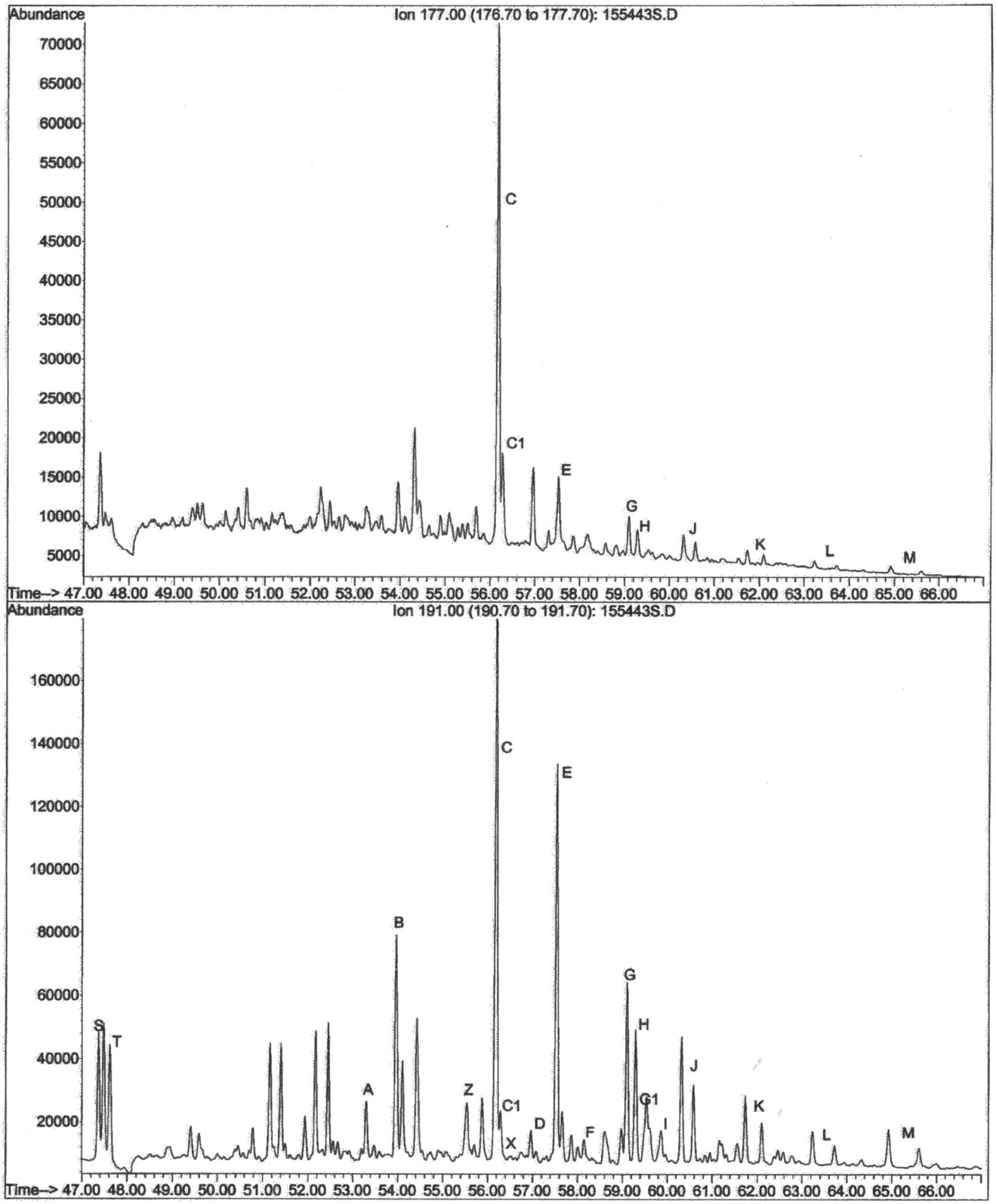

```
File       : C:\MSDCHEM\1\DATA\155443S.D
Operator   :
Acquired   : 24 Oct 2005  23:13     using AcqMethod BIOMARK
Instrument :   Instrumen
Sample Name: 15544-003 SATS
Misc Info  : 4574-003
Vial Number: 5
```

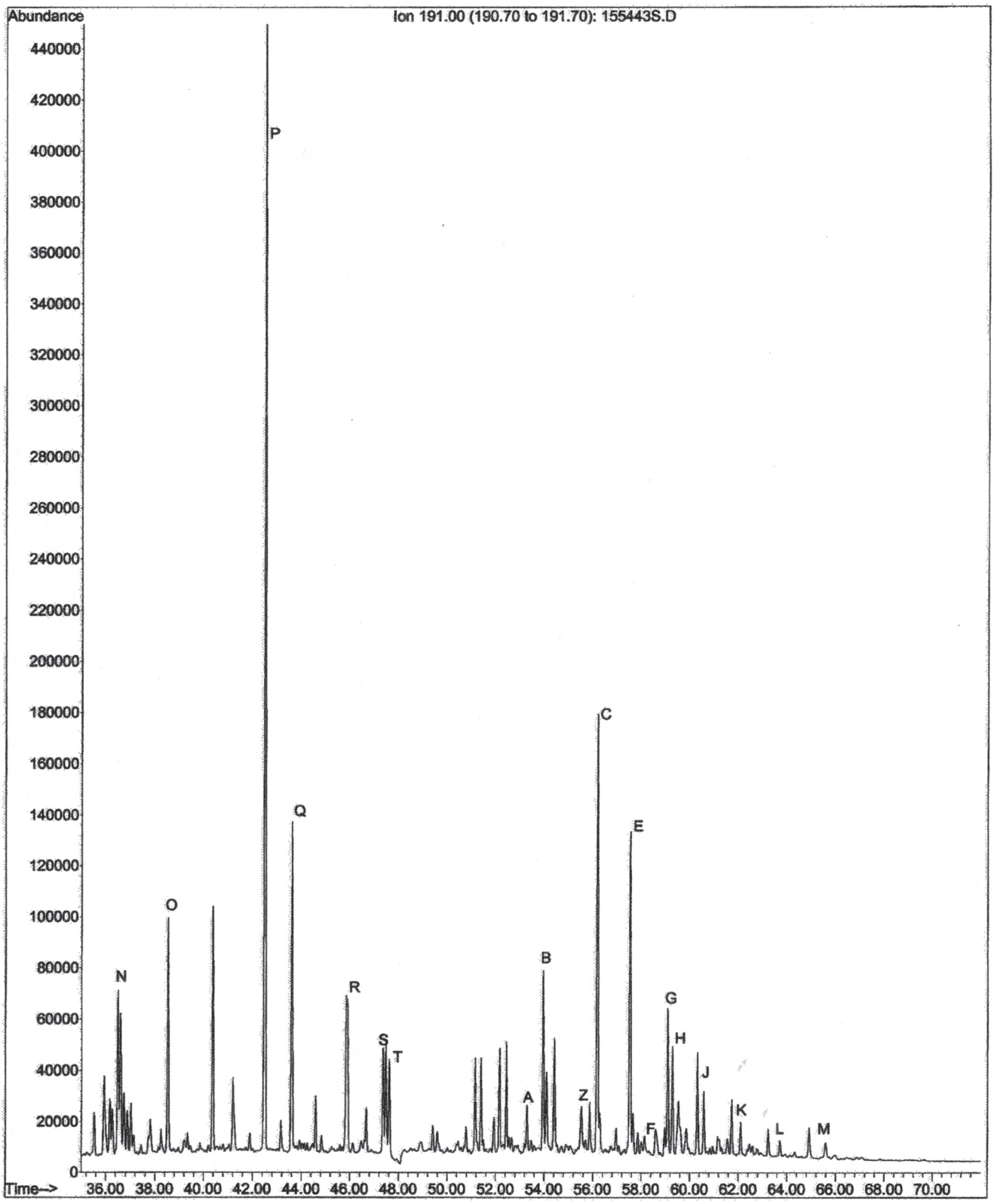

```
File        : C:\MSDCHEM\1\DATA\155443S.D
Operator    :
Acquired    : 24 Oct 2005  23:13      using AcqMethod BIOMARK
Instrument :   Instrumen
Sample Name: 15544-003 SATS
Misc Info   : 4574-003
Vial Number: 5
```

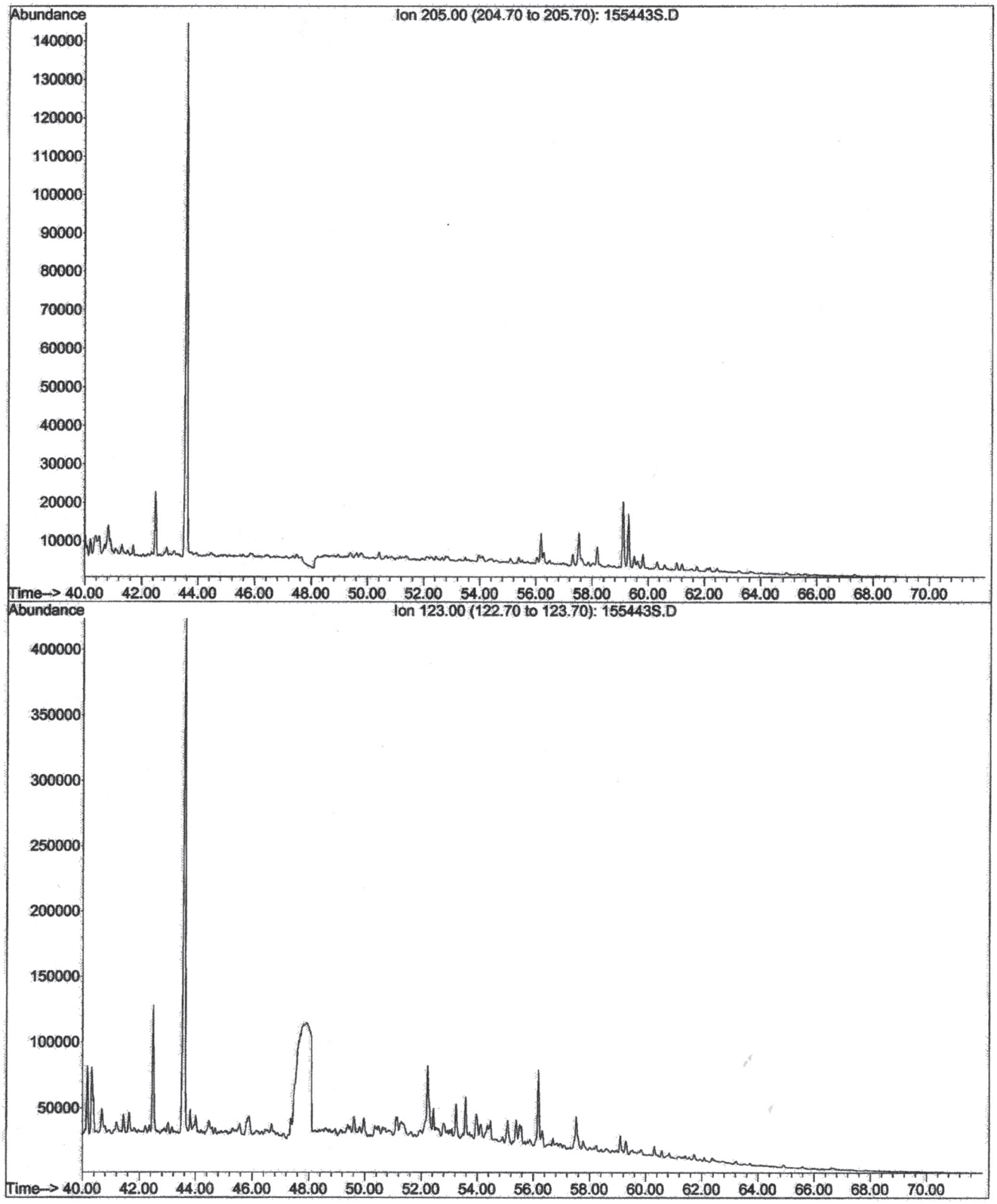

```
File        : C:\MSDCHEM\1\DATA\155444S.D
Operator    :
Acquired    : 25 Oct 2005  00:33     using AcqMethod BIOMARK
Instrument :   Instrumen
Sample Name: 15544-004 SATS
Misc Info   : 4574-004
Vial Number: 6
```

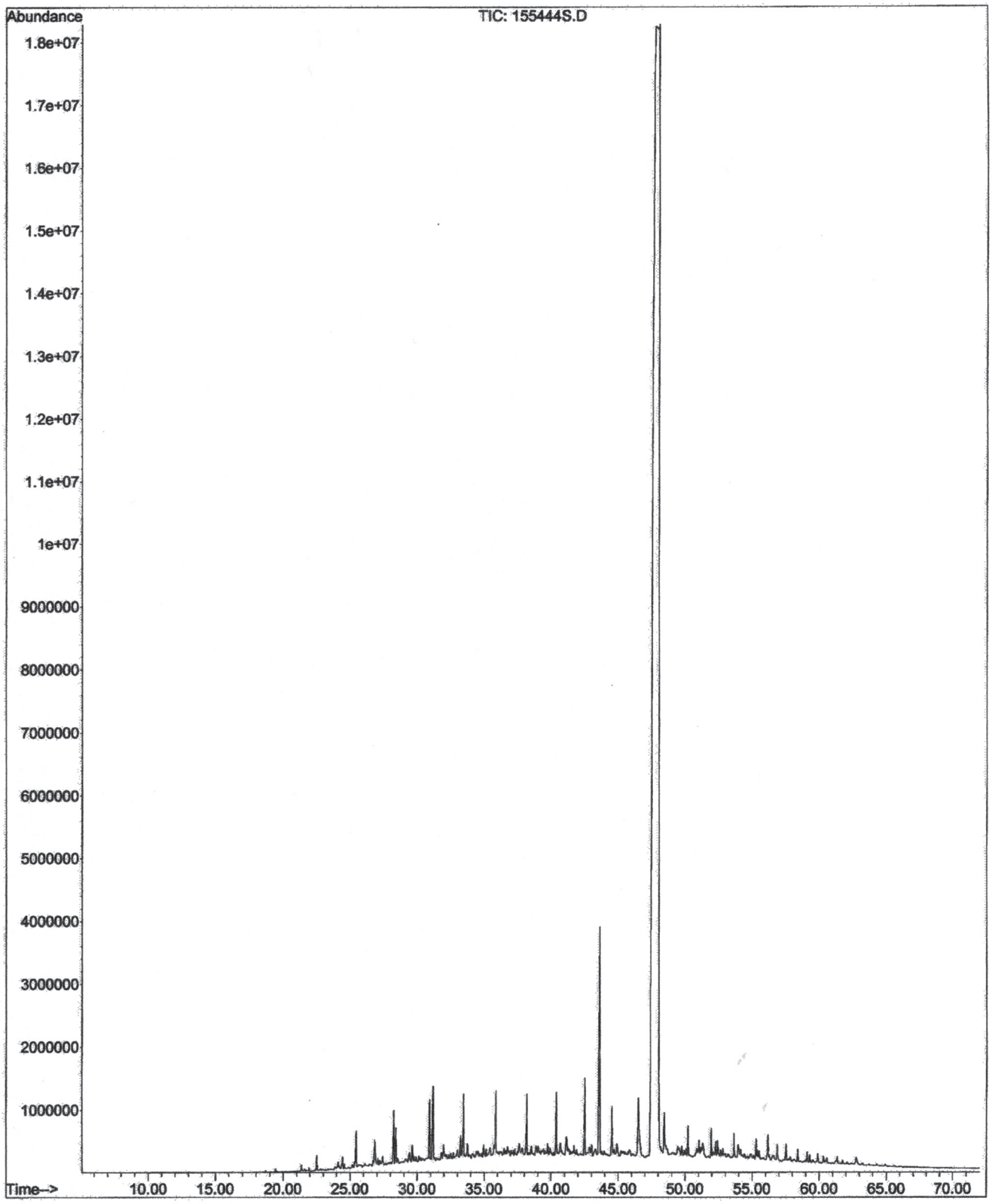

```
File        : C:\MSDCHEM\1\DATA\155444S.D
Operator    :
Acquired    : 25 Oct 2005  00:33     using AcqMethod BIOMARK
Instrument :   Instrumen
Sample Name: 15544-004 SATS
Misc Info   : 4574-004
Vial Number: 6
```

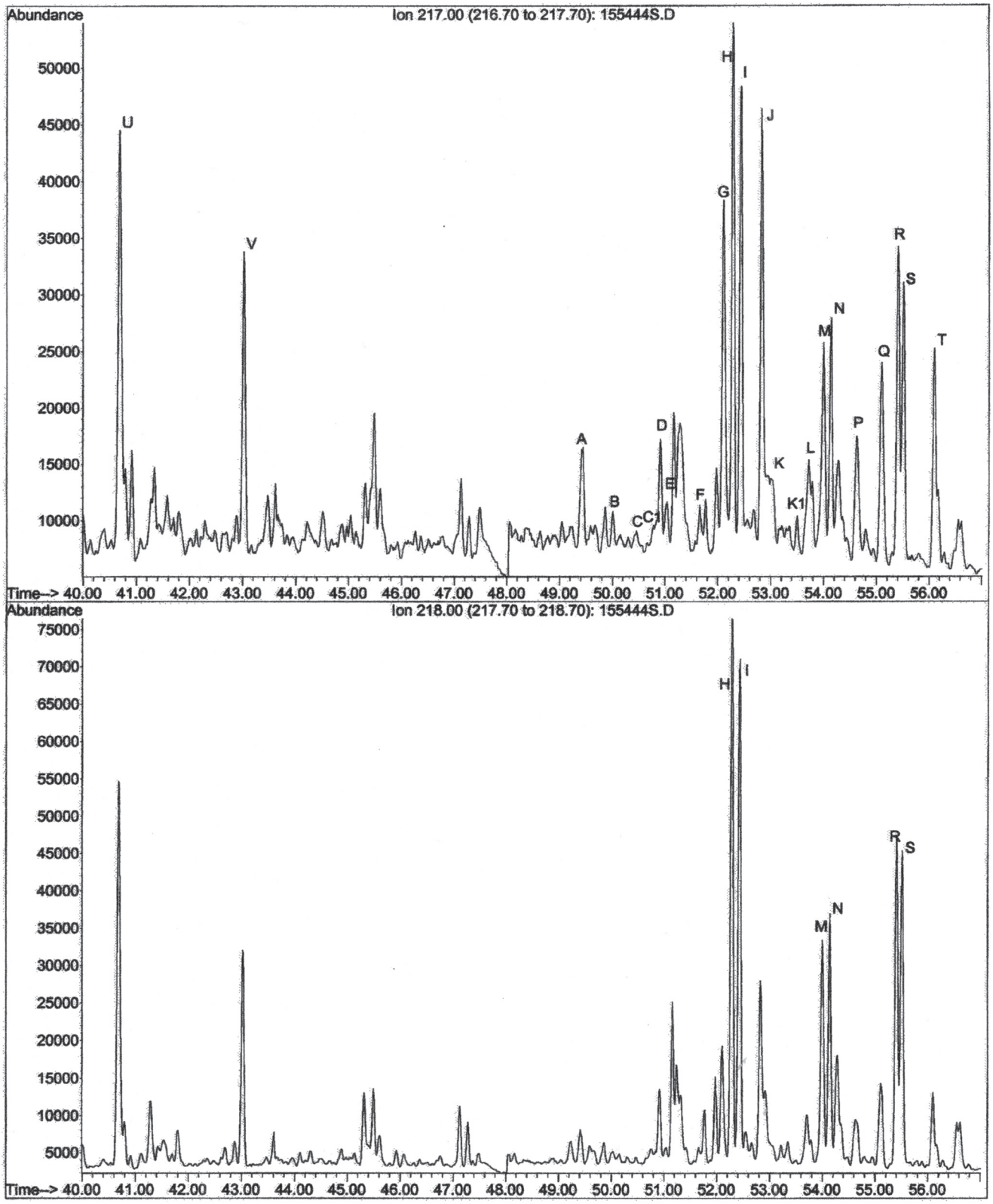

```
File        : C:\MSDCHEM\1\DATA\155444S.D
Operator    :
Acquired    : 25 Oct 2005  00:33      using AcqMethod BIOMARK
Instrument :   Instrumen
Sample Name: 15544-004 SATS
Misc Info   : 4574-004
Vial Number: 6
```

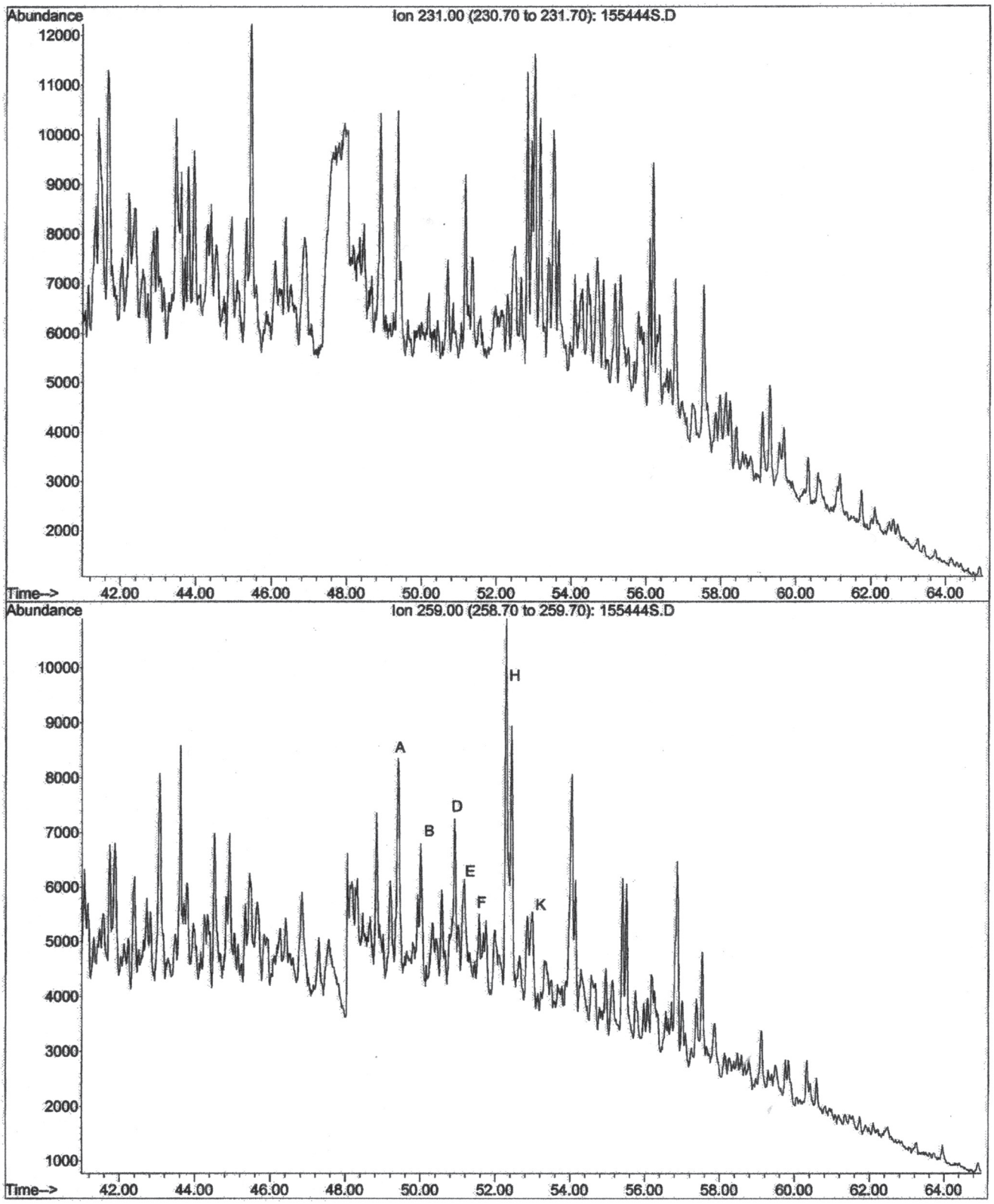

```
File        : C:\MSDCHEM\1\DATA\155444S.D
Operator    :
Acquired    : 25 Oct 2005  00:33     using AcqMethod BIOMARK
Instrument :   Instrumen
Sample Name: 15544-004 SATS
Misc Info   : 4574-004
Vial Number: 6
```

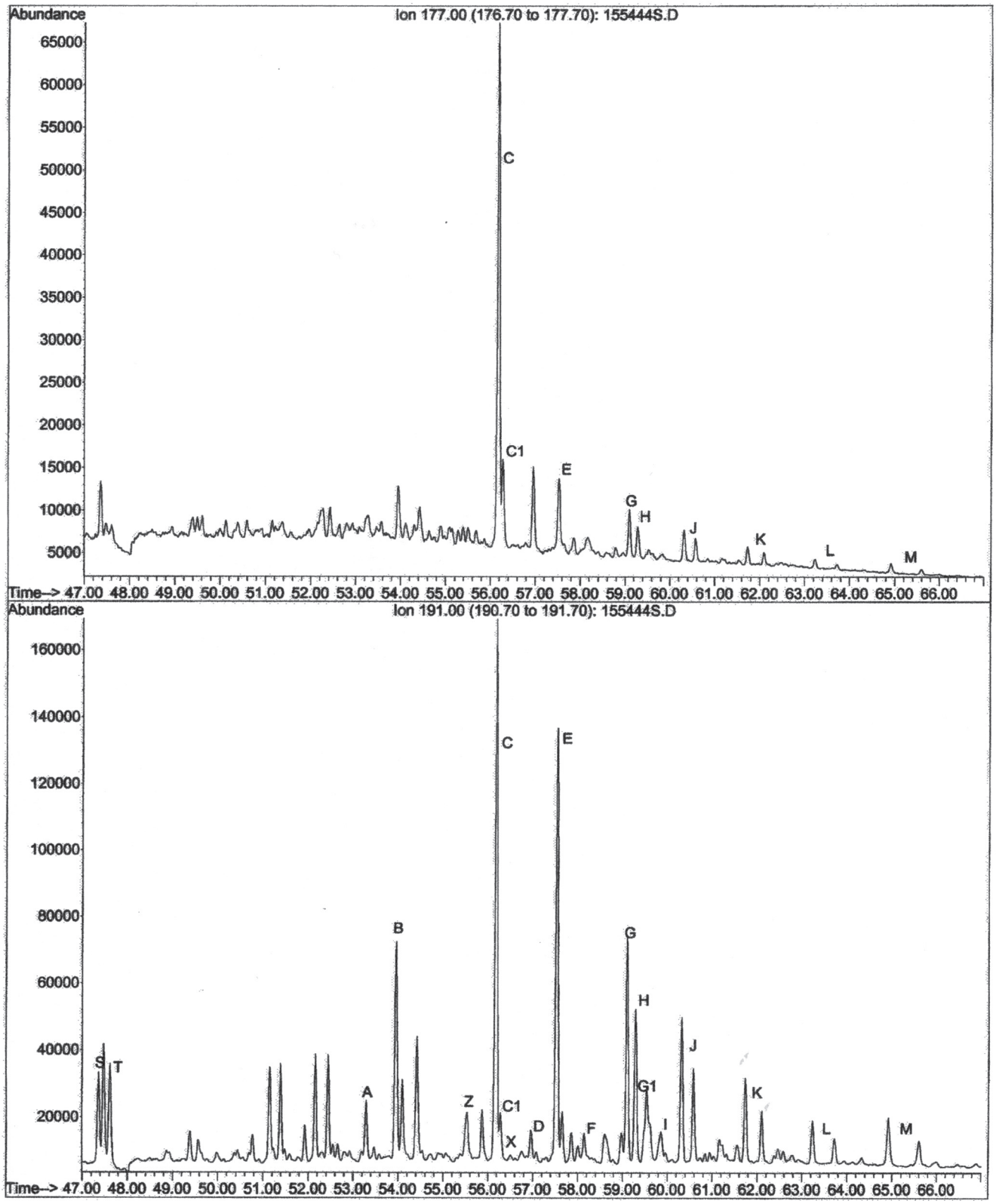

```
File        : C:\MSDCHEM\1\DATA\155444S.D
Operator    :
Acquired    : 25 Oct 2005  00:33     using AcqMethod BIOMARK
Instrument :   Instrumen
Sample Name: 15544-004 SATS
Misc Info   : 4574-004
Vial Number: 6
```

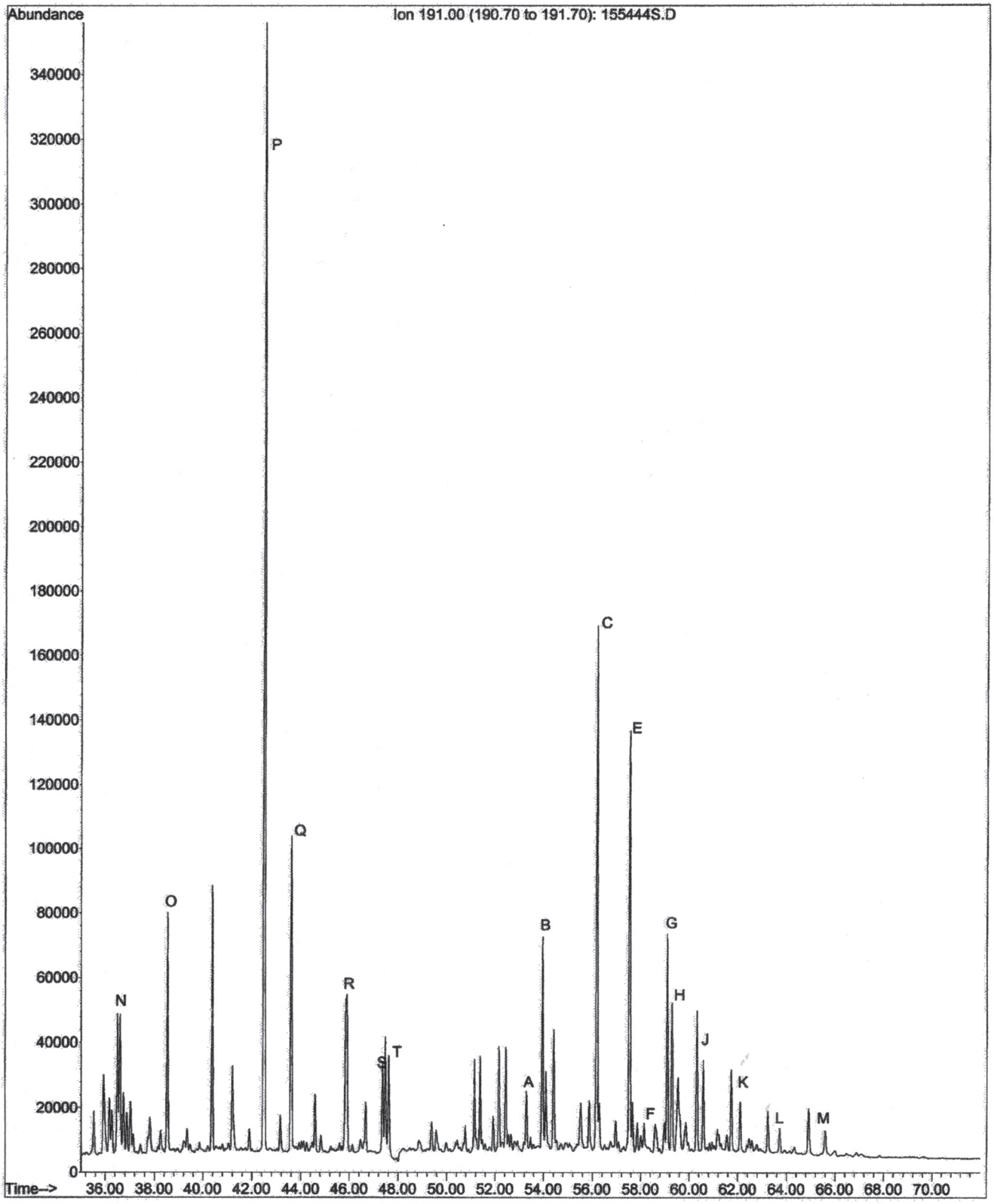

```
File        : C:\MSDCHEM\1\DATA\155444S.D
Operator    :
Acquired    : 25 Oct 2005  00:33      using AcqMethod BIOMARK
Instrument :   Instrumen
Sample Name: 15544-004 SATS
Misc Info   : 4574-004
Vial Number: 6
```

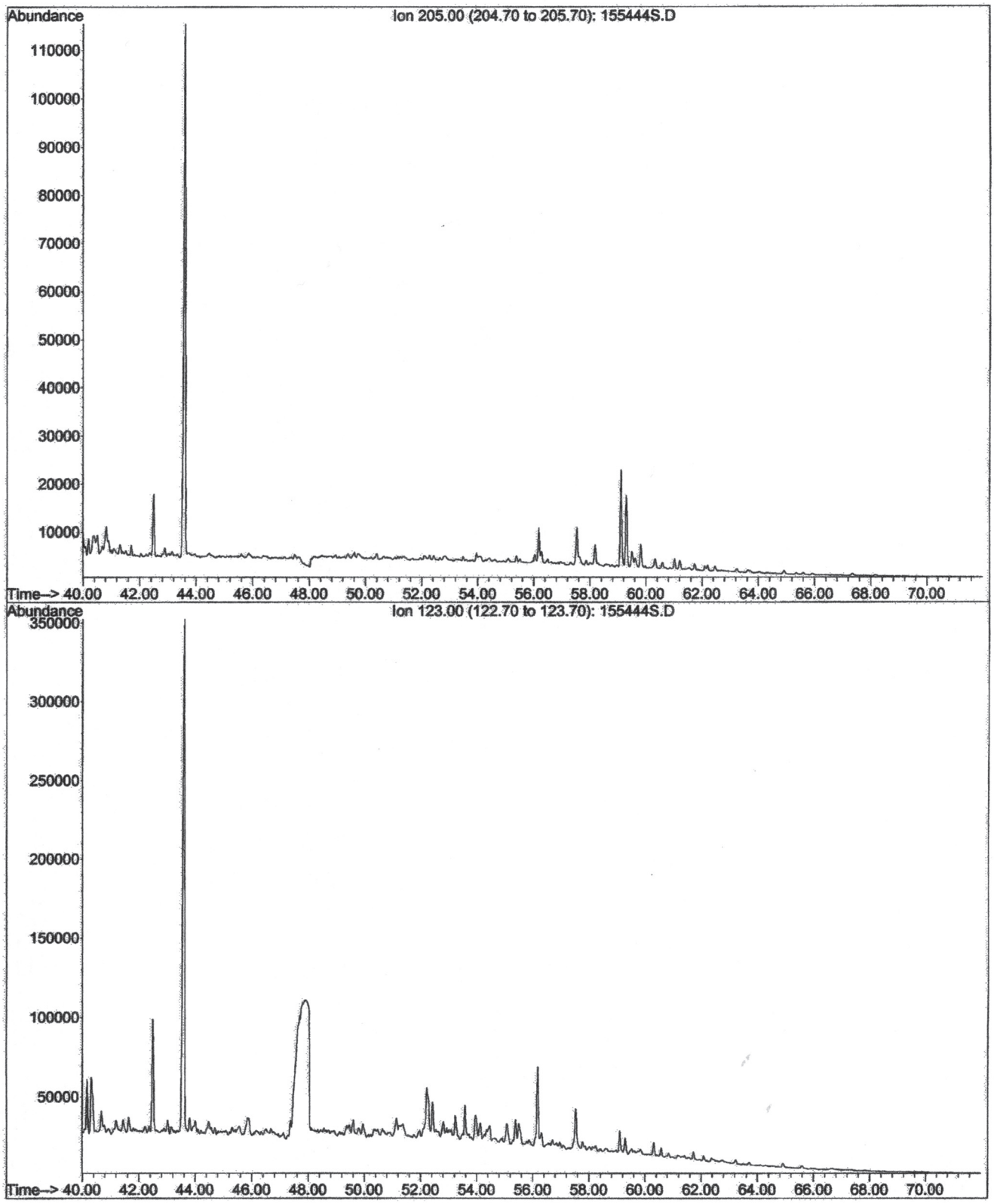

```
File        : C:\MSDCHEM\1\DATA\155444S.D
Operator    :
Acquired    : 25 Oct 2005  00:33      using AcqMethod BIOMARK
Instrument :   Instrumen
Sample Name: 15544-004 SATS
Misc Info   : 4574-004
Vial Number: 6
```